



รายงานวิจัยฉบับสมบูรณ์

โครงการ ผลกระทบของหมูปิ้งค์ชั้นบนพื้นผิวและโครงสร้างรูปพรุนต่อปรากฏการณ์การดูดซับแบบ
คัดเลือกของสารตกค้างจากยานยนต์กลางดูดซับชนิดไฮบริดสารอินทรีย์-อนินทรีย์

โดย รศ.ดร. ปฏิภาณ ปัญญาพลกุล และคณะ

กรกฎาคม พ.ศ. 2561

รายงานวิจัยฉบับสมบูรณ์

โครงการ ผลกระทบของหมูปิ้งค์ชั้นบนพื้นผิวและโครงสร้างรูพรุนต่อปรากฏการณ์การดูดซับแบบ
คัดเลือกของสารตกค้างจากยาบนตัวกลางดูดซับชนิดไฮบริดสารอินทรีย์-อนินทรีย์

รศ.ดร. ปฏิภาณ ปัญญาพลกุล จุฬาลงกรณ์มหาวิทยาลัย

สนับสนุนโดยสำนักงานกองทุนสนับสนุนการวิจัย
และจุฬาลงกรณ์มหาวิทยาลัย

(ความเห็นในรายงานนี้เป็นของผู้วิจัย สกว. และจุฬาลงกรณ์มหาวิทยาลัยไม่จำเป็นต้องเห็นด้วยเสมอไป)

เนื้อหางานวิจัย

สัญญาเลขที่ **RSA5880018**

โครงการ: ผลกระทบของหมู่ฟังก์ชันบนพื้นผิวและโครงสร้างรูพรุนต่อปรากฏการณ์การดูดซับแบบคัดเลือกของสารตกค้างจากยาบนตัวกลางดูดซับชนิดไฮบริดสารอินทรีย์-อนินทรีย์
Effects of surface functional groups and porous structures on selective adsorption mechanisms of pharmaceutical residues on organic-inorganic hybrid adsorbents

ระยะเวลาโครงการ 3 ปี

ชื่อหัวหน้าโครงการวิจัยผู้รับทุน : รศ.ดร. ปฏิภาณ ปัญญาพลกุล

รายงานในช่วงตั้งแต่วันที่ 1 กรกฎาคม พ.ศ. 2558 ถึงวันที่ 1 กรกฎาคม พ.ศ. 2561

Backgrounds

According to their large consumption pharmaceutical products by humans or animals either in households, industries or agriculture, they have been detected in sewage treatment plant including influent and effluents, surface waters (rivers, lakes, streams, estuaries, among others), groundwater, and drinking water. The metabolism of pharmaceutical compounds in human body are frequently incomplete that make excretion become one of the source. It is estimated that worldwide about 100,000-200,000t antibiotics (such as sulfonamide, tetracycline, and fluoroquinolone groups) were used in human therapy and veterinary medicine, and as growth promoters. Among a wide variety of pharmaceutical compounds and antibiotics residues in the environment is the special significance due to:

- i) Raw and treated effluents from pharmaceutical plant affected aquatic species growth.
- ii) Discharged pharmaceutical residuals were bio-concentrated in muscle and adipose tissue.
- iii) Pharmaceutical products and their degradation products tend to be endocrine disruptor (EDCs).
- iv) Discharged Antibiotic products have ability to facilitate the development of antibiotic-resistant human pathogens.

Previous literatures indicated that conventional treatment methods (coagulation, flocculation, sedimentation, sand filtration, and disinfection with chlorine), wastewater treatment (primary settling, activated sludge or trickling filter, and secondary settling), including advance oxidation processes (AOP) are not effective for removal of all pharmaceutical present in raw water and wastewater. This might be caused by their physico-chemical properties, biodegradability and fate in treatment facilities. Moreover, effects of degradation by-products from various treatment processes still have not been reported yet.

Adsorption is a preferable method for the removal of pharmaceutical residues, because it has the advantages of producing high-quality treated effluents, is easy and cheap to run, and does not have the problem of producing undesirable by-products. From the past, conventional materials such as activated carbon and silica are amorphous (molecular diffusion is limited by bottlenecks and dead volumes in their pore structures). This results in slow adsorption kinetics and lower capacities. In contrast, the materials contained ordered arrays of nano-sized pore channels were developed and improved the limitation from the previous materials. The open pore structures of ordered nanoporous materials allow fast access of ions and small molecules to their large ($>1,000 \text{ m}^2/\text{g}$) surface areas. Moreover, nanoporous sorbents can be created with controlled pore size and tailored pore chemistries to enhance their selectivity. Several papers have reported the synthesis of nanocomposites which are both attractive adsorbent with surface modifications and provide advantages on separation in different ways by encapsulating superparamagnetic iron oxide with well-ordered mesoporous silica structure. The superparamagnetic nanoparticles (SP) can be applied as the core of adsorbents to enhance the separation efficiencies by adding a magnetic field. For example, the application superparamagnetic material in classical cake filtration could reduce the overall filtration resistance (Wang et.al., 2010). Moreover, their surface modification, via the reaction of silanol groups with various organosilanes, is very helpful in improving the adsorptive capacity and selectivity as a result of specific interactions between the surface functional groups and adsorbate molecules.

Moreover, there are various organic-inorganic hybrid materials which synthesized and reported by many researcher and can be applied as an adsorbent for removal of organic contaminants from wastewater as well as application in purification unit for tap water systems. For example, graphene oxide modified mesoporous silicas which are supposed to have higher adsorption capacity comparing with pristine mesoporous silicas and attached graphene oxide can

enhance separation efficiency of graphene oxide which is the main drawback for applying graphene oxide in aqueous phase. Moreover, metal organic frameworks (MOFs) are also reported the extremely high adsorption capacities of some pharmaceutical residues, however, adsorption mechanism and effect of co-existing organic matters still have not been reported yet.

Natural organic matters (NOMs) are a complex chemical mixture with various molecular weights, produced mainly from the decomposition of plant and animal residues. According to their chemical molecule, NOM can be classified in to the hydrophobic- and hydrophilic NOM. The consisting polyaromatic carbon, having phenolic functional group and conjugated double bonds moieties in the molecular structure are classified as hydrophobic NOM, while a higher proportion of aliphatic carbon and nitrogenous compound is containing in hydrophilic NOM. According to their complex molecule hence the possibility of the interaction among NOM, adsorbent and other organic compound (pharmaceutical residues) due to π - π electron interactions, electrostatic interaction, ligand exchange between carboxyl/hydroxyl functional groups, etc, has considering as the important understanding. However, effects of surface functional groups and crystalline structure of organic-inorganic hybrid adsorbents on combined interaction with both pharmaceutical residues (including various oxidation by-products) and NOM is still unclear.

Objectives

The main objective of this proposal is to carry out a carefully designed parametric study of the physical and chemical factors that underlie three components interaction phenomena of pharmaceutical residues, NOM and surface of various functional groups grafted on surfaces of the alternative organic-inorganic hybrid adsorbents such as functionalized porous silicas (HMS, MCM-41, etc), PMOs and superparamagnetic porous silicas by adsorption/desorption phenomena. There are six sub-objectives of this research as follow;

1. To investigate the effects of surface functional groups, pore size, crystalline structures, hydrophobicity and surface area on adsorption/desorption capacities and mechanism of adsorption of pharmaceutical residues (i.e. hormones, antibiotics, antilipidemics, and non-steroidal anti-inflammatory drugs) onto functionalized porous and/or superparamagnetic porous silicates.
2. To evaluated effects of molecular characteristics of pharmaceutical residues on interaction with both NOM and organic-inorganic hybrid adsorbents.

3. To investigate the effects of pH on adsorption capacities and mechanism of adsorption of the pharmaceutical residues onto organic-inorganic hybrid adsorbents.
4. To determine the adsorption selectivity of difference pharmaceutical residues on organic-inorganic hybrid adsorbents.

Materials and methods

Experimental Approach

The experimental approach can be divided into 7 topics as follows :

1. To synthesize and characterize physico-chemical properties of the organic-inorganic hybrid adsorbents with the various types of organic functional groups.
2. To develop measurement method of pharmaceutical residues in aqueous phase and on organic-inorganic hybrid adsorbents surfaces.
3. To investigate the effect of surface characteristics and molecular structure of pharmaceutical residues on adsorption kinetic and isotherm.
4. To investigate the desorption phenomena of pharmaceutical residues from organic-inorganic hybrid adsorbents.
5. To study the selective adsorption mechanisms in mixed solution of pharmaceutical residues.
6. To study the three component adsorption mechanisms among adsorbent surface, PPCP and NOM.
7. To evaluate the separation efficiencies of superparamagnetic porous silicates adsorbents by ultrafiltration and High Gradient Magnetic Separation filter (HGMS).

Adsorbents

All synthesis adsorbents have been synthesized and characterized by various techniques such as Nitrogen adsorption isotherm, XRD, FT-IR, Elemental analysis, SEM, TEM, XPS and TGA. Synthesized hybrid adsorbents can be divided to be 5 groups of adsorbents which is :

1. Superparamagnetic Hexagonal mesoporous silicas (HMS-SPs)
 - 1.1 Amino functionalized HMS-SP (A-HMS-SP)
 - 1.2 Nitrile functionalized HMS-SP (N-HMS-SP)

- 1.3 Mercapto functionalized HMS-SP (M-HMS-SP)
- 1.4 Phenyl functionalized HMS-SP (P-HMS-SP)
- 1.5 Octyl functionalized HMS-SP (OD-HMS-SP)
2. Periodic mesoporous organosilicas (PMOs)
 - 2.1 Pristine periodic mesoporous organosilica (PMO)
 - 2.2 (3-Aminopropyl)trimethoxy PMOs (1N-silane) (1NX%PMOs)
 - 2.3 3-[2-(2-Aminoethylamino)ethylamino]-propyltrimethoxy PMO (2N-silane)(2NX%PMOs)
 - 2.4 [2-(2-Aminoethylamino)propyl]-trimethoxy PMO (N-silane) (3NX%PMOs)
3. Graphene modified mesoporous silicas (GO-porous silicas)
 - 3.1 Amino-porous silica modified by graphene oxide (A-GO-A-SBA-15)
 - 3.2 Mercapto, amino porous silica modified by graphene oxide (GO-A-HMS and GO-A5M5)
4. Metal organic frameworks (MOFs)
 - 4.1 MIL-53(Al)
 - 4.2 Amine or mercapto modified MIL-53(Al) (NH₂- MIL-53(Al))
 - 4.3 ZIF-8(Zn)
5. Mesoporous silicas
 - 5.1 SBA-15
 - 5.2 HMSs

Physico-chemical characterization of adsorbents

1. Porous structure: powder X-ray diffractometer (XRD)
2. Surface area and pore size: N₂ adsorption-desorption isotherm using BET theory
3. Pore size distribution: N₂ adsorption-desorption isotherm using BJH theory
4. Surface charge: Zeta potential analyzer
5. Functional group: Fourier Transform Infrared Spectroscopy (FT-IR) and X-ray Photoelectron Spectroscopy (XPS)
6. Hydrophilicity/Hydrophobicity: Tensiometer
7. Surface appearance: Scanning Electron Microscopy (SEM), Transmission Electron Microscope (TEM)
8. Stability of adsorbent : Thermogravimetric analysis (TGA)
9. Nitrogen content: CHONS analyzer
10. Sulfur content: Inductively Coupled Plasma Atomic Emission Spectroscopy (ICP-AES)

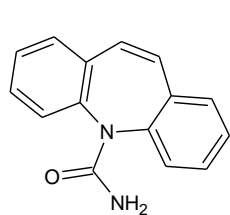
Target pollutants (pharmaceutical residues and disinfection by-products)

Nalidixic acid (NAL), Ciprofloxacin (CIP), Sulfamethoxazole (SMX), Acetaminophen (ACT), Naproxen (NAP), Diclofenac (DCF), Carbamazepine (CBZ) and Methyltestosterone (MT) will be chosen as the representative antibiotic in this research. The selected pharmaceutical residues represent main hormones, antibiotics, antilipidemics, and non-steroidal anti-inflammatory drugs which were detected in the aquatic environment. Moreover, carcinogenic disinfection by-products such as haloacetonitrile group was included in this study. Figure 1 shows the molecular structures of applied pollutants.

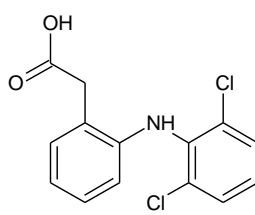
Target pollutants measurement

Pharmaceutical residues (PPCPs) was measured by high performance liquid chromatography (HPLC) for ppb level. The filtrated solute underwent a solid-phase extraction (SPE) with PEP cartridges (200 mg/6 ml, Cleanert PEP-H). The cartridges were equilibrated with methanol (5 ml) and water (10 ml), and then the filtrate sample was taken, eluted with methanol (10 ml), evaporated and resuspended with 0.5 ml of methanol. The quantities of antibiotic concentration in equilibrium solutions were analyzed by a reverse phase HPLC equipped with a photodiode array detector (260-280 nm). The determination of PPCP in solution was performed at 50 °C on a HPLC column (5mm, 250 mm x 4.6 mm; LiChrosorb NH₂, GLS Sciences, USA). The elution gradient was conducted using acetonitrile (A) and water (B). The initial elution condition was a mobile phase A 100% v/v reach to 0% v/v within 15 min, while the flow rate and injection volume was 1 ml min⁻¹ and 40 µl, respectively. The detection limit of applied PPCP of concentrated sample by HPLC was approximately 0.2 mg L⁻¹. Whereas the recovery percentage of the each surrogate standard was approximately 90 % and the applied PPCPs recovery percentage were nearly 80%. For example, the recovery percentage of CIP, NAL, and SMX were 79.44±24.80, 79.76±26.81, and 76.63±19.58, respectively. According to the surrogate standard, sulfamethoxazole (100 µg L⁻¹) was spiked in the obtained sample solution of CIP and NAL adsorption experiment. In case of SMX adsorption, CIP (100 µg.L⁻¹) was used as the surrogate standard instead.

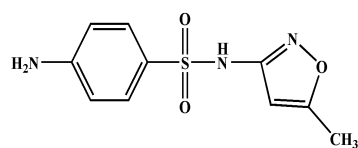
Target PPCPs and other emerging pollutants



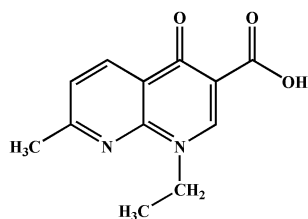
Carbamazepine



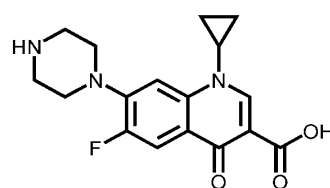
Diclofenac (DCF)



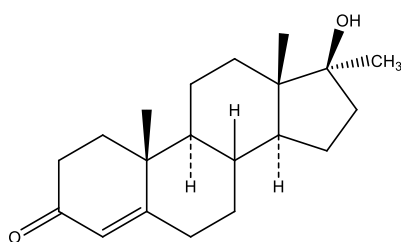
Sulfamethoxazole



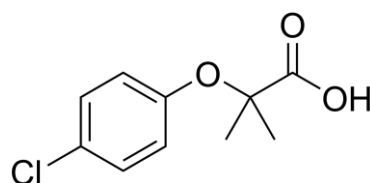
Nalidixic acid



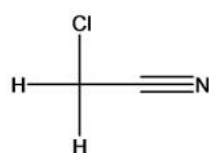
Ciprofloxacin



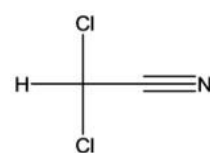
Methyltestosterone



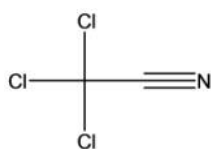
Clofibric acid



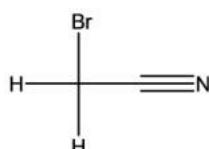
Monochloroacetonitrile



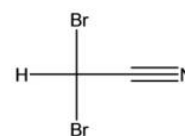
Dichloroacetonitrile



Trichloroacetonitrile



Monobromoacetonitrile



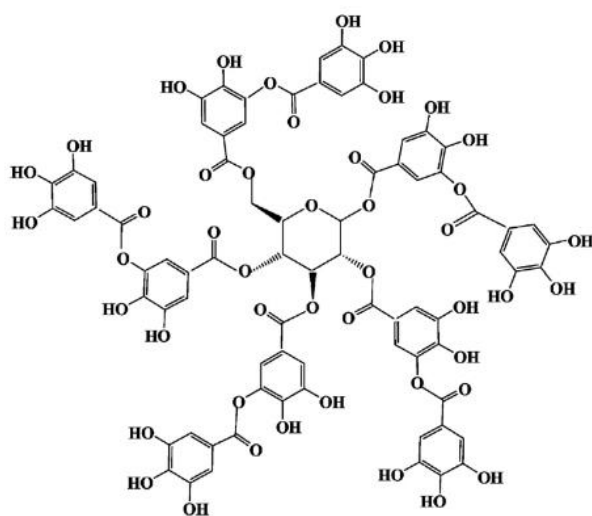
Dibromoacetonitrile

Figure 1 Chemical structures of the studied pharmaceutical residues (PPCPs), and disinfection by-products (DBPs).

Haloacetonitriles (HANs) was analyzed according to a modified EPA Method 551.1. Typically, a sample solution (30 mL) was placed in a 40 mL glass vial with a polypropylene screw cap and PTFE faced septum. Into each sample, 5 g of anhydrous sodium sulfate (Na_2SO_4) was added in order to increase the ionic strength of the aqueous matrix together with 2 mL of methyl tert-butyl ether (MtBE). The vial was then sealed with Teflon-faced septa and shaken for 2 min. After standing the resulting solution for 3 min, 500 μL of the MtBE layer was transferred into a 2-mL vial. The organic layer (1 μL) was injected into an Agilent GC6890 gas chromatograph equipped with an electron capture detector (GC/ECD).

Natural organic matter (NOM)

Since tannic acid (TA) can causes many problem for drinking water and wastewater such as the health problem from carcinogenic disinfection by-products, the qualities of water etc. Comparison on molecular structure, TA has the possible active site to interact with the organo-functional group on the adsorbent surface and the functional group of selected antibiotic. Therefore, TA was selected as a representative natural organic matter. The chemical structure of TA shows in Figure 3.1.



Tannic acid	($\text{C}_{76}\text{H}_{52}\text{O}_{46}$)
MW	1700 g/mole
Water solubility	2850 g/L
pKa	3.5

Figure 2 Chemical structure of Tannic acid (Yi et al., 2011)

Adsorption experiments

Batch adsorption experiment was studies in 100-mL Erlenmeyer flask containing 1 g.L^{-1} of the synthesized adsorbents. The solution pH and ionic strength was controlled by using a 0.01

M phosphate buffer. Selected pollutants and tannic acid stock was prepared in 50% methanol and 0.01 M phosphate buffer at pH 7.0, respectively. In addition, the stock concentration of each antibiotic and tannic acid was prepared at 1 mg. L⁻¹ and 80 mg L⁻¹, respectively. The experimental sample was conducted with shaking condition at 220 rpm (25 °C), and then filtered through a glass filter (GF/C, pore size 0.12 µm). The quantities of pollutants concentration in equilibrium solutions were analyzed by a solid phase extraction (SPE) and a reverse phase high performance liquid chromatography (HPLC) equipped with a photodiode array detector (260-280 nm). Then, the adsorption capacity was calculated from the difference between initial and equilibrium concentration divided by the amount of adsorbent as following Equation:

$$q_e = \frac{(C_0 - C_e)}{M} V$$

Where q_e is the adsorption capacity (µg/g), C_0 and C_e are the initial and equilibrium concentration (µg/L), respectively. V is the volume of the solution (L) and M is the mass of adsorbent (g).

Furthermore, the important parameter involved in adsorption mechanism was examined and summarized in Figure 5.

Adsorption Kinetic Study

Adsorption kinetics were performed by varying the contact time and initial pollutant concentration at 500 µg.L⁻¹ and 1 g.L⁻¹ of adsorbent in 0.01 M phosphate buffer pH 7.0. The sample was shaken at 220 rpm at 25 °C, and then the supernatant solution was filtrated through a glass filter (GF/C, pore size 0.12 mm). Then, the remaining pollutant concentration was analyzed by above analytical methods.

Adsorption isotherm study

Adsorption isotherm was conducted with an initial pollutants concentration range between 20-3000 µg.L⁻¹ and 1 g.L⁻¹ of adsorbent. The ionic strength of the solution was fixed using 0.01 M phosphate buffer at either pH 5, 7 or 9. The sample was shaken at 220 rpm at 25 °C, and then the supernatant solution was filtrated through a glass filter (GF/C, pore size 0.12 mm). the remaining pollutant concentration was analyzed by above analytical methods.

Selective adsorption study

Selective adsorption of three antibiotics in mixed solute solution

Adsorption selectivity was determined via a mixture of three selected antibiotics, CIP, NAL and SMX, on the synthesized adsorbents. The experiment was conducted in the same condition of the single solute solution at pH 7.0. The remaining antibiotics concentration in equilibrium solution was analyzed by a solid phase extraction (SPE) and a reverse phase high performance liquid chromatography (HPLC) equipped with a photodiode array detector (260-280 nm) as described in the analytical method.

Effect of tannic acid on antibiotic adsorption

According to the effect of tannic acid (TA) on antibiotic adsorption, the experiment was investigated by adjusting TA solution (40 mg.L^{-1}) to different antibiotic concentration at pH 7.0 and 0.01 M phosphate buffer. The residual concentration of TA in solution was analyzed by the HPLC equipped with a photodiode array detector (280 nm). The separation was performed at 50°C on a C18 HPLC column (5mm, 250 mm x 4.6 mm; Intersil, GLS Sciences, USA) using an acetonitrile-water mixture (85:15%, v) as the mobile phase at a flow rate of 1 ml min^{-1} . The quantities of antibiotic in the presence of TA were analyzed via the same adsorption procedure. The recovery of antibiotics was interfered by the presence of TA, therefore, double PEP cartridges (200 mg/6 ml, Cleanert PEP-H) were used in the same SPE procedure to increase the recovery efficiencies.

Magnetic adsorbents separation

High gradient magnetic separate filtration

The magnetic filtration system consists of wire stainless steel filter, 3 acrylic pipe diameter 0.8 cm and height 5 cm, pair of permanent magnets and peristaltic pump that show as Figure 3. The gap between permanent magnets was 3 cm.

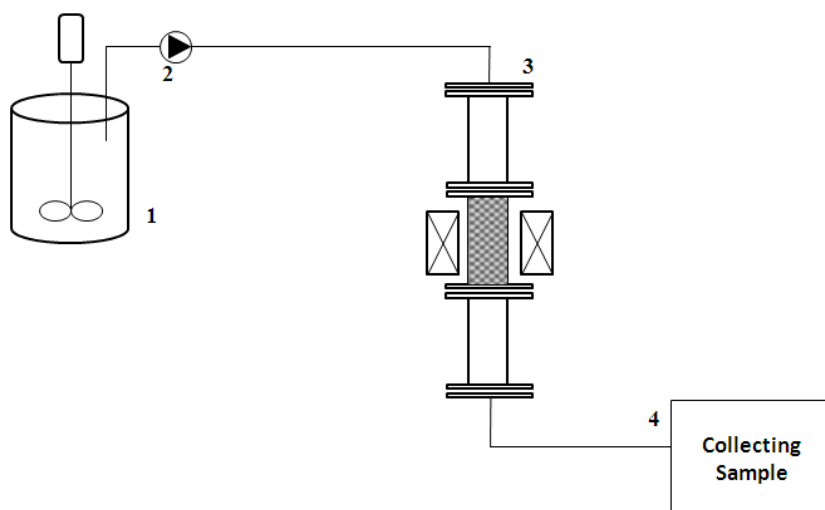


Figure 3 System filtration process; stirrer (1), peristaltic pump (2), magnetic filtration (3) and collecting sample (4).

Ultrafiltration unit (UF)

The completely mixed of solution will be fed to the dead-end flow membrane system while pressure head was controlled to be 1 bar by valve of by-pass line (temperature at 25 ± 2 °C) as shown in figure 14.

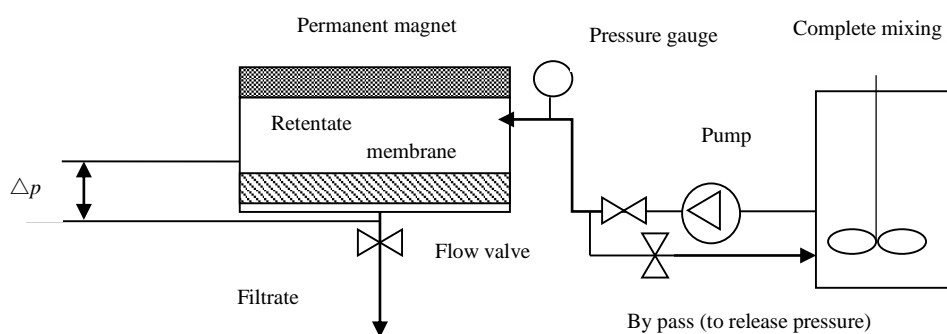


Figure 4 Diagram of magnetic system applied to UF

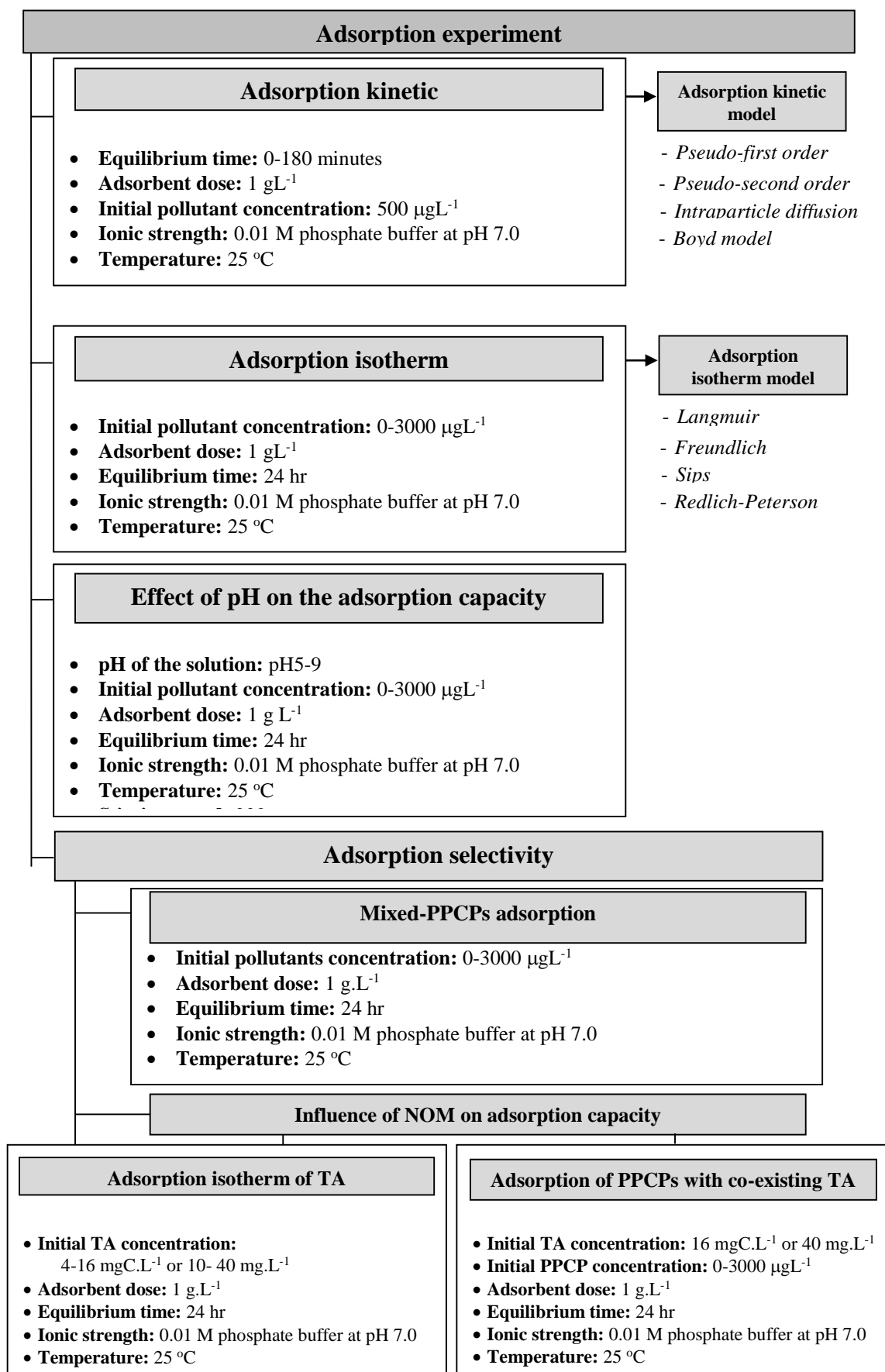


Figure 5 Adsorption experimental framework of this study

Results and discussions

Physico-chemical characteristics

Physico-chemical characteristics of studied adsorbents have been concluded in table 1-3 such as surface area, pore structure, surface charges and surface functional groups, etc. TEM, SEM images and XPS spectra also have been shown in figure 4-9.

Synthesized adsorbents have been identified and proved their crystalline structure and morphology by standard techniques. Effects of surface and structure modification on characteristics and their relationship with adsorption capacities and mechanisms were also reported in further publication. Moreover, used adsorbents which adsorbed pollutants (PPCPs, DBPs and emerging pollutants) were also investigated to identify the signal that can be proved adsorption mechanisms.

To study the physico-chemical characteristics of the synthesized adsorbents, the properties of superparamagnetic particles as the core-shell of the adsorbents, the structures of hexagonal mesoporous silica, and the organo-functional groups at the surfaces were determined in this chapter. Summary of synthesized HMS-SP, and functionalized HMS-SPs as the adsorbents used in this study are shown in Table 1.

Table 1 Physico-chemical characteristics of Superparamagnetic Hexagonal mesoporous silicas (HMS-SPs)

Adsorbents	Surface functional groups	Surface Characteristic ^s	Contact angle (θ)	Pore diameter (nm)	BET surface area (m^2/g)	Pore volume (mm^3/g)	Particle Diameter (μm)	pH_{zpc}
SP	-	-		-	95	-	-	-
HMS-SP	Silanol	Hydrophilic	45	3.28	380	344	0.33	4.5
A-HMS-SP	Amino	Hydrophilic	50	3.70	141	265	0.15	9.0
N-HMS-SP	Nitrile	Hydrophilic	53	3.32	362	589	0.21	4.5
M-HMS-SP	Mercapto	Hydrophobic	60	2.51	492	609	0.39	6.4
P-HMS-SP	Phenyl	Hydrophobic	77	2.52	345	471	0.21	5.5
OD-HMS-SP	Octyl	Hydrophobic	90	3.21	403	237	0.18	3.5

The results showed the BET surface area of the adsorbents followed the order: M-HMS-SP>OD-HMS-SP>HMS-SP>N-HMS-SP>P-HMS-SP>>A-HMS-SP whereas the decrease of pore volume and surface area of N-HMS-SP, P-HMS-SP and A-HMS-SP in comparison with pristine HMS-SP could be detected. Considering with the narrow pore size distribution results are calculated from the Barrett-Joyner-Halenda (BJH) method (the mean pore size are summarized in Table 1). The selected antibiotics molecular size; ciprofloxacin (CIP) molecular dimension (0.73 nm in width and 1.2 nm in length), nalidixic acid (NAL) molecular dimension (0.71 nm in width and 1.05 nm in length), and sulfamethoxazole (SMX) molecular dimension (0.43 nm in width and 1.27 nm in length), are smaller than the mean pore size of all adsorbents. Therefore, selected antibiotics molecule could be available for adsorption both on the external and internal of the surface area of the synthesized adsorbents. Moreover, due to the higher molecular size of tannic acid (TA) (2.7 and 2.8 nm in width and length, respectively), the representing natural organic matter than antibiotics molecule, it can be suggested that the accessibility of selected antibiotics into internal surface area should be higher than TA. Nevertheless, normalization of adsorption area per molecule of each antibiotic should be further calculated to evaluate to internal surface accessibility of each synthesized adsorbents.

Structural properties of the extracted PMO and the functionalized PMOs are listed in Table 2. Specific surface area of the materials was calculated using BET equation. These materials had very large specific surface areas and pore volume. Their specific surface areas ranged from 963.5 m²/g to 1252 m²/g and their pore volumes ranged from 0.524 cm³/g to 0.85 cm³/g. Virgin PMO had the largest and 2N40PMO had the smallest specific surface area. Virgin PMO had the largest and 3N40PMO the smallest pore volume.

In regard to the structural properties of PMO functionalized with n-silane, it was found that the BET surface area and the pore volume of the functionalized PMO decreased as the concentration of added N-silane increased. This could be explained by the occupying of the pore framework by the terminal organic functional groups protruding into the terminal surface of the pores [Saad et al., 2008]. However these functionalized materials still have larger surface area than other materials which were functionalized with amine-functional group such as HMS, MCM-41 or SBA-15 [Prarat et al., 2011; Saad et al., 2008]. The corresponding pore sizes of PMO, 1N10PMO, 1N25PMO and 1N40PMO materials were 26.5 Å, 26.0 Å, 23.5 Å and 21.5 Å respectively. It was found that further increasing of the concentration of organosilane in the reaction mixture resulted in reduction of the pore diameter of 1NPMOs materials. Dimos et al. (2009) reported that reduction of the specific surface area and pore diameter of the

Table 2 Physico-chemical characteristics of Periodic mesoporous organosilicas (PMOs)

Sample	BET surface area (m²/g)	Total pore volume (cm³/g)	Pore diameter^a (Å)
PMO	1252.1	0.851	26.5
1N10PMO	1176.0	0.723	26.0
1N25PMO	1095.5	0.611	23.5
1N40PMO	1086.5	0.601	21.5
2N10PMO	1122.5	0.735	25.5
2N25PMO	1086.1	0.682	25.3
2N40PMO	963.5	0.581	20.5
3N10PMO	1230.3	0.652	23.5
3N25PMO	1188.1	0.601	20.5
3N40PMO	1037.4	0.524	18.5

materials provided evidence that the pores were filled with organic molecules which were dispersed uniformly throughout the pores.

The result of BET surface area in table 3 showed that SBA-15 has larger surface area than A-SBA-15, GO-A-SBA-15, and A-GO-A-SBA-15. It might be caused by the damage of silicate structure after modification with amine group on pristine SBA-15 and some structure was covered by GO in GO-A-SBA-15. Similarly, pore volume was decrease after functionalized amine group and modified with GO following the order; SBA-15 > A-SBA-15 > GO-A-SBA-15 > A-GO-A-SBA-15. Whereas, pore size distribution of A-GO-A-SBA-15 was more than A-SBA-15, GO-A-SBA-15, and SBA-15 as shown in Figure 4.4. SBA-15 reported the smallest pore size. Owing to amine functionalized SBA-15, it might ruin the structure of SBA-15 and modification of GO might affect pore size distribution. According to the pore size of all synthesized adsorbents, CFA could access to the internal surface area, since molecular size of CFA (0.94 nm (9.4 Å)) are smaller than the pore size. However, NAP (64 nm (640 Å)) could be adsorbed only on external surface of the adsorbents (de Villiers et al., 2008; Nie et al., 2014).

Moreover, table 3 also shows the pore size, pore volume, and BET surface area of pristine HMS, grafted HMS, and GO modified HMS, which was typical of materials containing mesopores. The results show the BET surface area of HMS and grafted HMS followed the order: M-HMS

HMS > GO-A5M5 > A5M5 > A-HMS > GO-A-HMS whereas the decrease of pore volume and surface area of A-HMS could be detected. It can be concluded that hydrophilic functional group could be more grafting onto HMS surface.

Table 3 Physiochemical characteristic of SBA-15s, HMSs and graphene oxide modified mesoporous silicas

Adsorbents	Surface functional groups	Surface characteristic	BET surface area (m ² /g)	Pore volume (cc/g)	Pore diameter (Å)	pH PZC	%N
SBA-15	Silanol	Hydrophilic	734.77	1.2780	34.79	5.26	0.00
A-SBA-15	Amine and silanol	Hydrophilic	310.79	0.7421	47.76	9.60	3.53
GO	Carboxylic, epoxy, and hydroxyl	Hydrophobic	-	-	-	3.19	0.00
A-GO	Amine, carboxylic, epoxy, and hydroxyl	Hydrophilic	-	-	-	7.63	7.71
GO-A-SBA-15	Carboxylic, epoxy, hydroxyl, amine, and silanol	Hydrophobic	96.15	0.1957	40.70	9.24	3.13
A-GO-A-SBA-15	Amine, carboxylic, epoxy, hydroxyl, and silanol	Hydrophilic	72.84	0.1931	53.01	9.35	3.44
HMS	Silanol (-OH)	Hydrophilic	873.49	1.0620	24.32	5.3	-
A-HMS	Amino (-NH ₂)	Hydrophilic	52.32	0.2183	83.46	9.3	3.27
M-HMS	Mercapto (-SH)	Hydrophobic	1233.1	0.6828	11.07	5.6	-
A5M5	Amino and mercapto (-NH ₂ and -SH)	Hydrophilic	518.98	0.4743	18.28	8.5	1.77
GO-A-HMS	Epoxides, hydroxyl, ketones, and silanol (-OH)	Hydrophobic	49.85	0.2085	83.65	3.3	3.33
GO-A5M5	Epoxides, hydroxyl, ketones, and mercapto (-SH)	Hydrophobic	546.59	0.4903	17.94	8.8	1.76

Scanning electron microscopy (SEM) was applied to inspect surface appearance of all magnetic hexagonal mesoporous silicas (HMS-SPs) shown in figure 6. All material were spherical particles, when superparamagnetic particle (SP) were aggregated with mean diameters of 0.14 μm that were synthesized as the core-shell of the adsorbents. After the coated with pristine and functionalized hexagonal mesoporous silica the mean particle size in diameter were increased to

be the diameters range 0.15-0.39 μm . The larger size of M-HMS-SP than HMS-SP was caused by the thiol group on M-HMS-SP surface enhance the agglomerate adsorbent particle. However, these obtained results reveal the silica base surface coats the superparamagnetic core-shell of the adsorbents.

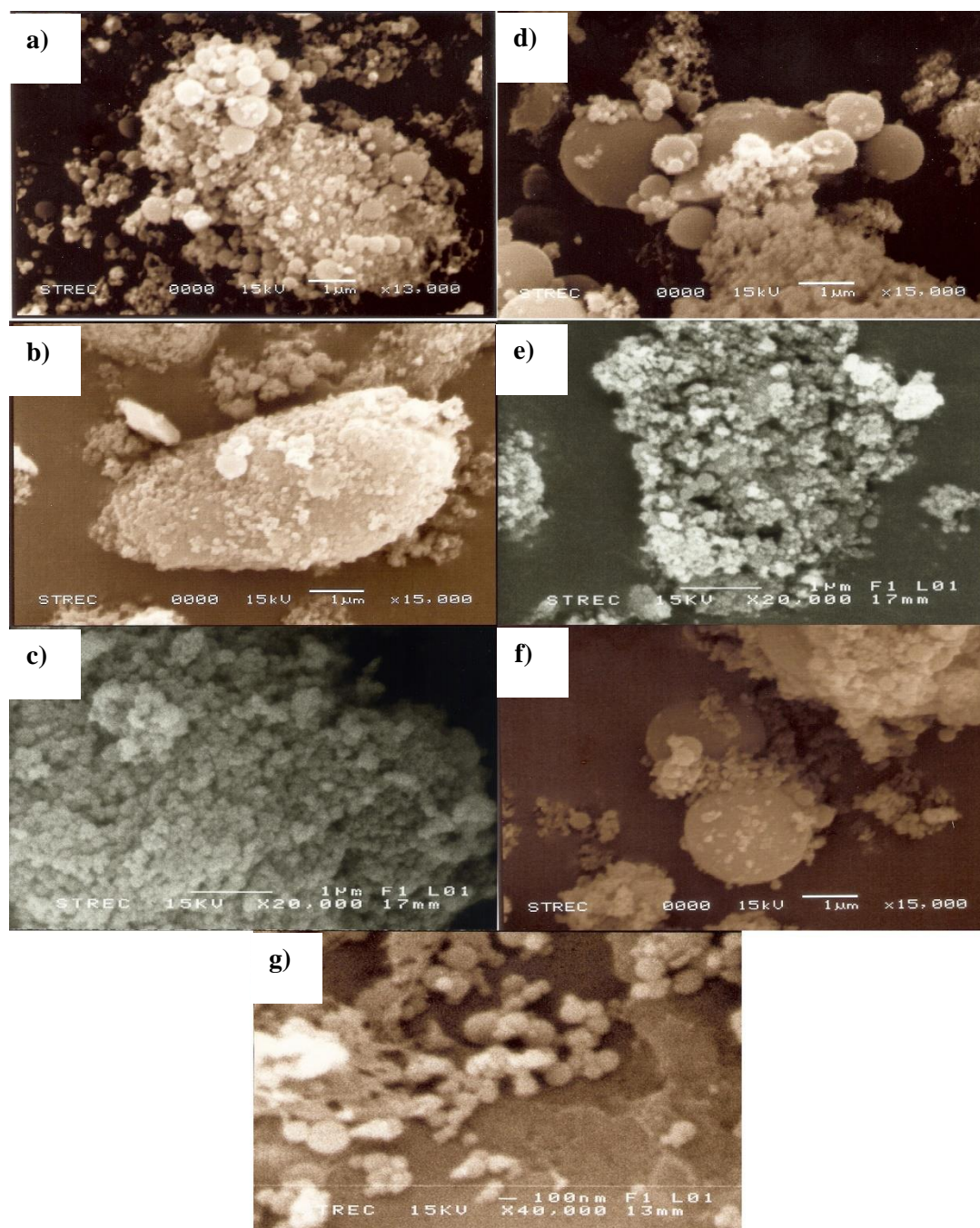


Figure 6 Representative SEM pictures of magnetic adsorbents a) HMS-SP, b) A-HMS-SP, c) N-HMS-SP, d) M-HMS-SP, e) P-HMS-SP, f) OD-HMS-SP, and g) magnetic particle (Fe_3O_4)

TEM microphotographs of PMO, 1N25PMO, 2N25PMO and 3N25PMO are shown in figure 7. The well ordered meso-structure of PMO and PMO derivatives was confirmed by TEM images. This was consistent with the results of nitrogen gas adsorption-desorption isotherms and x-ray diffraction patterns studies.

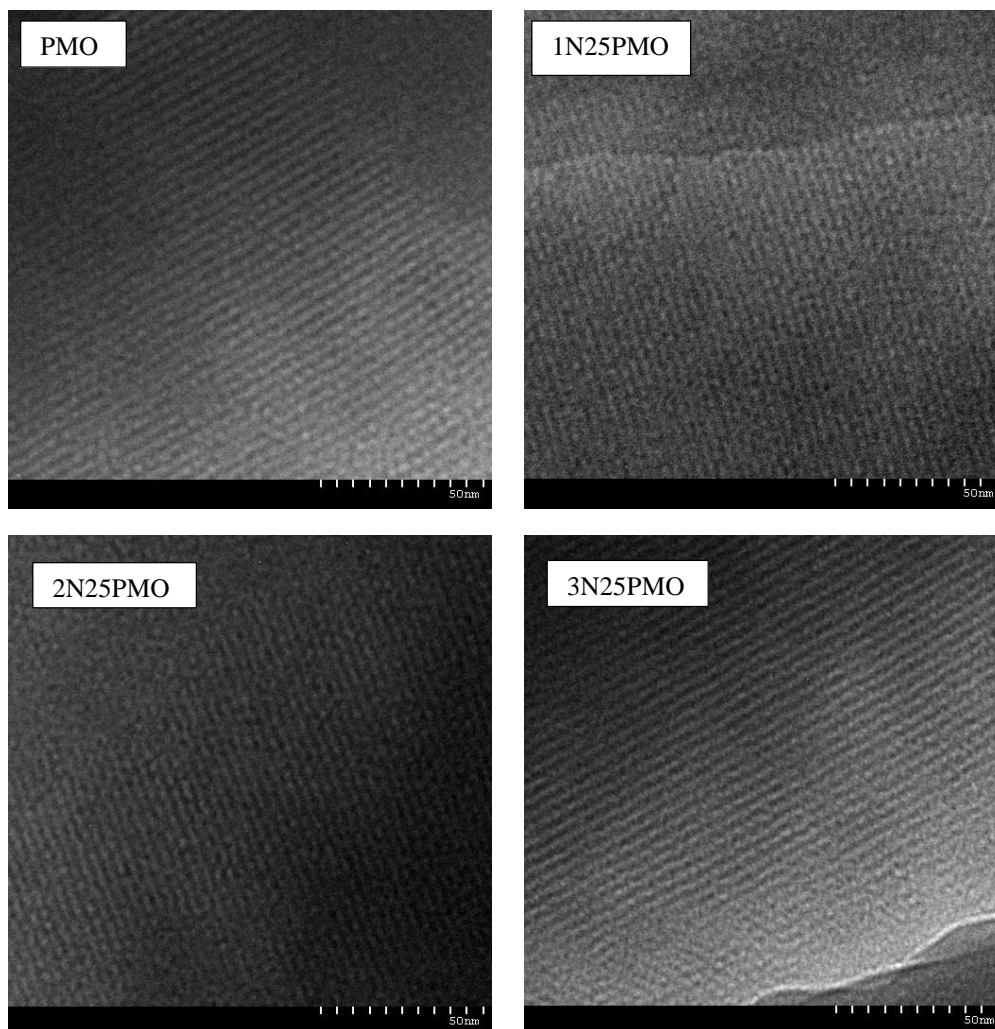


Figure 7 TEM microphotographs of PMO, 1N25PMO, 2N25PMO and 3N25PMO.

Figure 8 displays SEM and TEM images of GO and GO modified HMS. SEM and TEM images of GO shows the layer of GO nanosheets and the agglomeration on the surface. After combination, A-HMS and A5M5 particles were attached on the GO layer, as can be seen in the figure 8. The surface of GO is quite more transparent than individual GO sheets due to the dispersion during the synthesis process and the particle of A-HMS and A5M5 were wrapped up on GO flakes as quite the same porous structure.

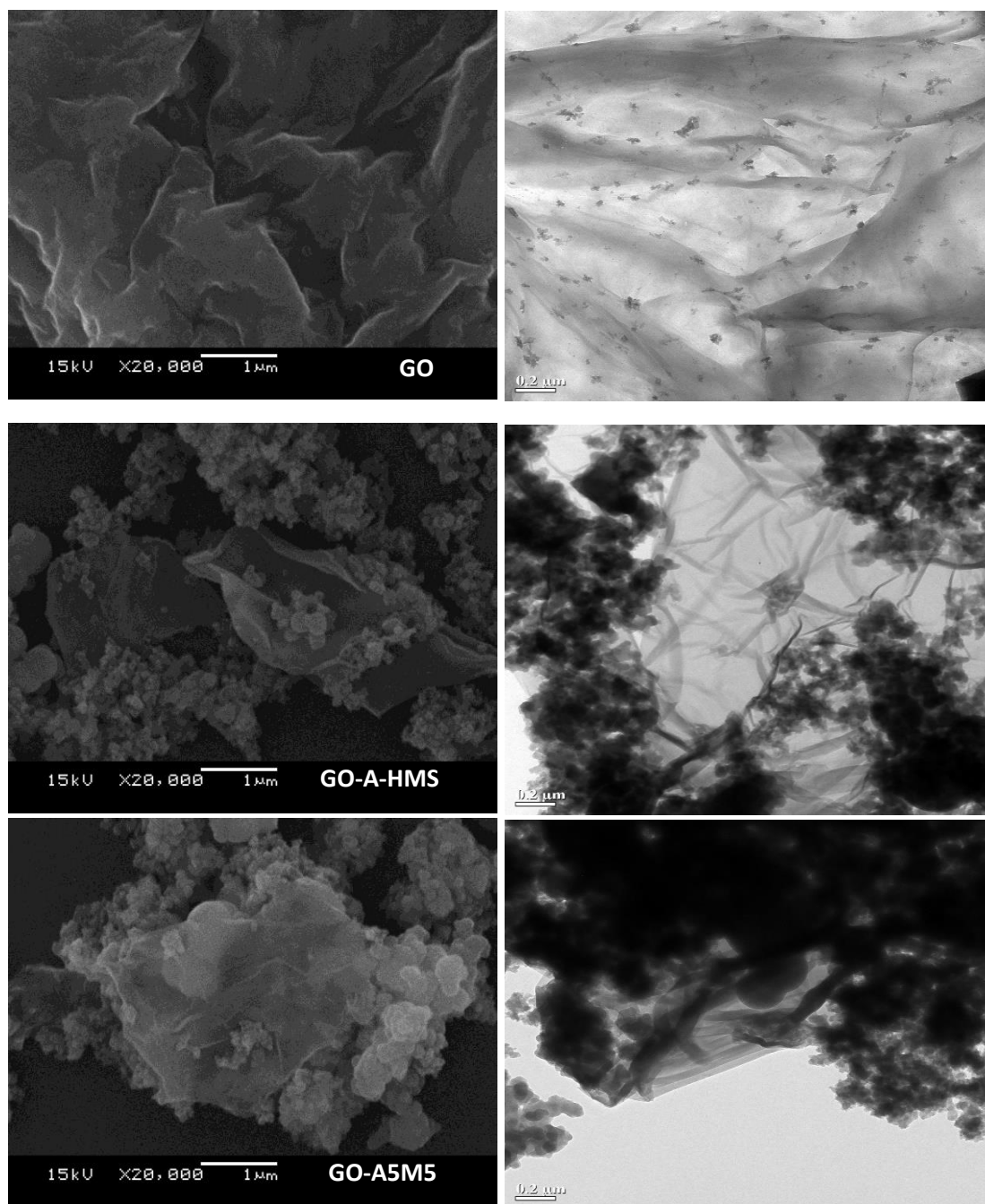


Figure 8 Representative SEM and TEM images of the GO, GO-A-HMS, and GO-A5M5 (x20000)

The internal morphologies of synthesized GO modified SBA-15s were also observed using transmission electron microscopy (TEM) as shown in figure 9. Synthesized SBA-15 presented the U-shaped which was indeed almost straight, indexing the high ordering of hexagonal mesoporous silica as figure 9a (Janssen et al., 2002). Additionally, the TEM image of GO reported the smooth sheet and also the aggregation of GO (as figure 9c). As showed in figure 9d, after functionalized amine functional group, A-GO was presented rough curled surface comparing with

GO. It might be caused by the H-bonding and hydrophilic interaction making A-GO sheet to be crumpling sheet (Yang et al., 2015). TEM image of GO-A-SBA-15 (figure 9e) illustrated the mixture of well ordering mesoporous silica of A-SBA-15 and smooth sheet of GO. Moreover, A-GO-A-SBA-15 TEM's image (figure 9f) showed the structure of A-SBA-15 encapsulated in curled surface of A-GO sheet.

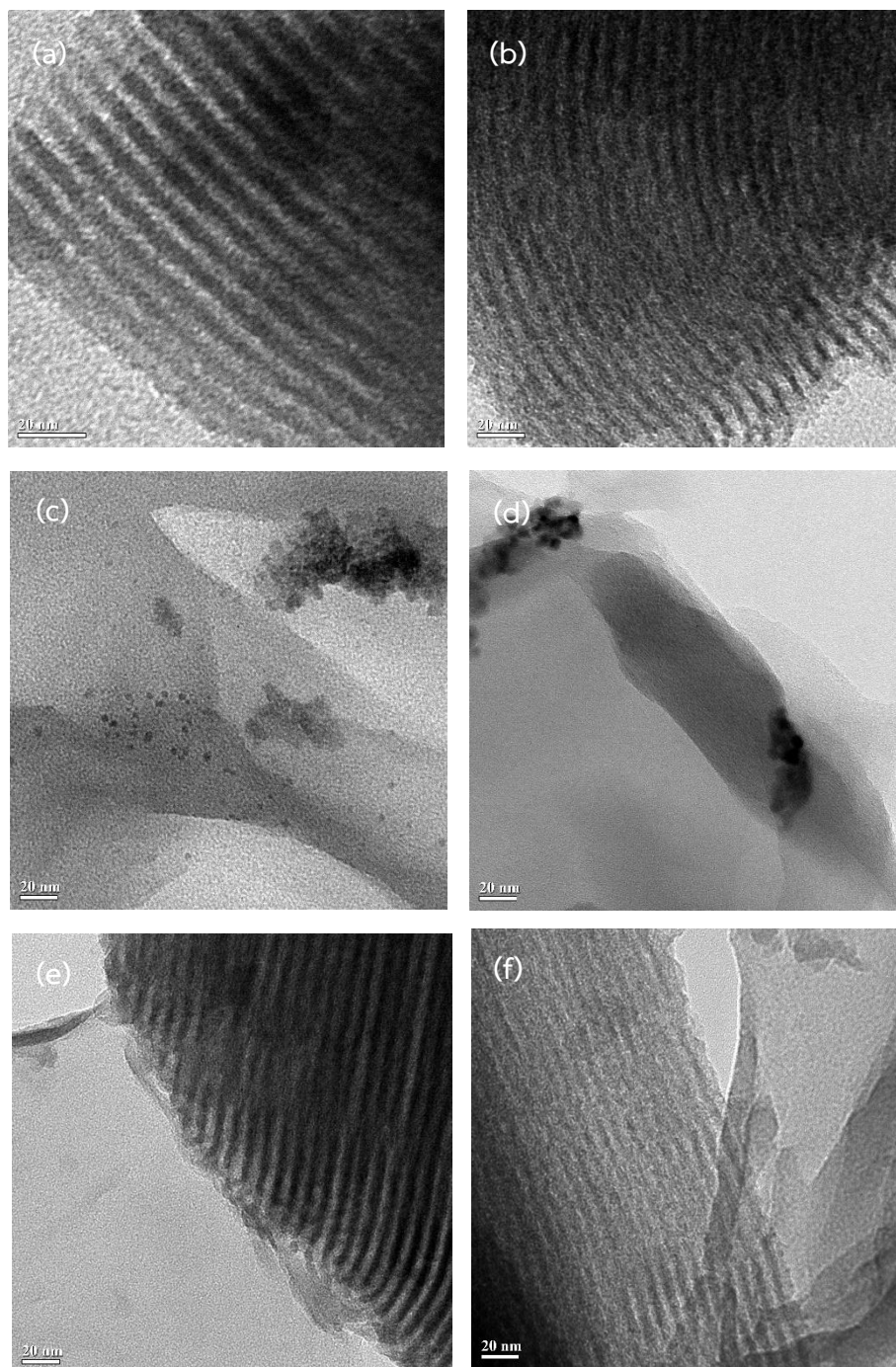


Figure 9 TEM images of a) SBA-15, b) A-SBA-15, c) GO, d) A-GO, e) GO-A-SBA-15, and f) A-GO-A-SBA-15

Elemental composites on surface of A-GO-A-SBA-15 were measured by X-ray photoelectron spectroscopy (XPS) as shown in figure 10. A-GO-A-SBA-15 showed the bond of C-C, C-N, C-O-C of epoxy group, C-O, and O-C=O at 284.6, 285.6, 286.5, 287.2 and 288.3 eV, respectively, in C1S, as well as NH and NH₂ (in N1S) at 397.9 and 399.4 eV, respectively. This could not be discussed the successful modification of amine functional group on GO-A-SBA-15 (Huang et al., 2011; Lai et al., 2011; Pulido et al., 2012; Yang et al., 2015).

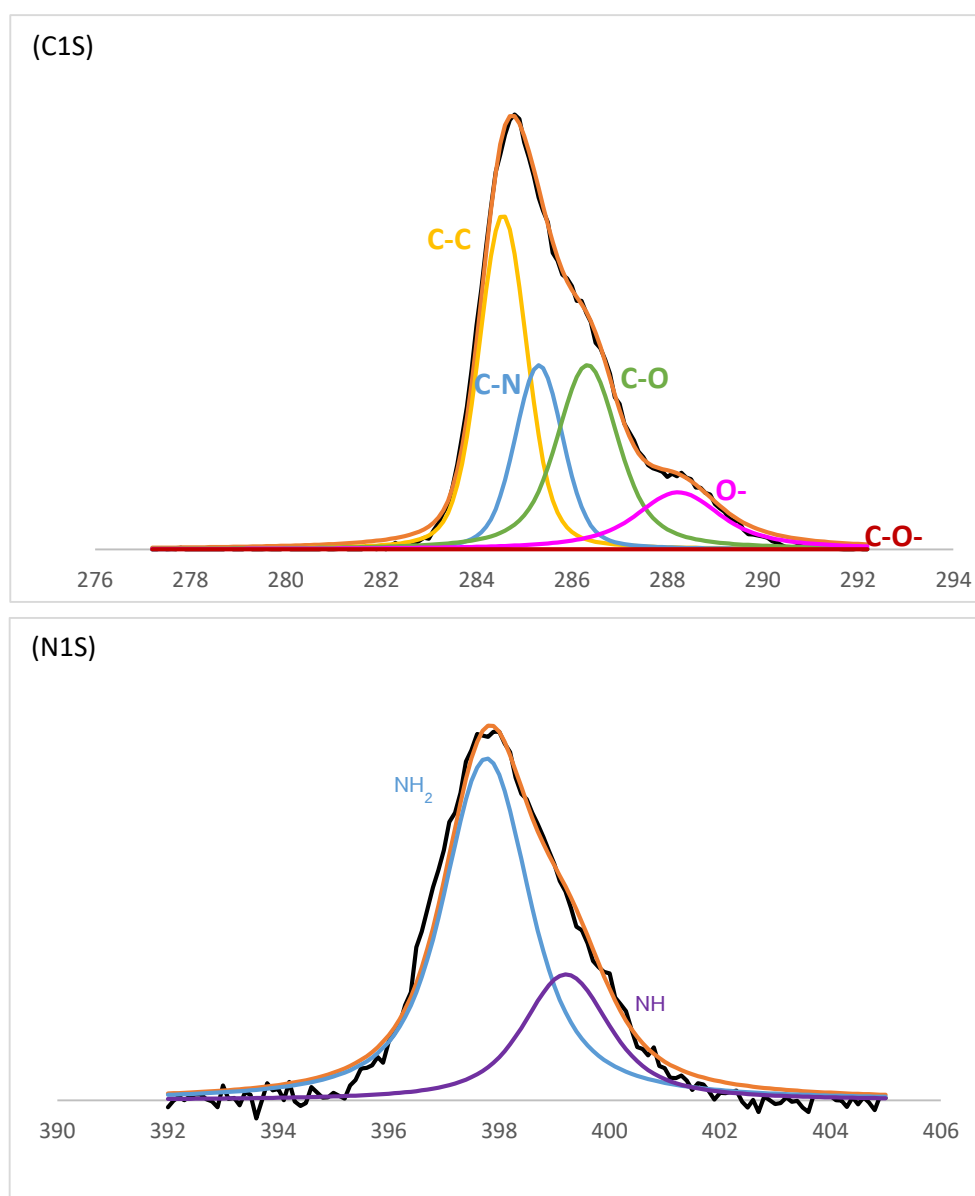


Figure 10 XPS spectra of A-GO-A-SBA-15

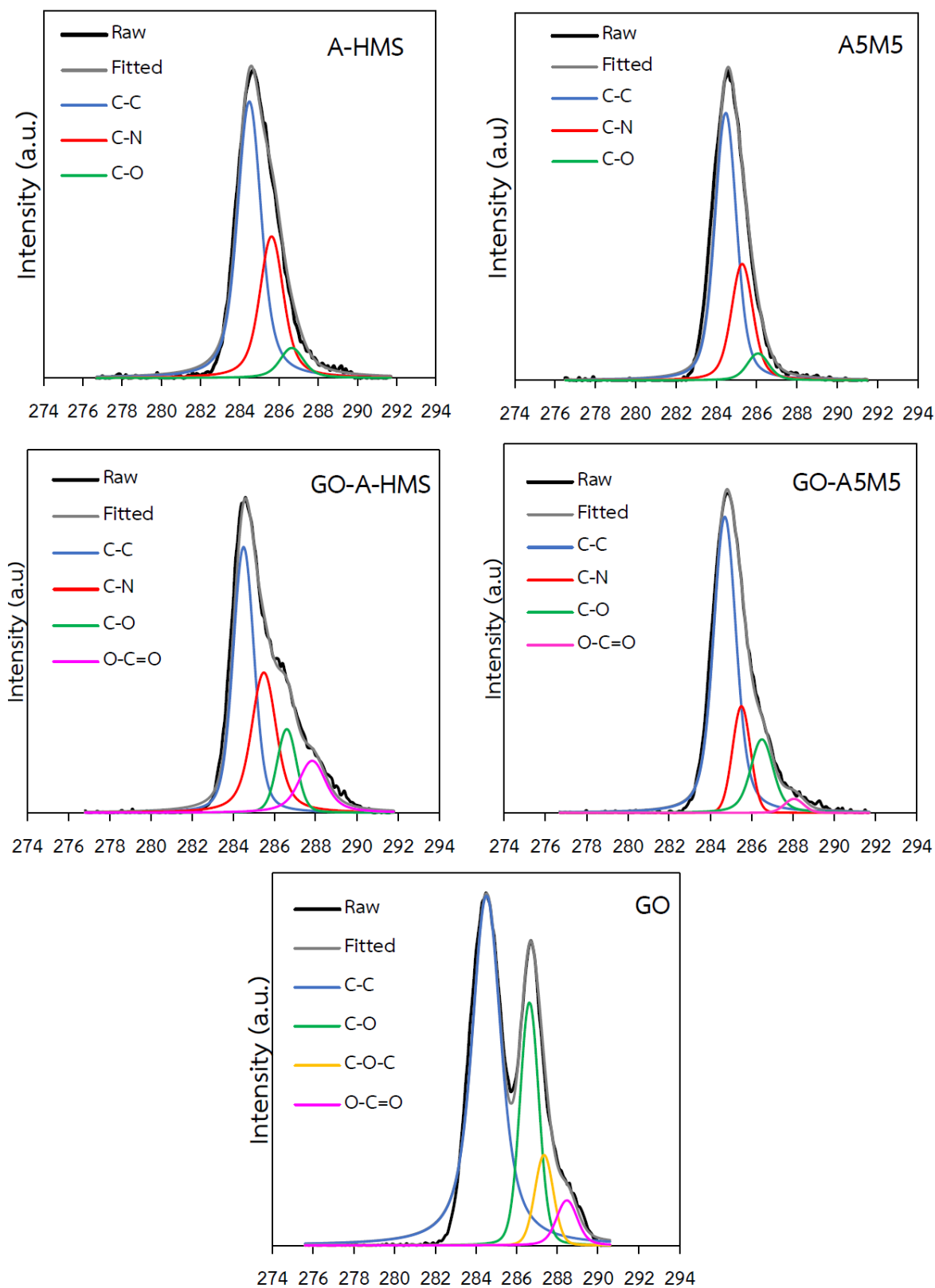


Figure 11 Representative XPS spectra C1s of A-HMS, A5M5, GO-A-HMS, GO-A5M5, and GO

Figure 11 shows XPS spectra of A-HMS, A5M5, GO-A-HMS, GO-A5M5, and GO in term of C 1s using X-ray photoelectron spectroscopy. It can be seen A-HMS and A5M5 contained C-C, C-N, and C-O at 284.6, 285.4, and 286.3 eV, respectively. In case of GO, the bond included C-C, C-O-C, C-O, and O-C=O at 284.6, 286.2, 286.3, and 288.2 eV, respectively. For GO-A-HMS, the bonds of C-C, C-O, O-C=O and C-N at 284.6, 286.3, 288.2, and 285.6 eV, respectively, were observed. It can be conclude that GO was chemical bonded with HMS due to C-N bond (Yang et al., 2015).

Adsorption kinetic

Adsorption kinetic information is the important data to calculate uptake rate, and to identify the rate-controlling parameters for adsorption process. Obtained adsorption rate and equilibrium time can be used to suggest the possible diffusion mechanism by comparing between the physico-chemical characteristics of synthesized adsorbents and diffusion rates. Since the synthesized adsorbents were mostly the porous material, the overall adsorption rate mainly involves in two steps such as film diffusion, and intraparticle diffusion.

HMS-SPs versus antibiotics (at ppb level)

Fluoroquinolone (Ciprofloxacin (CIP), and Nalidixic acid (NAL) and sulfonamide (Sulfamethoxazole (SMX)) were selected to be the antibiotic models in this study. According to their physico-chemical properties, CIP was reported to have high water solubility and highly interaction compound, while SMX was characterized as a low reactive antibiotic. Furthermore, the smaller molecular size of nalidixic acid (NAL) was evaluated the adsorption kinetic parameter comparing with both CIP and SMX to identify their internal diffusion rate affected by the molecular size. Adsorption kinetics of three antibiotics onto pristine-HMS-SP and functionalized-HMS-SPs were evaluated and expressed in figure 12. Their concentration decreased gradually in the first 15 min, and then the equilibrium stages were reached after approximately 30 min on all synthesized adsorbents. Both pseudo-first-order and pseudo-second-order adsorption kinetics model were determined; however, the experimental data was well-fitted with the pseudo-second-order kinetic model (data was not shown). Thus, a pseudo-second-order rate model could be used to describe their adsorption kinetics.

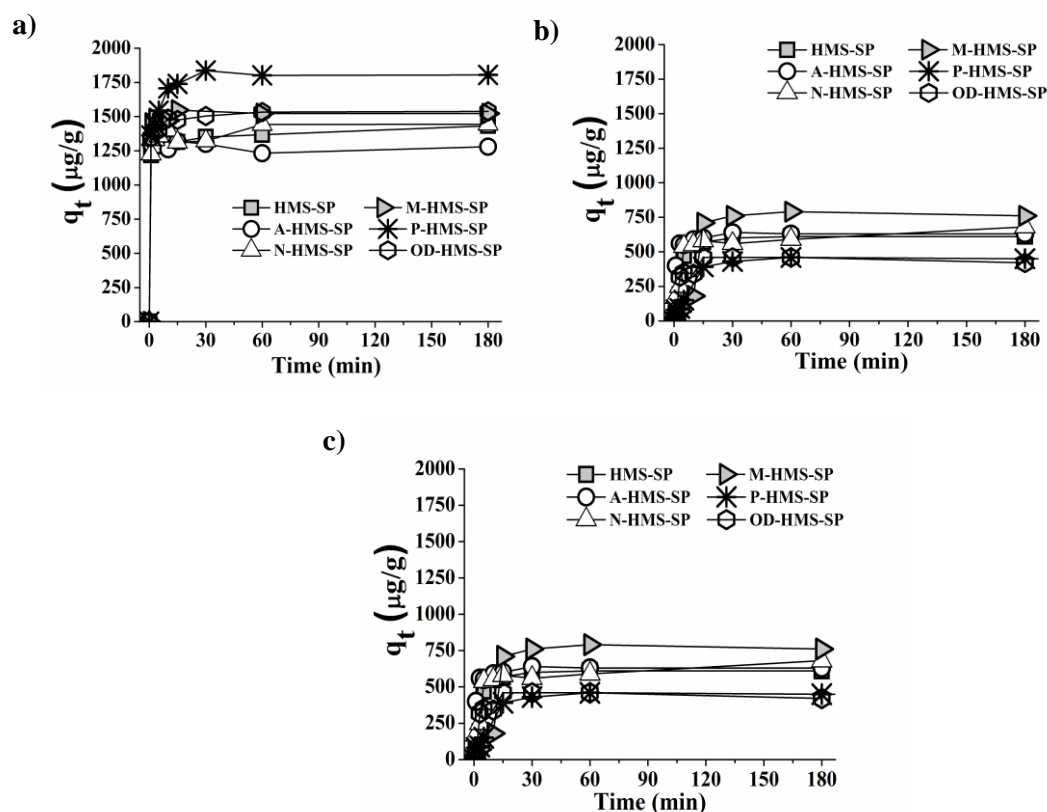


Figure 12 Adsorption kinetics of CIP (a), NAL (b), and SMX (c) by pristine HMS-SP and functionalized HMS-SPs at $250 \mu\text{g L}^{-1}$ (pH 7 and IS 0.01 M).

PMOs versus clofibric acid (CFA) at (ppb level)

The kinetics of CFA adsorption are shown in figure 13. For all PMOs, the concentration of CFA in the solution decreased rapidly in the first 30 min and then gradually decreased thereafter until they reached equilibrium within 4 h. The adsorption of CFA onto the PMOS is most likely represented by pseudo-second-order kinetics (data was not shown). The initial adsorption rates (h) of virgin PMO and PMOs functionalized with 1N-silane were found to range from $2.18 \mu\text{g/g.min}$ to $8.14 \mu\text{g/g.min}$. Virgin PMO has the lowest h value. The h values of the adsorbents seemed to increase as the amount of added n-silane was increased. The half-life values ($t_{1/2}$) of these adsorbents seemed to decrease when the concentration of added n-silane was increased. The functionalized PMOs (1N10PMO, 1N25PMO and 1N40PMO) had lower half-life values ($t_{1/2}$) than the virgin PMO. The same pattern of relationship between the initial adsorption rate and the concentration of added silane was also found in PMOs functionalized with 2N-silane and

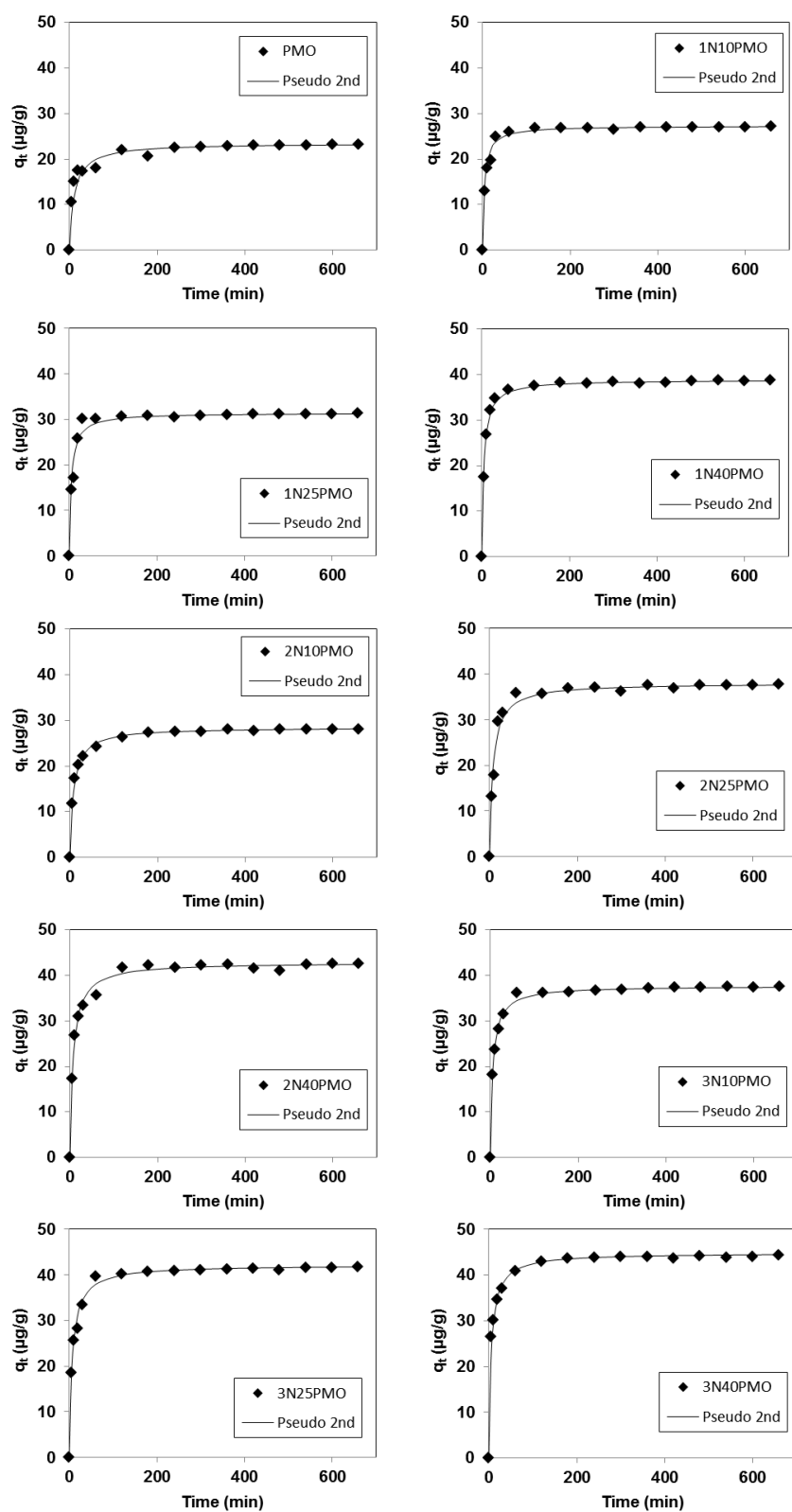


Figure 13 Adsorption kinetics of CFA adsorbed onto different kinds of mesoporous silicates (pH 7, 25 °C and IS 0.01M).

3N-silane. The initial adsorption rates and half-life values of the adsorbents had no relationship with the types of the added functional groups. The results of this study suggested that the surface functional groups of the adsorbent had an effect on the adsorption process. The surface modification with 1N-amine, 2N-amine and 3N-amine functional groups improved the adsorption ability of the silica based porous materials.

GO modified SBA-15s versus clofibric acid (CFA) at (ppm level)

CFA adsorption kinetic of SBA-15, A-SBA-15, GO, A-GO, GO-A-SBA-15, A-GO-A-SBA-15, comparing with PAC showed the same equilibrium time that was a few minutes (figure 14). At the beginning of all kinetic experiments, the concentration of CFA was dramatically decreased (CFA adsorption capacity was increased). Whereas, all adsorbents had different surface such as smooth sheet of GO, porous silica of SBA-15, complex surface functional group of PAC, these factors did not affect the adsorption kinetic of CFA. Moreover, adsorption kinetic of all synthesized adsorbents showed the best correlation coefficient value of R^2 on the pseudo-second order model (data was not shown). The initial rate adsorption (h) of all adsorbents was investigated from the calculation of the pseudo-second order model as ordering; PAC > GO > GO-A-SBA-15 > A-GO-A-SBA-15 > A-GO > SBA-15 > A-SBA-15. It can be seen that the initial rate adsorptions of amine surface functional group adsorbents were less than pristine adsorbents. It could be summarized that complexity of surface structure might decrease the initial rate of adsorption due to steric effect of surface functional groups (except PAC).

GO modified HMSs versus ciprofloxacin (CIP) at (ppm level)

In case of GO modified HMSs, the concentration of CIP decreased in the first 30 minutes and then achieved the equilibrium stage at approximately 6 hours as shown in Figure 15. The higher equilibrium time of GO-A-HMS and GO-A5M5 could be the results of the presence of GO on the materials. Considering the pseudo-second-order kinetic parameters by comparison on the initial adsorption rate (h), the initial adsorption rate of CIP decreased followed the order of GO < GO-A-HMS < GO-A5M5 < M-HMS < A5M5 < HMS < A-HMS (data was not shown). Moreover, the experimental data were plotted between q_t versus $t^{0.5}$ (data was not shown). The intraparticle plot could exhibit a multi-linearity pattern of three steps in the adsorption process. From comparison among each slope of multi-linearity, the rate limiting step for CIP adsorption on all adsorbents were controlled by intraparticle diffusion, and also related to low porosity of the

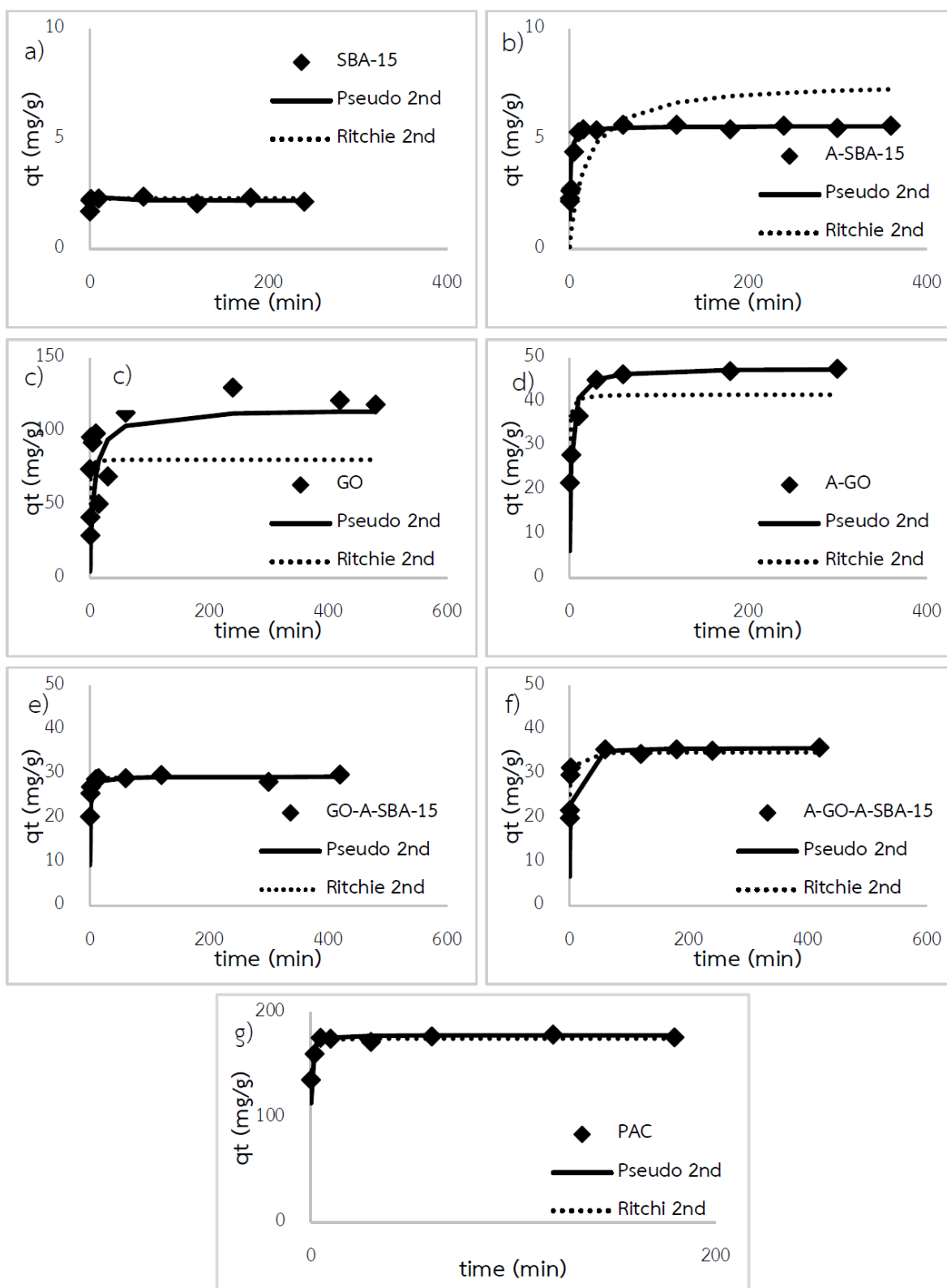


Figure 14 The kinetic curves of CFA on a) SBA-15, b) A-SBA-15, c) GO, d) A-GO, e) GO-A-SBA-15, f) A-GO-A-SBA-15, and g) PAC

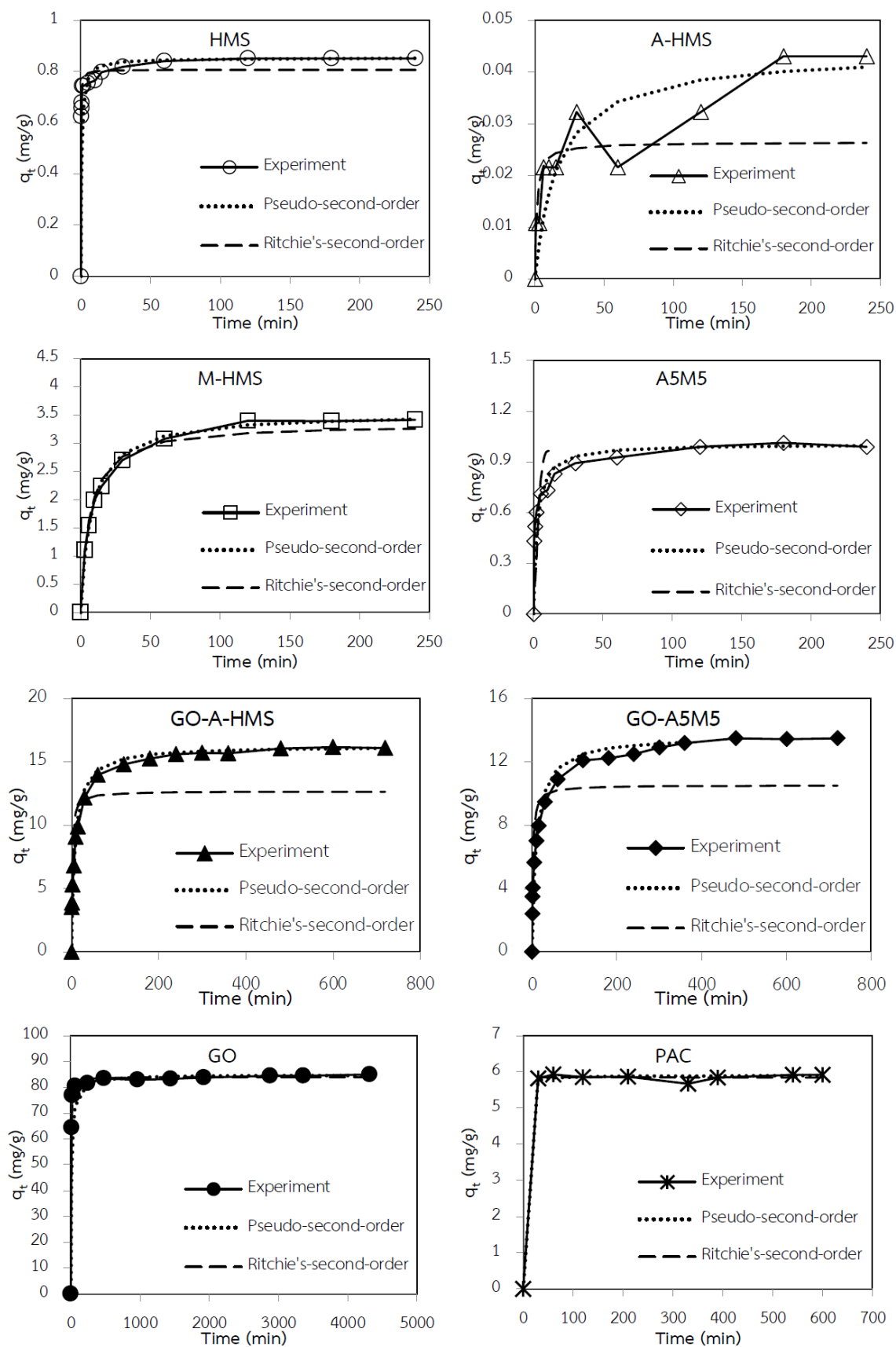


Figure 15 Adsorption kinetics of CIP on the synthesized adsorbents and PAC

adsorbents. Except for A-HMS, the film diffusion was limited by a high hydrophilic surface of A-HMS.

Porous silicas versus haloacetonitriles (HANs)

The kinetic curves of the dichloroacetonitril (DCAN) adsorption on the porous materials, as plot of the relative adsorption capacity (q_t) versus time, are shown in figure 16. The DCAN uptake by all four adsorbents (HMS, Ti-HMS, SBA-15 and NaY) was rapid at the beginning (within the first 4 h) and reached the equilibrium stage after ca. 18 hr. However, the amount of adsorbed DCAN (q_t) varied between the adsorbents being highest for HMS followed by NaY > Ti-HMS > SBA-15. To describe the adsorption phenomena, the adsorption kinetics were modeled using several mathematical expressions. The experimental data were fitted with the pseudo-first order and pseudo-second order equations. For all four adsorbents the pseudo-second order model gave a better fit to the data, as defined by the higher R^2 than the pseudo-first order model.

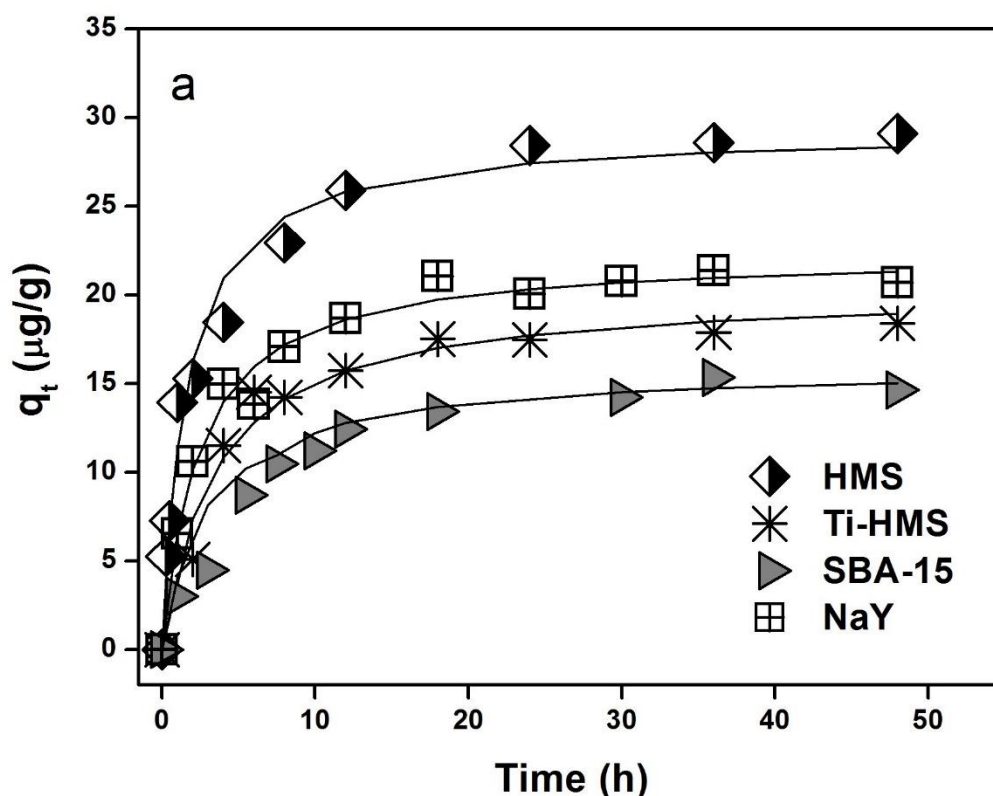


Figure 16 DCAN adsorption kinetics of HMS, Ti-HMS, SBA-15 and NaY at 100 µg/L at pH solution of 7 (ionic strength of 10 mM). Solid lines present the data derived from the pseudo-second-order kinetic model.

Adsorption isotherms

Information of equilibrium adsorption can be used to investigate the nature of adsorption phenomena which can be applied for the further design and optimization of adsorption treatment process. The main objective of all experiments in this part was to investigate the adsorption mechanism and predominant factors controlling the adsorption of three selected pollutants, such as CIP, NAL, SMX, CFA and haloacetonitriles onto the studied adsorbents.

HMS-SPs versus antibiotics (at ppb level)

To neglect the effect of the surface area of adsorbents, the specific adsorption capacities of each antibiotic per square meter was shown in figure 17. As seen in figure 17 (a), the CIP adsorption isotherms of the hydrophobic adsorbents (P-HMS-SP~OD-HMS-SP>M-HMS-SP) had higher adsorption capacities per square meter than the hydrophilic ones at pH 7.0. Among hydrophobic adsorbents, P-HMS-SP had the highest adsorption capacity per specific area without relying on the contact angle value (OD-HMS-SP>P-HMS-SP>M-HMS-SP). That might be caused by the dispersive interaction between the π electrons in the aromatic ring of CIP and phenyl group on the surface of P-HMS-SP or the interaction between the π electrons in phenyl group and free electrons in CIP molecule (Carabineiro et al., 2011). Therefore, it can be suggested that a combination between the hydrophobicity via van der Waals interaction and π - π electron-donor-acceptors interaction were the main CIP adsorption interaction.

Nevertheless, it could be seen that A-HMS-SP provided similar adsorption capacity per square meter to the hydrophobic adsorbents. This might be caused by a combination between attractive electrostatic interaction and hydrogen bonding. At pH 7, A-HMS-SP has a strong positive surface charge density compared with other synthesized adsorbents which might interact with negative part of zwitterionic molecule of CIP.

As same as CIP adsorption condition, the order of NAL adsorption capacities per specific area was shown in figure. 17(b) in order as following: A-HMS-SP>OD-HMS-SP>>P-HMS-SP>M-HMS-SP~N-HMS-SP~HMS-SP. As reveal in these results, the higher hydrophobic surface had a higher adsorption capacity than hydrophilic one. These results were suggesting that the competitive adsorption between water and NAL onto the adsorbent surface might probably reduced by the hydrophobic functional surface (Prarat et al., 2011). However, A-HMS-SP has the highest adsorption capacity per specific area; hence the hydrogen bonding between the hydroxyl-, and/or ketone-group of NAL and amine group of A-HMS-SP is expected to be the key role in

the adsorption mechanism. Nevertheless, adsorption mechanisms of various similar antibiotic molecular structures to NAL on carbonaceous adsorbents have been proposed that the electrostatic interaction seem to play important roles in their adsorption by previous literatures (Carabineiro et al., 2011; Carabineiro et al., 2012). Thereby, the NAL adsorption mechanism has further investigated the electrostatic interaction under the pH function.

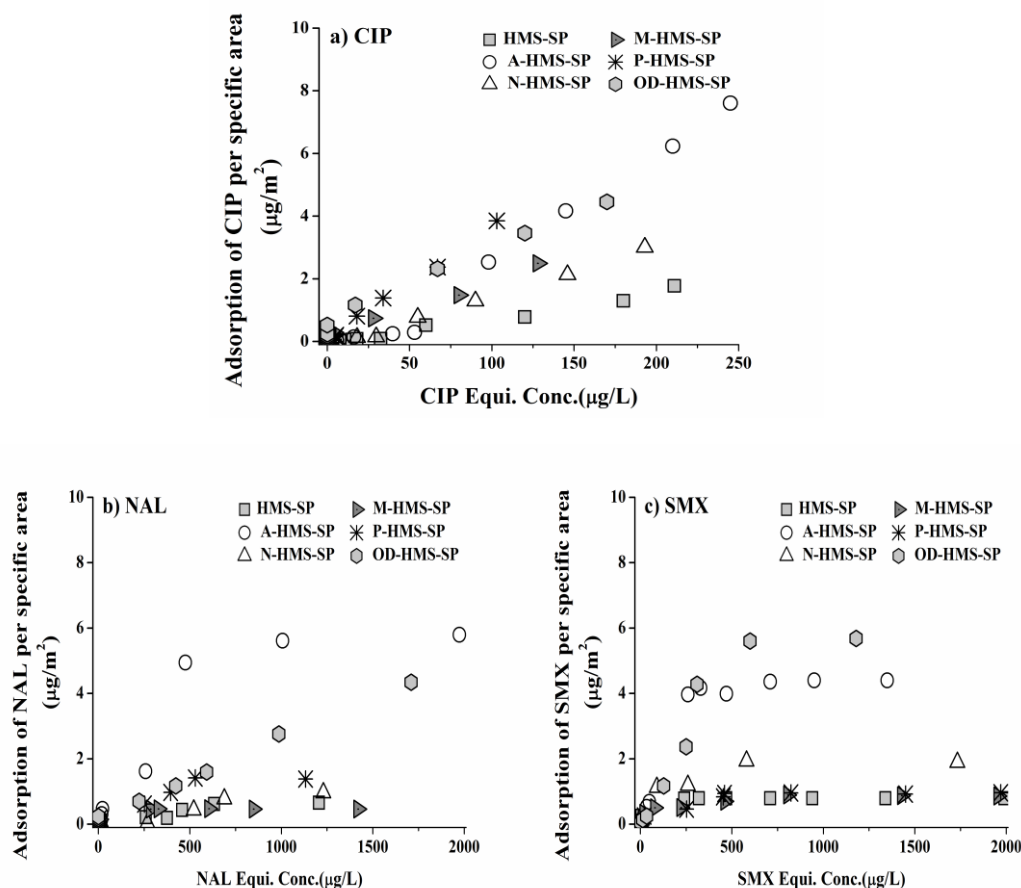


Figure 17 Effect of organo-functional group on adsorbent surface onto adsorption capacities per specific surface area of (a) CIP, (b) NAL, and (c) SMX at pH 7 with IS 0.01 M phosphate buffer (25 °C).

Additionally, the adsorption isotherms of SMX (figure 17(c)) showed adsorption capacity per specific area followed the sequence OD-HMS-SP>A-HMS-SP>>N-HMS-SP>M-HMS-SP~P-HMS-SP~HMS-SP, respectively. As the obtained results, the increased hydrophilicity of adsorbents can be enhanced the adsorption capacity per specific area of SMX except OD-HMS-SP and HMS-SP. According to HMS-SP, the highest hydrophilic adsorbent, it has the lowest adsorption capacity per specific area which contrasting with the other high hydrophilic one. This might be

caused by the competitive adsorption between water and SMX with silanol group surface. Due to the silanol surface might be surrounded with water molecules hence it was no free for SMX adsorption. When the hydrogen bonding might be occurred between the functional group of SMX and residual silanol groups (non-grafted silanol) on the OD-HMS-SP surface also. Therefore, hydrogen bonding was supposed to be the main interaction for SMX adsorption onto the synthesized adsorbents

PMOs versus clofibric acid (CFA) at (ppb level)

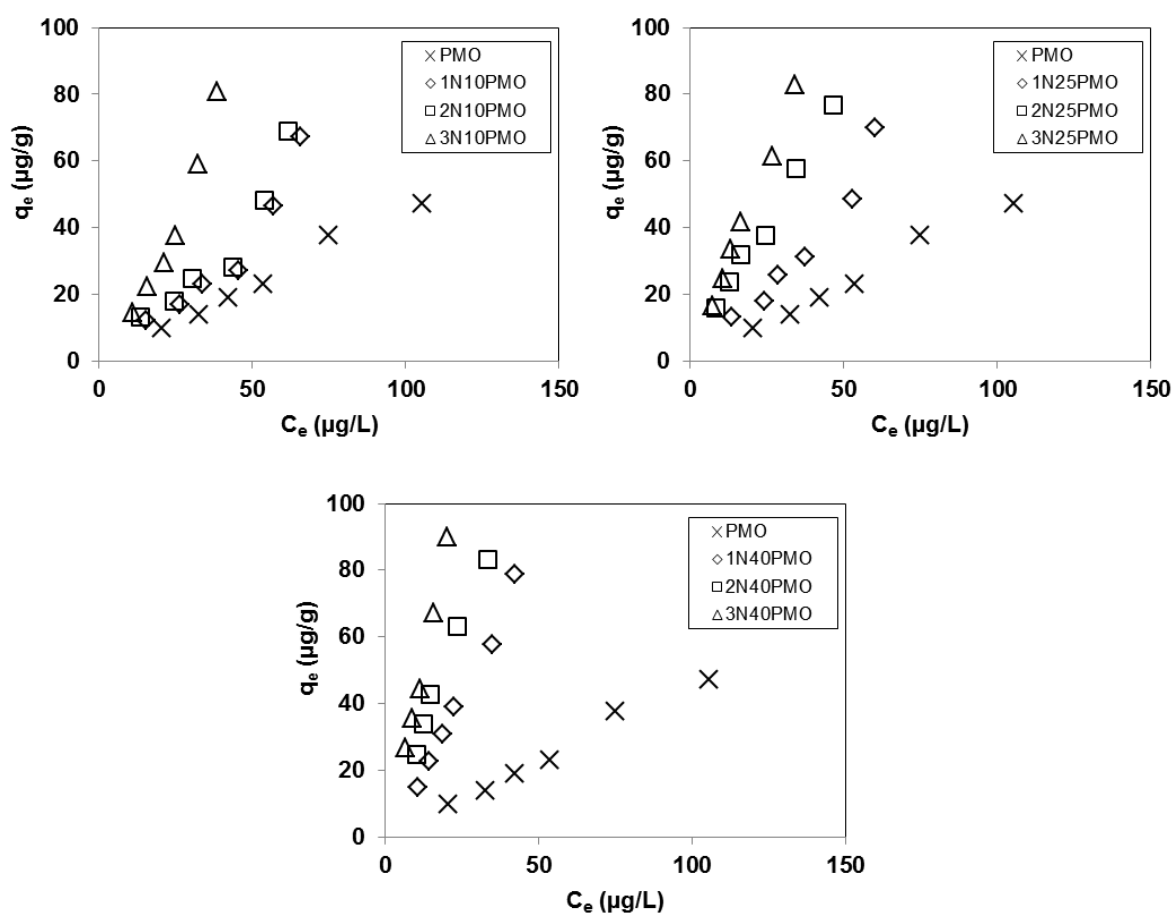


Figure 18 Adsorption capacity of PMOs with different functional groups (pH 7, 25 °C and IS 0.01M).

The adsorption capacity of PMO and the functionalized PMO adsorbents at pH 7 are shown in figure 18. Analysis of that for PMO and the functionalized derivatives allows the effect of different surface functional groups, hydroxyl (silanol), 1N-amine, 2N-amine and 3N-amine, on the adsorption capacity of the adsorbents to be inferred.

For adsorption of CFA, there are three possible mechanisms for their adsorption onto PMO and the functionalized PMO derivatives. The first mechanism is electrostatic interaction (by Coulomb's law) between the deprotonated CFA molecules and the surface charges of the adsorbents. The second mechanism is hydrogen bonding, a form of dipole-dipole interaction, and the third mechanism is hydrophobic interactions such as Van der Waals interaction, π - π electron acceptor-donor, etc. In this study, the adsorption capacities of functionalized PMOs were found to be higher than the virgin PMO. At pH 7 CFA's molecules have negative charges. The molecules of PMO, 1N10PMO, 1N25PMO, 2N10PMO and 3N10PMO also have net negative surface charges, but the molecules of the rest of functionalized PMOs have net positive surface charges (See Table 6.5). The enhancement of the adsorption of CFA onto the adsorbents which have positive surface charges (i.e. 1N40PMO, 2N25PMO, 2N40PMO, 3N25PMO and 3N40PMO) could be explained by the electrostatic interaction between the CFA's and the adsorbent's molecules. From the measurement in this study, PMO was found to have a zeta potential of -8.46 mv. Compared with all other adsorbents, PMO has the highest negative surface charges. The electrostatic repulsion between the adsorbent's and CFA's molecules is therefore highest when the adsorbent is PMO. The enhancement of the adsorption of CFA after surface modification of the adsorbents having negative surface charge (1N10PMO, 1N25PMO, 2N10PMO and 3N10PMO) could therefore be explained by the reduction in electrostatic repulsion. The increase in adsorption capacity of functionalized PMOs after modification with 1N-amine, 2N-amine or 3N-amine functional groups could be explained by either the enhancement of the electrostatic interaction or the reduction of the electrostatic repulsion between the CFA's and adsorbent's molecules.

The adsorption capacities of the adsorbents for CFA were ranked (highest to lowest adsorption capacity) as 3NPMOs > 2NPMOs > 1NPMOs > PMO. This could be explained by the electrostatic interaction. The zeta potential of the adsorbents functionalized with the different types (but same concentration) of organosilane was different. The zeta potentials of the adsorbents functionalized with different types of organosilane were ranked (highest to lowest) as 3NPMOs > 2NPMOs > 1NPMOs. This might be related to the differences in length and amount of nitrogen contents of the functional groups which were dispersed at the adsorbents surface. The zeta potential of the extracted 3NPMOs samples was higher than the extracted 1NPMOs and 2NPMOs samples because 3N-amine functional group is longer and contains higher amount of nitrogen content than 1N-amine and 2N-amine functional groups. The adsorption capacity of 3NPMOs was highest because their zeta potential was highest, or in other words higher than 2NPMOs and

1NPMOs. So it could be concluded that the adsorption capacity of the functionalized PMOs was affected by the type of added amine functional groups (i.e. 1N-amine, 2N-amine or 3N-amine).

GO modified SBA-15s versus clofibric acid (CFA) at (ppm level)

Adsorption isotherms on GO-A-SBA-15 and A-GO-A-SBA-15 were shown in figure 19. The adsorption capacity of GO-A-SBA-15 was reported around 29 mg/g at the equilibrium concentration 10 ppm. The main factors might be π - π interaction, hydrophilicity, H-bonding, and electrostatic attraction between negative charge of CFA and positive charge on the surface of GO-A-SBA-15. Moreover, adsorption of CFA on GO-A-SBA-15 was reported the best correlation coefficient value of R^2 on Linear isotherm model which always occurs in the beginning part of many adsorption isotherms.

After modification of amine functional group, the adsorption capacity of A-GO-SBA-15 was slightly increase to 35 mg/g at equilibrium concentration 10 ppm. As a result of adsorption isotherm, Langmuir isotherm model showed the best fit with adsorption of CFA on A-GO-A-SBA-15 meaning that the adsorption was monolayer. The obtained results showed the opposite trend comparing with the data set of GO and A-GO. The presence of amine group on A-GO attached on A-SBA-15 (A-GO-A-SBA-15) did not reduce the CFA adsorption capacity. It can be suggested that after fixing printine GO sheet on A-SBA-15, GO could not move freely or hardly move so that the intra-interaction of double amine functional group of Diethylenetriamine on GO surface might rarely occurred in A-GO-A-SBA-15 case.

Thus amine functional group on A-GO-A-SBA-15 could increase adsorption capacity of CFA due to π - π interaction, hydrophilicity, H-bonding, and electrostatic attraction between amine functional group and CFA.

Interestingly, when comparing the adsorption capacity of pure GO and GO-A-SBA-15 which were 117 and 29 mg/g at the equilibrium concentration 10 ppm, respectively. The obtained results showed the significant difference adsorption capacity between both adsorbents. The percentage of GO in pure GO was 100% and the percentage of GO in GO-A-SBA-15 was 12.44%. After calculation of CFA adsorption capacity of GO 12.44% from pure GO and from GO-A-SBA-15, the approximately capacitivities were showed at 14.5 mg/g and 18.3 mg/g, respectively. The CFA adsorption capacity GO on GO-A-SBA-15 at the same percentage of pure GO was exhibited the

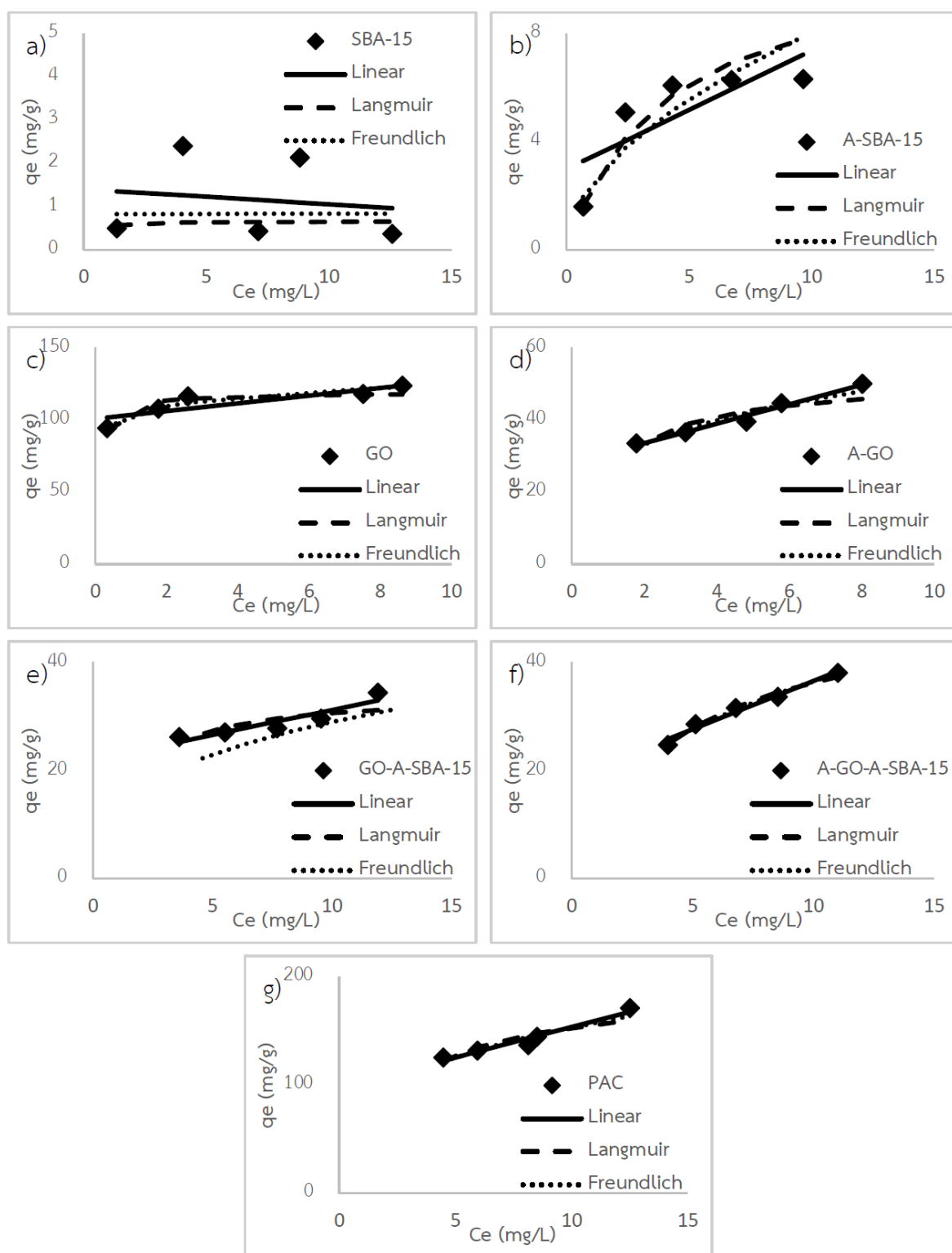


Figure 19 The adsorption isotherm of CFA on a) SBA-15, b) A-SBA-15, c) GO, d) A-GO, e) GO-A-SBA-15, f) A-GO-A-SBA-15, and g) PAC

higher than pristine GO. One possible discussion might be the agglomeration of pure (or pristine) GO. Therefore, the results of GO and GO-A-SBA-15 were reasonable when discussion in the quantitative analysis of GO.

Nevertheless, the comparison between A-GO and A-GO-A-SBA-15 did not follow the quantitative analysis as the series of A-GO like discussed above. It might relate to the folding phenomena of A-GO, which did not occur when double amine functional group of Diethylenetriamine was attached on GO-A-SBA-15 surface. Hence, if we compare the effect of A-GO on A-GO-SBA-15 with the same ratio of pristine GO, the approximately same level of CFA adsorption capacity of A-GO ratio (on A-GO-SBA-15) and pure GO ratio can be detected. Moreover, the effect of amine functional group might be increase adsorption capacity of CFA on A-GO-A-SBA-15.

GO modified HMSs versus ciprofloxacin (CIP) at (ppm level)

Figure 20 displays the comparison between the adsorption capacities of CIP on grafted HMS and GO modified HMS. Firstly, it can be seen the modification of GO on HMS could be enhanced the adsorption capacity even for A-HMS, which had less CIP adsorption capacity. Among GO modified HMS, GO-A-HMS provided slightly higher adsorption capacity than GO-A5M5. Although GO-A5M5 had mercapto functional group on the surface which could be enhanced the adsorption capacity more than silanol group on the surface of GO-A-HMS; therefore, the effect of surface functional group can be neglected. In addition, the presence of GO on each adsorbents was recommended to describe the main interaction. The approximated quantity of GO on GO-A-HMS (22.35%) was higher than GO-A5M5 (18.39%). Thereby, the adsorption mechanism of CIP on GO-A-HMS tend to be the results of cationic CIP species and carboxyl or phenyl groups on GO and hydrogen bonding via silanol group (non-grafted silanol) on A-HMS surface. As same as GO-A-HMS, electrostatic interaction could occur between CIP and GO on GO-A5M5. Moreover, it had mercapto functional group on A5M5 surface that could increase the adsorption capacity by hydrophobic interaction. The comparison of CIP adsorption on GO-A-HMS and GO-A5M5 was showed in Figure 21.

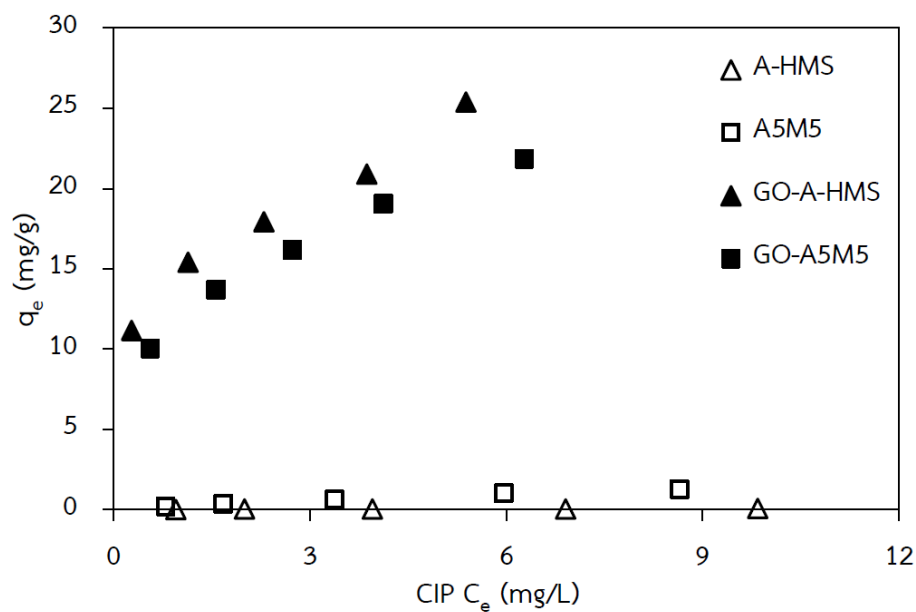


Figure 20 Adsorption capacities of CIP on grafted HMS and GO modified HMS.

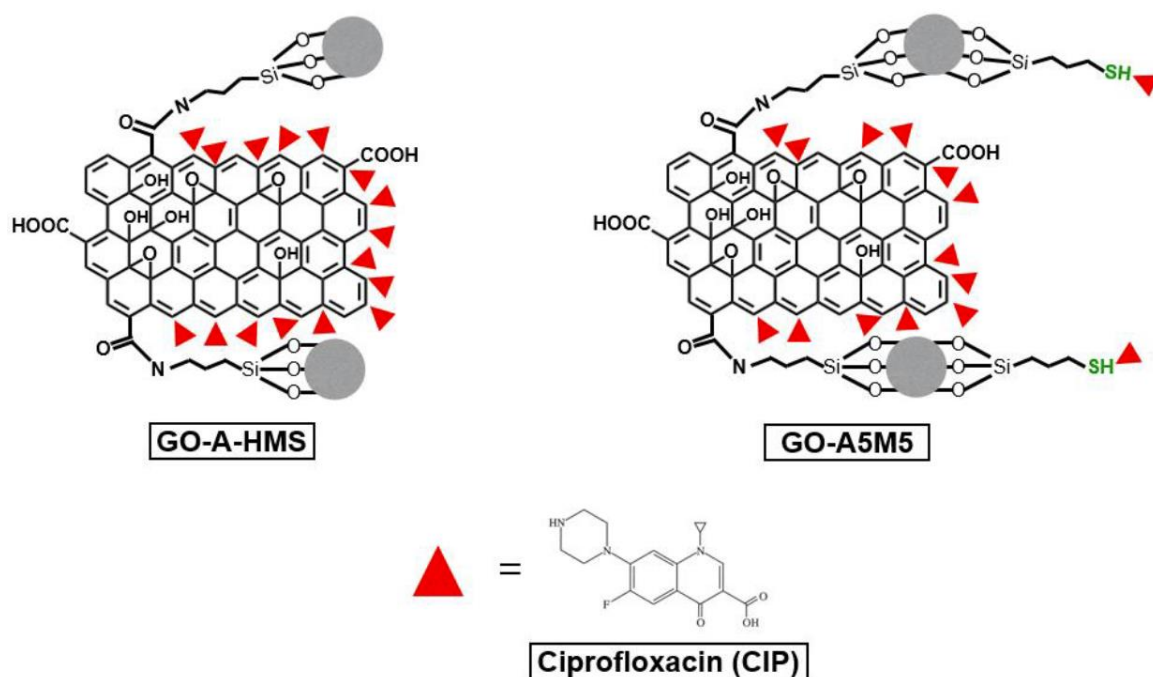


Figure 21 The comparison of CIP adsorption on GO-A-HMS and GO-A5M5

Porous silicas versus haloacetonitriles (HANs)

The effect of the porous and crystalline structures of the four adsorbents on the adsorption capacities of the five different HANs (MCAN, DCAN, TCAN, MBAN and DBAN) at pH 7 are shown in figure 22. To exclude the effect of the differences in surface area between the four adsorbents, the adsorption capacities were standardized for the surface area and are presented accordingly as $\mu\text{g}/\text{m}^2$. Ti-HMS had the highest adsorption capacities of both mono-HANs (MCAN and MBAN). Of the three mesoporous adsorbents, although HMS had a somewhat similar mean pore size to Ti-HMS (81.8% of the Ti-HMS level), the observed adsorption capacities of MCAN and MBAN were slightly and significantly lower, respectively, for HMS than that for Ti-HMS. This is probably due to the significantly (1.65-fold) higher pore volume of Ti-HMS, as determined by N_2 adsorption. Thus, the accessibility of the mono-HANs molecules to the internal pores of Ti-HMS is better than that for HMS leading to a higher adsorption capacity. In addition, the Lewis acid site on the Ti-HMS surface, is a stronger acid than the weak acidic silanol group in the pure silica-based HMS and SBA-15, and so could enhance the adsorption capacity by the synergic adsorption of the ion-dipole interactions from both functional groups. Previous reports have found that the active Lewis and Brønsted acid sites can promote adsorption by interacting with the nitrile ($\text{N}\equiv\text{C}$) and nitroso ($\text{N}=\text{NO}$) groups in the adsorbate molecules (Busca et al., 2008; Dai et al., 2009). Thus, the surface functional group of the adsorbent also plays an important role in adsorption.

However, the mesopore SBA-15 showed the lowest adsorption capacity of all four adsorbents for the two mono-HANs, MCAN and MBAN, compared with the other adsorbents. The negative surface charge derived from dissociation of silanol groups could contribute to the electrostatic interaction with the ion-dipole of the HANs and thus HAN adsorption. The significantly larger mean pore size (6.0 nm) of SBA-15 might reduce its ability to confine smaller sized adsorbates, such as these two mono-HANs. A similar result has been reported previously, where the adsorption capacity of nitrosamine on SBA-15 was lower than on the smaller (2.22-fold) pore diameter of MCM-41 (2.7 nm) (Wei et al., 2009). Thus, the pore size is clearly likely to be a key factor controlling mono-HAN adsorption.

In the case of NaY, the positively charged surface is due to the combination of the protonated silanol group and the Na^+ at pH 7. Since the N-atom of each HAN possesses a negative dipole, they can be electrostatically adsorbed onto the positively charged surface. As seen, the adsorption

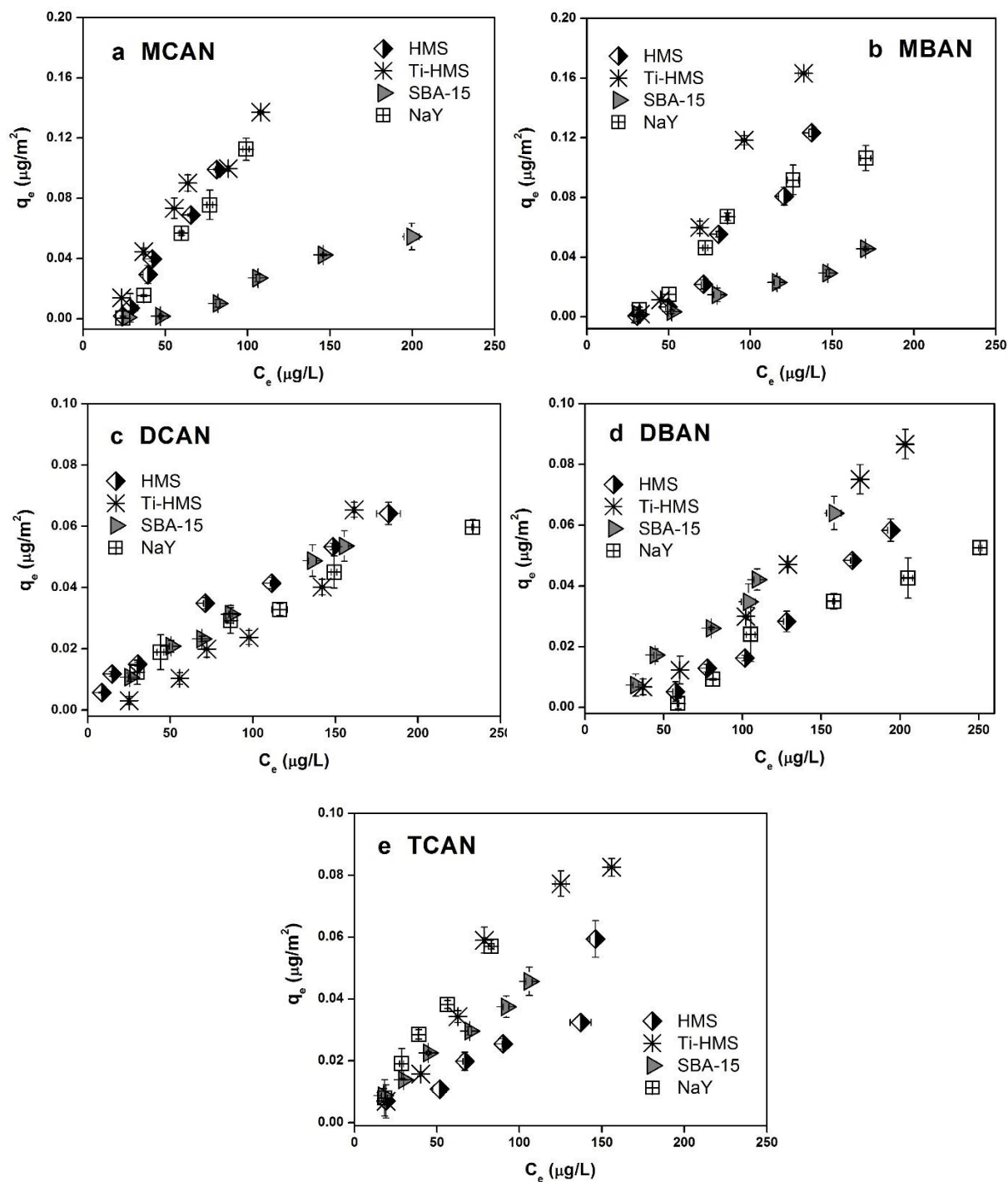


Figure 22 Adsorption isotherms of the five different HANs on the four adsorbents (HMS, Ti-HMS, SBA-15 and NaY) at pH solution of 7 (ionic strength of 10 mM). Isotherms are shown for (a) MCAN, (b) MBAN, (c) DCAN, (d) DBAN and (e) TCAN.

of the mono-HANs exhibited a comparable adsorption capacity to that for HMS and Ti-HMS (excepting for the adsorption of MBAN that was less than Ti-HMS), although NaY has a relatively low surface area and pore volume. One possible explanation is that the small pore size (0.74 nm) and porous structure of NaY could be effective in retaining the mono-HANs. In this scenario, the crystalline structure and narrow diameter pore size (micropores) of zeolite NaY provides a delicate geometric confinement of small adsorbate molecules (Zhou and Zhu, 2005), and so suggests that the crystalline structure of the adsorbent can affect the adsorption capacity of mono-HANs.

The adsorption capacities of the di-HANs (DCAN and DBAN) on HMS, Ti-HMS and NaY (figure 22c & 22d) were less than that of the mono-HANs, whereas, in contrast, SBA-15 showed a slightly higher capacity. However, the adsorption capacities are likely to be related to the molecular structure of the HANs in terms of the amount of halogen atoms in the molecule and their molecular weight. Moreover, that the adsorption capacity of DBAN is higher than DCAN might be because of the stronger positive dipole of the H-atom in DBAN.

The TCAN adsorption isotherm (Fig. 22e) showed the adsorption capacity followed the sequence Ti-HMS > NaY > SBA-15 > HMS, and suggests that the Lewis acid sites of Ti-HMS and the Na⁺ of NaY significantly influenced the adsorption capacities. This supports the notion that the surface functional group plays a crucial role in adsorption.

Adsorption selectivity

Adsorption selectivity of antibiotic residues on HMS-SPs

To investigate the selective adsorption mechanisms, the entire synthesized adsorbents were determined the adsorption isotherms of mixed solute of three selected antibiotics comparing with the individual antibiotic adsorption. For possible comparison with the individual solute, the mixed solutes were carried out in the same condition as individual solute (in 0.01 M phosphate buffer, pH 7.0). Under this experimental conditions, CIP, NAL, and SMX were exhibited the zwitterions, anionic, and anionic as their predominant speciation in the solution, respectively.

The adsorption isotherm of mixed antibiotics onto the hydrophilic adsorbent was shown in figure 23. Beside the HMS-SP, the adsorption capacity of three antibiotics was increasing in comparing with the single solute (as showed in figure 23 (a, d)). Hydrogen bonding between the silanol group on the surface and functional group of antibiotic might be the main mechanism onto

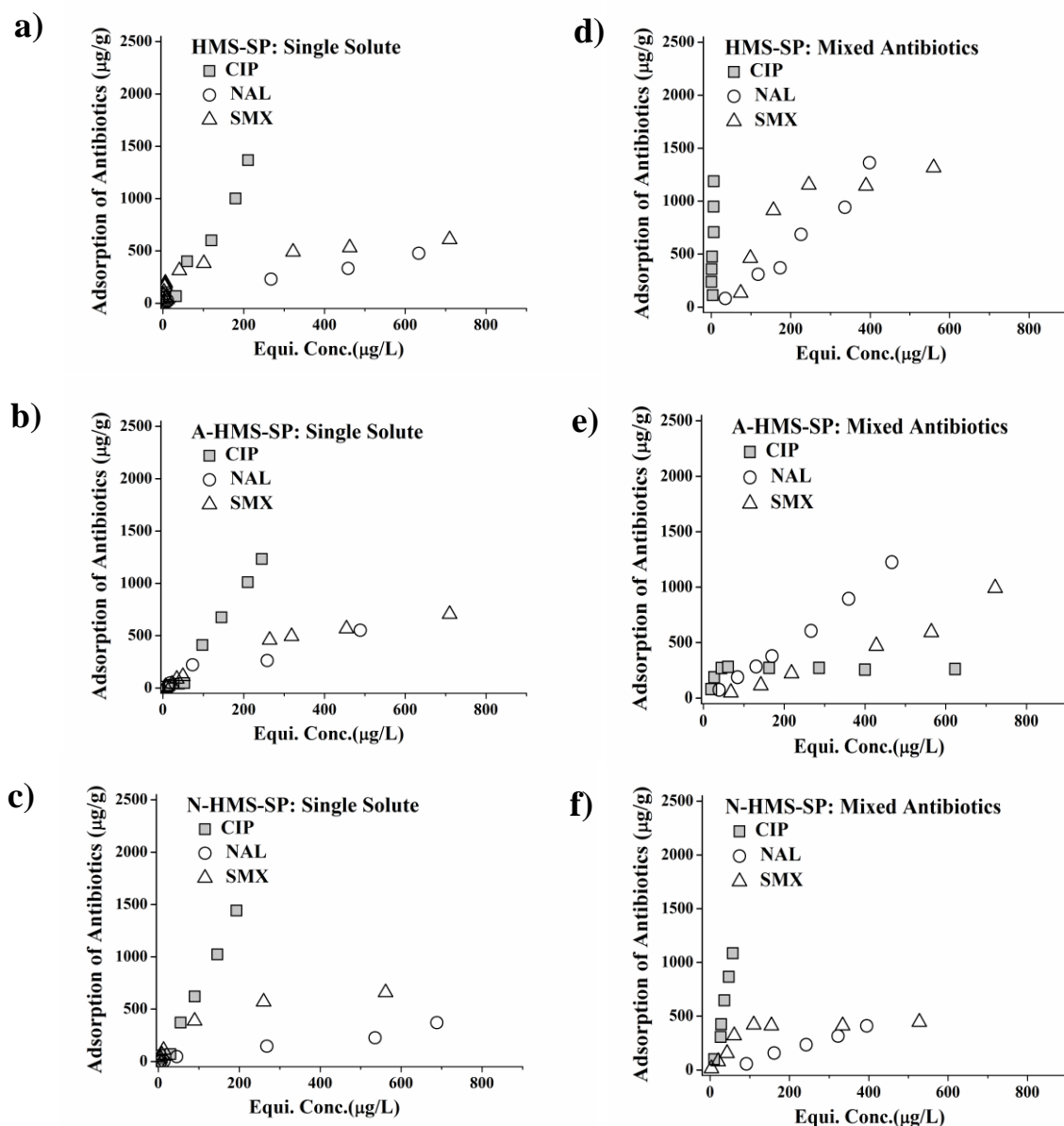


Figure 23 Adsorption isotherm of three antibiotics on hydrophilic synthesized adsorbents; HMS-SP, A-HMS-SP and N-HMS-SP, in a single solute (a, b, c), and mixed solute (d, e, f) in 0.01 M phosphate buffer pH 7.0 (25 °C).

the surface. Since the attractive interaction between a positive site of zwitteric CIP molecule (CIP^{\pm}) and a negatively charge of the other antibiotics might be occurred. Hence, that could enhance the adsorption capacities in the mixed solute onto HMS-SP. Nevertheless, the order of adsorption capacity in the mixed solutes was stilled the same as the single solute. These results were implied that there was no competitive interaction among three antibiotics adsorption by HMS-SP.

For A-HMS-SP, the adsorption capacities of NAL and SMX in mixed solute were increased than single solute condition in contrast with CIP molecule as showed in figure 23 (b, e). While the order of adsorption capacities in mixed solutes was different from the single solute results; being as NAL>SMX>CIP, thus hydrogen bonding could not be the only adsorption mechanism on A-HMS-SP as same as HMS-SP. Due to the positively charge on the adsorbent surface and the negatively speciation of both NAL and SMX was performed thus the electrostatic interaction was suggesting to be involve in this adsorption mechanism also.

Figure 23 (c, f) showed the adsorption isotherm of the single and mixed solutes of three antibiotics onto N-HMS-SP. The obtained results showed that the order of adsorption capacities in the mixed solutes was not different from the single solute. However, the adsorption capacities of CIP and NAL in mixed solutes were slightly increased in comparing with single solute. Similarly to HMS-SP, the hydrogen bonding between nitrile functional group of N-HMS-SP surface and antibiotics molecule might be the main adsorption interaction in this condition.

According to the hydrophobic adsorbents, the comparison on the adsorption interaction between the mixed and the single solute were shown in figure 24. In case of M-HMS-SP, the adsorption capacities order in mixed solutes was different from the single solute as followed; NAL>SMX>CIP, thus the competitive adsorption among three antibiotics could be occurred onto the M-HMS-SP surface. The adsorption capacity of CIP in mixed solute was extremely decreased. It might be caused by the competition between the hydrophobic interaction of NAL and SMX and hydrogen bonding of CIP onto the surface. Moreover, interaction between hydrophobic moiety of each antibiotics via van der Waals interaction might cause the increasing of NAL and SMX adsorption capacities.

In contrasting with the adsorption capacities order on P-HMS-SP, there was no change from the single solute condition as showed in figure 24 (b, d). However, the slightly decreased adsorption capacities of CIP and increased adsorption capacities of the other antibiotics were investigated in the mixed solute condition. These obtained results were suggesting that the strong π - π interaction between CIP and aromatic ring of phenyl functional group on P-HMS-SP surface could be involved in this adsorption interaction. Therefore, the combination between hydrogen bonding and π - π electron donor acceptor was suggested to be the key role adsorption mechanism.

In order to evaluated the antibiotics adsorption by OD-HMS-SP, the highest hydrophobic synthesized adsorbent, the adsorption capacities of NAL was increased in mixed solutes than single solute as showed in figure 24 (c, f). Unexpected result, the decreased adsorption capacity

of CIP in mixed solutes was decreased. Moreover, adsorption capacity of CIP was the lowest value in the adsorption range in mixed solute. These obtained results were implied that the adsorption of CIP molecule could be easier interrupted than the other antibiotics (NAL and SMX) via hydrophobic interaction. However, the hydrogen bonding between the CIP and the residual silanol functional group surface should be also considered for the rest adsorption capacity of CIP. Nevertheless, these obtained results could be concluded that active surface area were enough for adsorption of three antibiotics in mixed solute in this applied total concentration range.

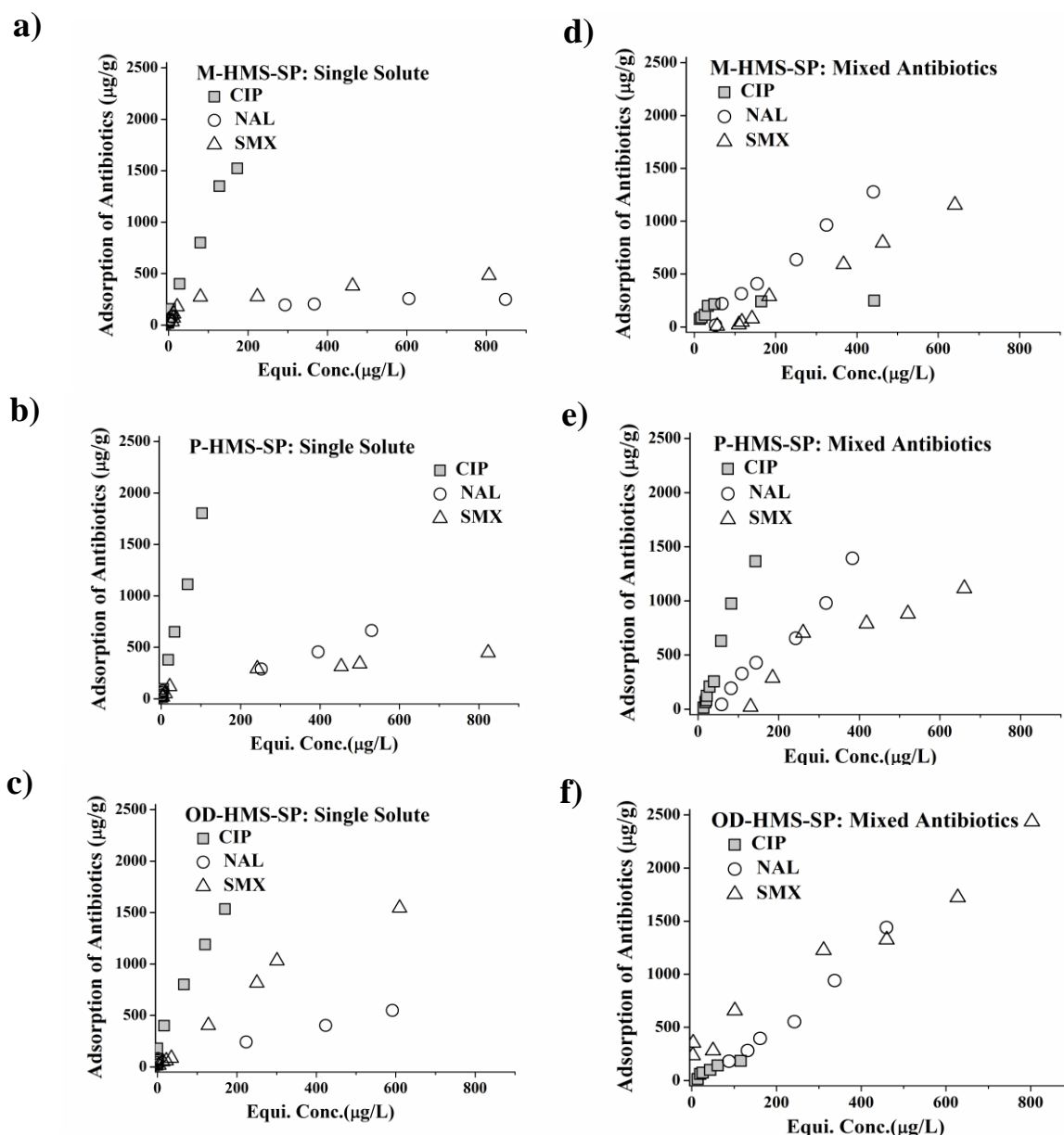


Figure 24 Adsorption isotherm of three antibiotics on hydrophobic synthesized adsorbents; M-HMS-SP, P-HMS-SP and OD-HMS-SP, in a single solute (a, b, c), and mixed solute (d, e, f) in 0.01 M phosphate buffer pH 7.0 (25 °C).

Adsorption selectivity on CFA and NAP on GO-A-SBA-15 (ppm concentration)

GO-A-SBA-15 was selected because this adsorbent showed the highest adsorption capacity of NAP comparing with all synthesized adsorbents. The adsorption selectivity on GO-A-SBA-15 was conducted by varying concentration of NAP between 2-13 ppm and fix concentration of CFA at 7 ppm. And then, the concentration CFA was varied between 10-20 ppm and fixed concentration of NAP at 15 ppm in controlling of phosphate buffer 0.01M at pH 7.

Obtained results showed that in the vary concentration of NAP between 2-13 ppm and fix CFA concentration at 7 ppm on GO-A-SBA-15 exhibited the decrease of adsorption capacity of both NAP and CFA. However, the adsorption capacity of CFA was reduced from the single solute around 28.98% but the concentration of NAP was exhibited the reduction around 39.39% as Table 4.17. Therefore, the adsorption of NAP on GO-A-SBA-15 might be easily disturbed by the existence of CFA.

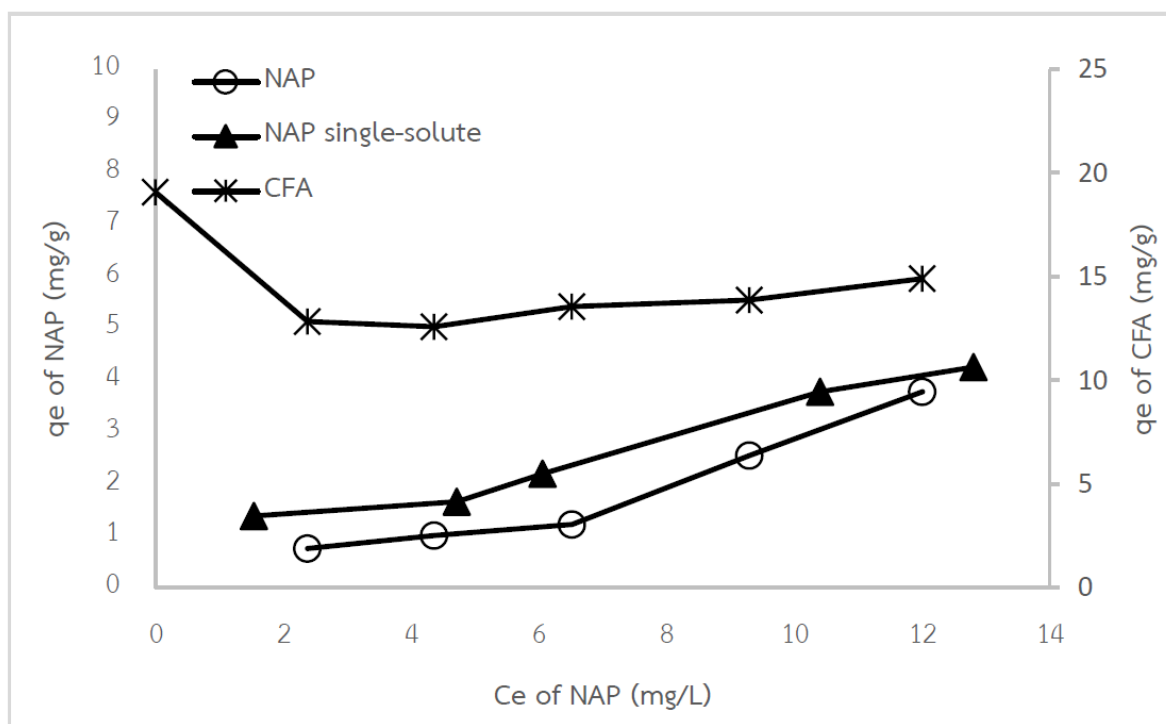


Figure 25 Adsorption isotherm of varied NAP concentration (with fixed CFA concentration) on GO-A-SBA-15 in multi-solute.

Whereas, the results of varying concentration of CFA between 10-20 ppm and fix concentration of NAP at 15 ppm on GO-A-SBA-15 also showed the significantly decline of

adsorption capacity of both CFA and NAP as figure 26. The adsorption capacity of CFA was dropped from the single solute around 26.07%. And for NAP, the adsorption capacity was showed the decrease around 38.82%. The obtained results exhibited the same as shown in the varying concentration of NAP between 2-13 ppm and fix CFA concentration at 7 ppm on GO-A-SBA-15. Thus the adsorption of CFA on GO-A-SBA-15 might be also interrupted by the presence of NAP.

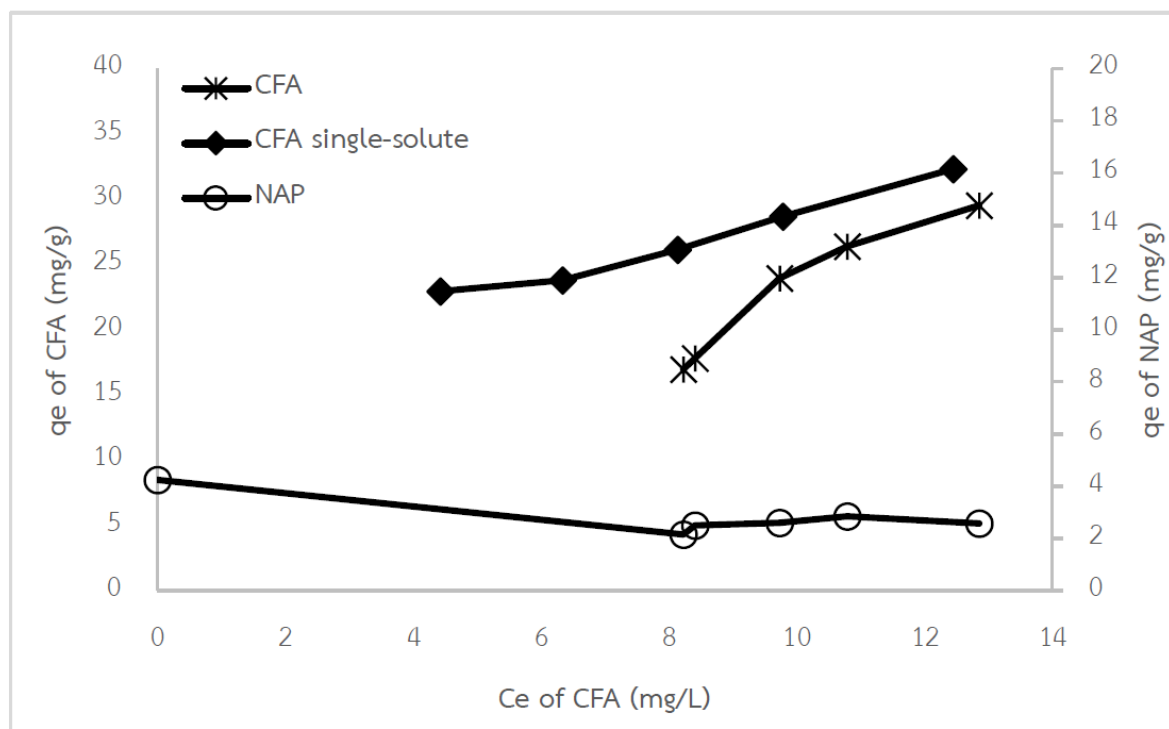


Figure 26 Adsorption isotherm of varied CFA concentration (with fixed CFA concentration) on GO-A-SBA-15 in multi-solute

Adsorption selectivity on CIP and CBZ on GO modified HMSs (ppm concentration)

The competitive adsorption of binary solute solution of CIP and CBZ was performed by fixing one pharmaceutical as the same concentration and varying initial concentration another one to investigate the selective adsorption of GO-A-HMS and GO-A5M5 as shown in figure 27 GO-A-HMS had a higher adsorption capacity for CIP than for CBZ in both single and binary solute solution. It can be observed the adsorption capacity of CIP in binary solute solution was extremely lower than in single solute solution. In case of GO-A5M5, it shows the similar result as GO-A-HMS, but the adsorption capacity of CBZ in binary solute solution was slightly lower than in single

solute solution. These results could be explained the competition between CIP and CBZ adsorb on the adsorbents. Firstly, the higher adsorption capacity of CIP on GO-A-HMS and GO-A5M5 in both single and binary solute solution might be related to the molecular size of pharmaceuticals. CIP has a lower molecular size than CBZ that could enhance the movement to the inner surface of the adsorbents. Moreover, the adsorption mechanism of CIP and both GO modified HMS tend to be the results of π - π interaction between CIP molecule and surface of GO. In case of CBZ, the lower adsorption capacities of both adsorbents in binary-solute solution were observed. However, the adsorption capacity of CBZ on GO-A5M5 was not extremely reduce that might be the result of hydrophobicity of mercapto functional group on the surface of GO-A5M5.

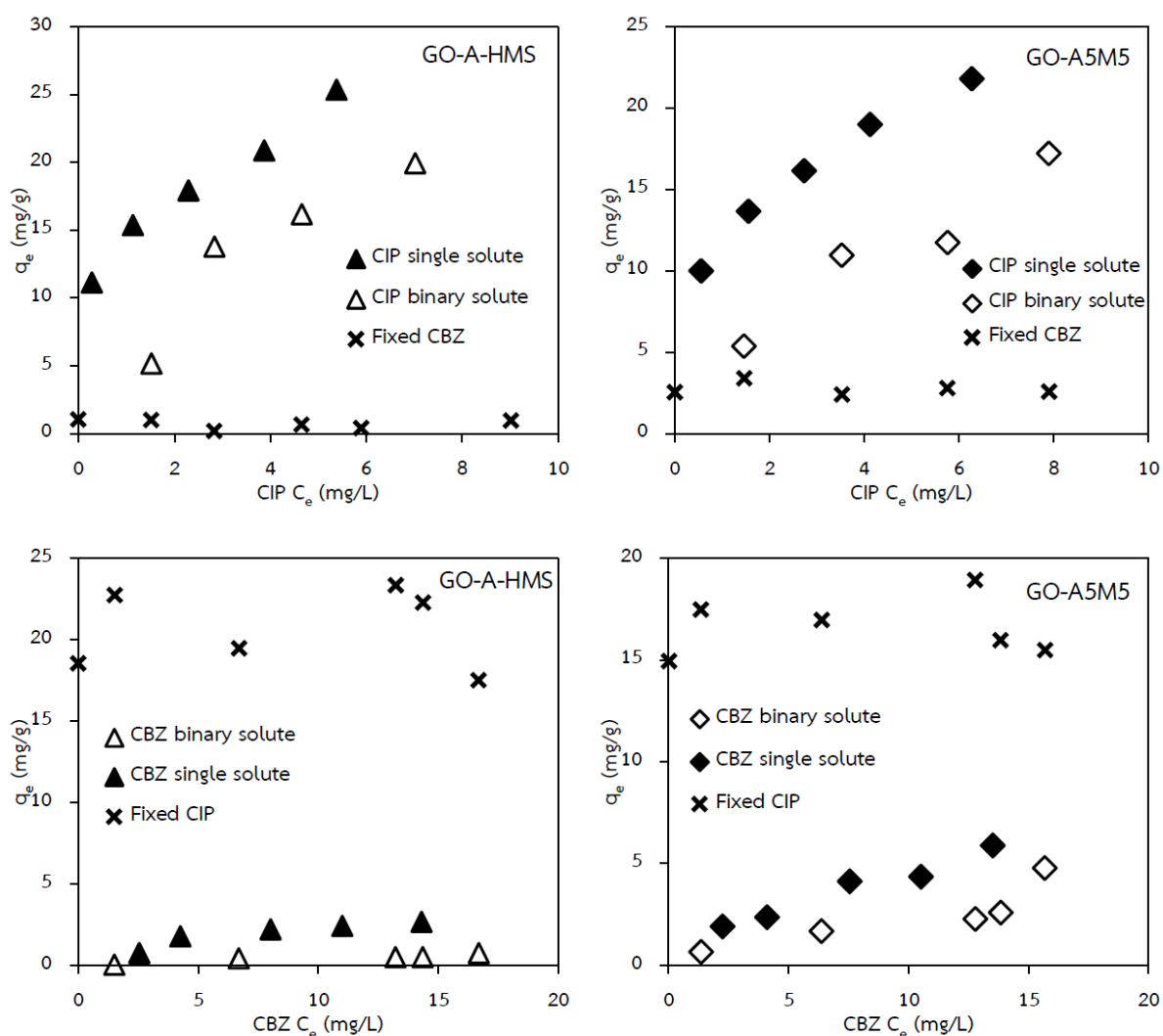


Figure 27 Selective adsorption isotherms of CIP and CBZ on GO-A-HMS and GO-A5M5

Selective adsorption of five-HANs in single-solute and mixed-solute solutions

Adsorption isotherms for the five-HANs alone (single solutes) on HMS, Ti-HMS, SBA-15 and NaY are shown in figure 28 (a), (c), (e) and (g), respectively. The order of adsorption preference (highest to lowest) was MCAN > MBAN > DCAN > DBAN > TCAN on HMS, Ti-HMS and NaY, which implies that the adsorption capacities may relate to the strength of the positive/negative dipoles in the respective HANs. The strongest positive dipole of the two H-atom of the mono-HANs provides an enhancement of the ion-dipole electrostatic force and the strongest negative dipole of N-atom in mono-HANs molecule could interact with Lewis acid site of Ti-HMS and Na⁺ of NaY, leading to a higher adsorption capacity. Moreover, these selective adsorption behaviors might be linked to the surface characteristics of each adsorbent. The hydrophilic surface characteristics of all four adsorbents would be expected to selectively adsorb a hydrophilic adsorbate in the order of mono-HANs > di-HANS > tri-HAN. However, except for SBA-15, the adsorption of the five HANs displayed a reverse order of adsorption preference (figure 28e). For SBA-15, the larger molecular weight of tri-HAN was adsorbed more than the di-HANs and mono-HANs. This difference may be related to the porous structure of SBA-15, which seems to be a more important factor in controlling adsorption. A larger pore size might enhance the internal surface accessibility and let the larger molecular structure HANs be adsorbed better than on adsorbents with smaller sized pores. Regardless, these results indicate that the adsorption capacity of the five different HANs on the four adsorbents is related to the molecular structure of the HANs. Moreover, the hydrophilic / hydrophobic nature of both the adsorbent and the adsorbate can influence the selective adsorption.

The adsorption isotherms for the five HANs when presented as an equimolar mixed solute on the four adsorbates (figure 28) are consistent with the notion that the active surfaces of each adsorbent had been divided between all five-HAN species causing a decrease in the observed adsorption capacity of each HAN. The order of adsorption capacities in this equimolar mixed HAN solute on HMS, Ti-HMS and NaY were significantly different from the single solute results (TCAN > DBAN \cong DCAN > MBAN \cong MCAN). The large molecular weight of the tri-HAN and the two di-HANs are more easily adsorbed than the smaller molecular weight mono-HANs at low concentrations. Unlike SBA-15, the order of adsorption capacities of all five HANs was not different compared to that observed for the single HAN solute (figure. 28f), which might be caused by the higher accessibility to the active sites due to larger pore size.

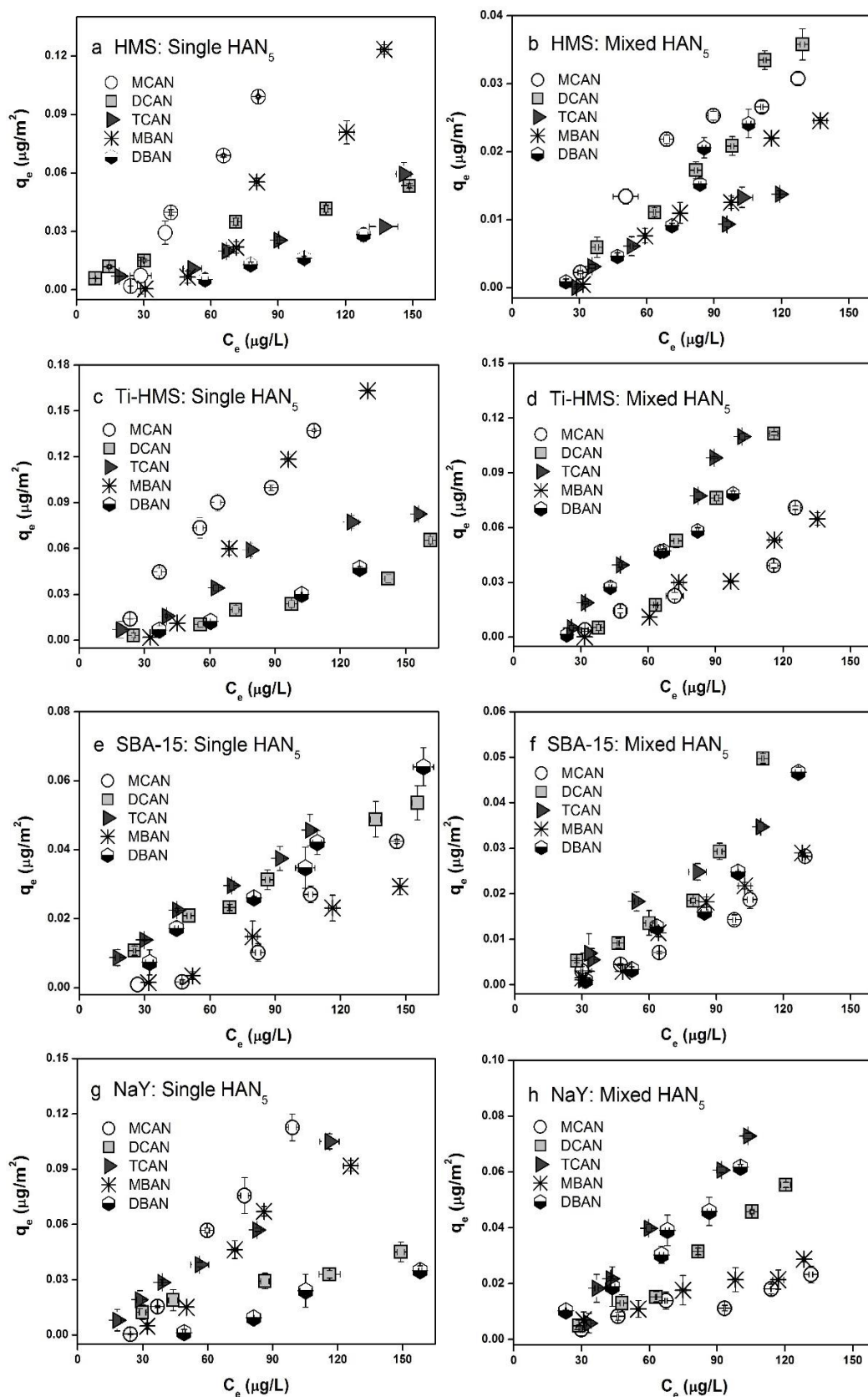


Figure 28 Adsorption isotherms of the five different HANs alone (single solute) or as an equimolar mixture on the four adsorbents (HMS, Ti-HMS, SBA-15 and NaY) at pH solution of 7 (ionic strength of 10 mM).

Adsorption mechanisms among adsorbent surface, PPCP and NOM.

Adsorption isotherms of tannic acid (TA) on HMS-SPs

Concerning the fate and transport of antibiotics on environment, the effect of natural organic matter (NOM) on the adsorption of antibiotics has been investigated in several reports (Brigante et al., 2010; Bui et al., 2010). Tannic acid (TA), consisting of hydrophilic phenolic groups and hydrophobic aromatic rings, was selected to be the model of NOM in this study. The adsorption isotherm of TA in 0.01 M phosphate buffer pH 7.0 onto six synthesized adsorbents were examined and shown in figure 29 (a). A-HMS-SP had the highest adsorption capacity of TA comparing with all the synthesized adsorbents. In this respect, electrostatic interaction between the positively charge of adsorbent surface and negatively charge of TA molecule was suggesting to be the main interaction mechanism in this condition. Consistent with previous reports, the interaction between TA and the amino-functional group on A-HMS-SP had been suggested to be the main adsorption mechanism (Lin et al., 2011; Wang et al., 2011; Wang et al., 2010). In order to the adsorption of TA on OD-HMS-SP, the lowest TA adsorption capacities, the hydrophobic interaction without the specified active site was suggesting to involve in this adsorption mechanism. However, the adsorption capacity of all synthesized adsorbents was still lower than the universal adsorbent as PAC as showed in figure 29 (b).

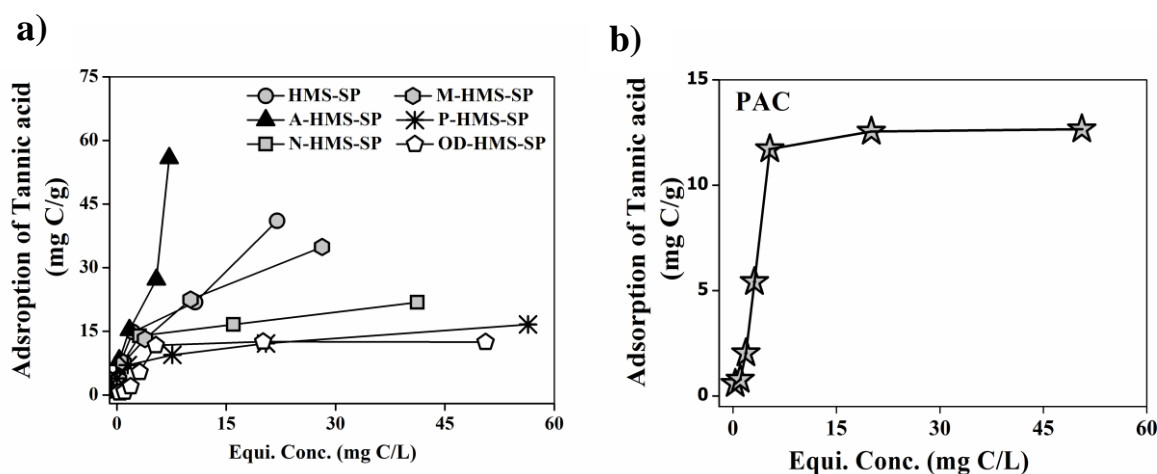


Figure 29 Adsorption isotherm of Tannic acid (TA) onto a) synthesized HMS-SPs and b) PAC in phosphate buffer pH 7.0 (25°C) and IS 0.01 M.

Effects of tannic acid on antibiotic adsorption (CIP, NAL and SMX)

Since A-HMS-SP and OD-HMS-SP had highest antibiotics adsorption capacities comparing to the other HMS-SPs adsorbents. Moreover, TA also had higher affinity with A-HMS-SP, while the adsorption capacity on OD-HMS-SP was lowest. Therefore, A-HMS-SP and OD-HMS-SP were chosen as the representing synthesized adsorbents for the investigation of the effect of TA on single antibiotic adsorption selectivity.

Figure 30 showed the adsorption of individual antibiotic; CIP, NAL, and SMX at pH 7.0 and IS 0.01 M in coexisting solution with and without tannic acid by A-HMS-SP and OD-HMS-SP. As seen in figure 30 (a, d), the obtained results were consistent with previous results that A-HMS-SP and OD-HMS-SP were preferable to TA and CIP, respectively. However, the adsorption capacity of CIP on A-HMS-SP in mixed solute was extremely increased in the presence of TA, while the adsorption capacity of TA on A-HMS-SP seemed not to be changed significantly in mixed solute. Firstly, TA might form a layer on the surface via the electrostatic interaction between negatively TA molecules and positively charge of adsorbent surface. After that CIP (CIP^{\pm}) molecules could create a new layer on TA former layer via the formation between protonate amine group of CIP and negatively surface charge of TA molecule according to the electrostatic interaction, which could increase the CIP adsorption capacity on A-HMS-SP. This proposed adsorption mechanism was illustrated as showed in figure 31.

In the case of OD-HMS-SP, there was a slightly increased CIP adsorption capacity in the presence of TA. Furthermore, the adsorption capacity of TA increased slightly compared with a single solute. Similarly to A-HMS-SP, multilayer adsorption between TA and CIP associated with interaction between onto OD-HMS-SP. CIP was suggested to be adsorption onto the first layer and created the positively charged surface by amine moiety for TA adsorption. Hence, the electrostatic interaction might be occurred between TA and CIP at the second layer. Moreover, adsorbed TA on second layer might enhance the adsorption capacity of CIP again due to electrostatic interaction. However, the adsorption interaction of CIP without specific selectivity of n-octyldimethoxy surface can be suggested. This expected phenomenon could be illustrated and showed in figure 32.

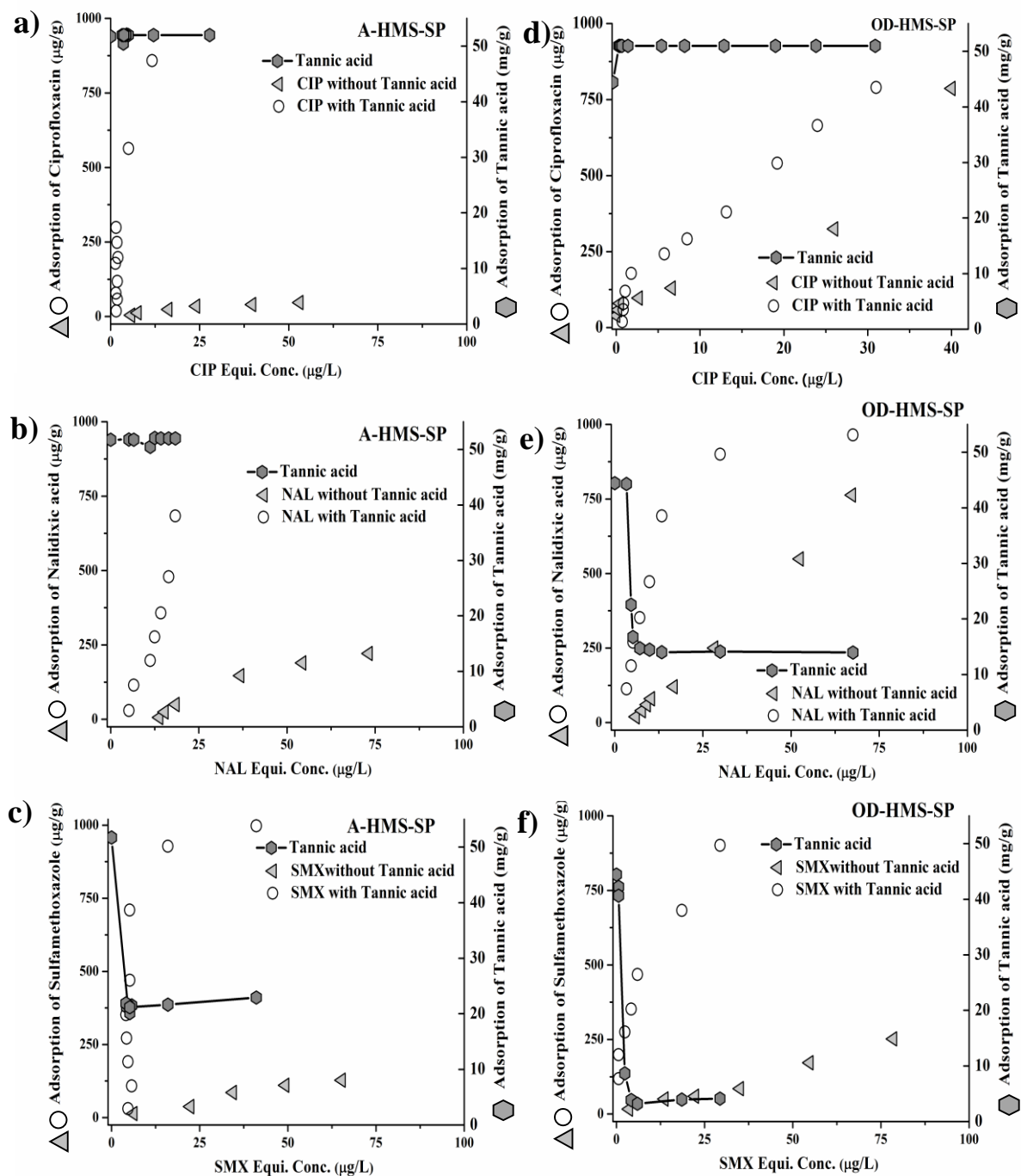


Figure 30 Effect of tannic acid on the adsorption of CIP (a, d), NAL (b, e), and SMX (c, e) on A-HMS-SP and OD-HMS-SP in 0.01 M phosphate buffer pH 7.0 (25°C).

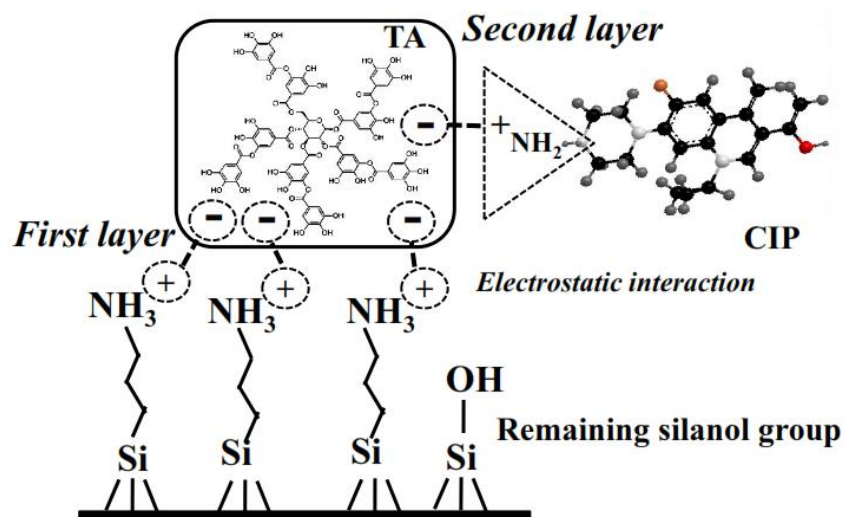


Figure 31 The proposed CIP adsorption mechanism in co-existing TA onto A-HMS-SP.

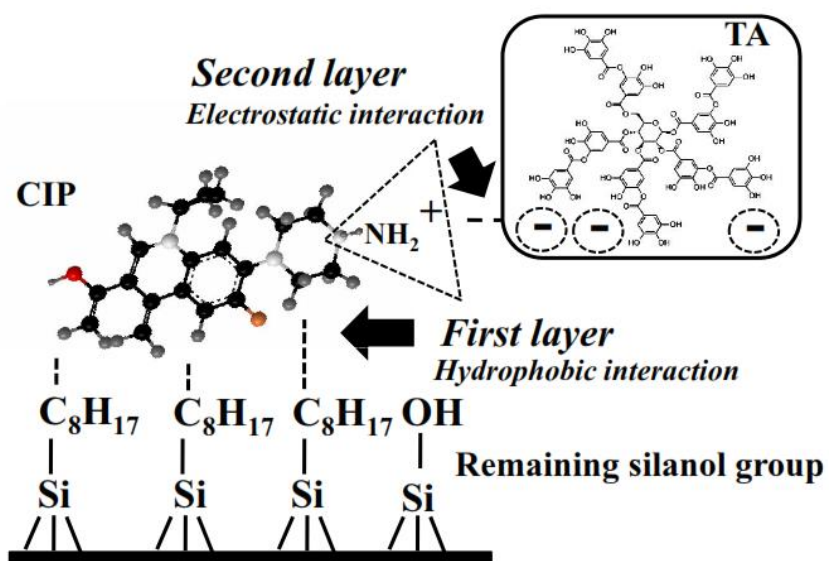


Figure 32 The proposed CIP adsorption mechanism in co-existing TA onto OD-HMS-SP.

Interestingly, the adsorption capacities of TA in the presence of each NAL and SMX were decreased on OD-HMS-SP as similar as the adsorption of TA in the presence of SMX on A-HMS-SP as shown in figure 30 (c, e, f). On contrary, the adsorption capacities of both antibiotics (NAL and SMX) were increased in the presence of TA as a co-existing compound. According to adsorption of NAL and SMX, the increased adsorption capacities of NAL and SMX might be caused by the driven force of the repulsive charge between negatively antibiotic and negatively TA molecule in this pH solution. That might be enhanced the driving force of NAL and SMX for adsorption on the surface of A-HMS-SP and OD-HMS-SP.

Additionally, TA preferred to be adsorbed to amine functional group as described above, hence the TA adsorption capacity should be related to the amino functional groups of A-HMS-SP. From the figure 30 (b), the adsorption of TA on A-HMS-SP did not change significantly, which might indicate that the NAL was not be adsorbed via amino functional groups of A-HMS-SP. However, the increasing of NAL adsorption capacity might be caused by the interaction between NAL and already adsorbed TA via π - π electron donor acceptor between benzene ring of both TA and NAL. The expected adsorption of NAL onto A-HMS-SP surface was illustrated as showed in figure 33.

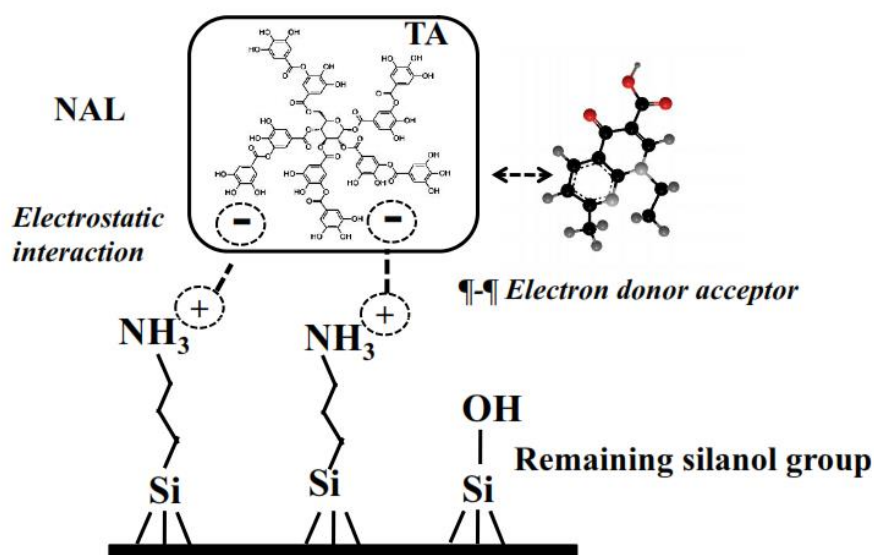


Figure 33 The proposed NAL adsorption mechanism in co-existing TA onto A-HMS-SP.

In case of TA adsorption on OD-HMS-SP in the presence of NAL (Figure 30 (e)), the adsorption of TA might be occurred via the hydrophobic interaction and hydrogen bonding via free silanol groups of OD-HMS-SP which was supposed to be the same mechanism as NAL adsorption. This Figure clearly indicated that the surface of OD-HMS-SP preferred to adsorb higher hydrophobic NAL much more than TA. Moreover, the adsorption capacity of NAL on OD-HMS-SP was increased by π - π electron donor acceptor between benzene ring of both adsorbed TA and NAL. This phenomenon was illustrated as showed in figure 34.

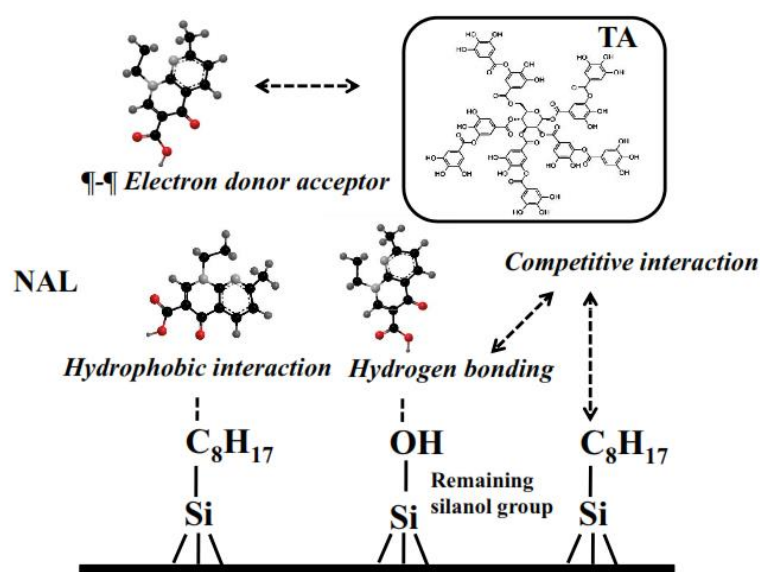


Figure 33 The proposed NAL adsorption mechanism in co-existing TA onto OD-HMS-SP.

As mention earlier, the adsorption capacities of TA in the presence of SMX on both adsorbents (A-HMS-SP, and OD-HMS-SP) were decreased as showed in Figure 30 (c, f). Although TA can be adsorbed by amino groups on A-HMS-SP surface very well, the hydrogen bonding between SMX molecule and amino groups (and/or remained silanol group) on the A-HMS-SP surface seem to be stronger than the TA adsorption. Therefore, there was the competitive adsorption between SMX and TA onto the active sites of the surface (amine- and remained silanol groups). Considering on the increased adsorption capacities of SMX in the presence of TA, that might be caused by the interaction between SMX and TA via hydrogen bonding of the active functional site of both molecules such as carboxylic- and amine- group, together with π - π electron donor acceptor between benzene ring. The expected adsorption mechanism of SMX in the presence of TA onto A-HMS-P was illustrated and showed in figure 34.

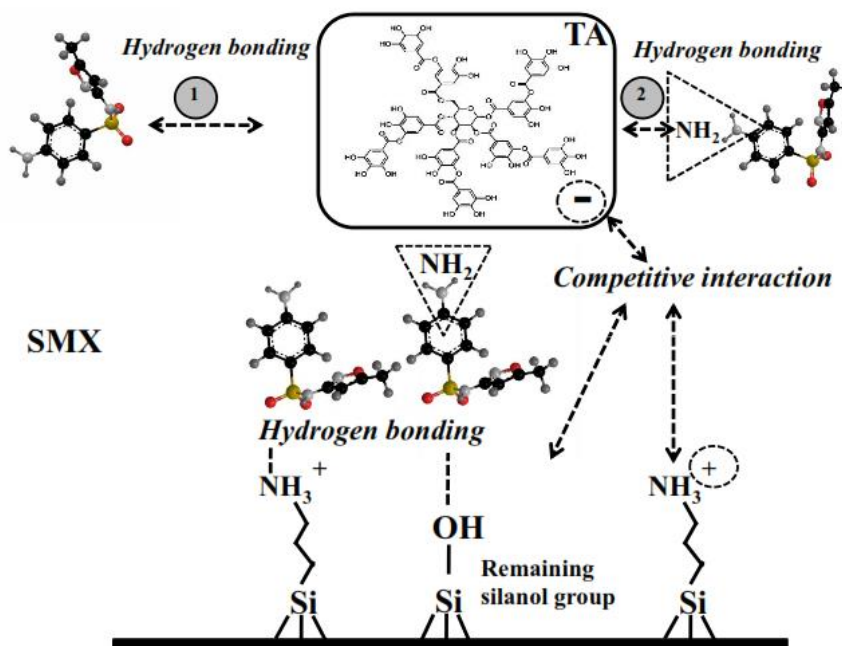


Figure 34 The proposed SMX adsorption mechanism in co-existing TA onto A-HMS-SP.

Similarly to the adsorption behavior onto A-HMS-SP, the competitive interaction between SMX and TA was supposed to be occurring onto the OD-HMS-SP surface. That revealed on the increased SMX adsorption capacity but the adsorption capacity of TA was decreased as showed in Figure 30 (f). The adsorption capacities of SMX could be increased by two possible phenomenons; the adsorption of SMX onto the OD-HMS-SP surface via hydrogen bonding (the carboxylic group of SMX and the active site of adsorbent surface) and the interaction of SMX and the already adsorbed TA via π - π electron donor acceptor between benzene ring between SMX and TA,. The expected adsorption mechanism of SMX in the presence of TA onto OD-HMS-P was illustrated and showed in figure 35.

Selectivity of mixed antibiotics (SMX CIP and NAL) in the presence of co-existing tannic acid

Figure 7.12 showed adsorption isotherms of the mixed three antibiotics in the presence of tannic acid as a co-existing compound. The order of adsorption preferable on A-HMS-SP was CIP>>NAL>SMX as seen in figure 36 (d). There were different from the mixed antibiotic solution without the TA (as showed in figure 36 (a)). However, the adsorption capacities of NAL and SMX on A-HMS-SP with the co-existing TA were not as high as in mixed antibiotic solute without TA (figure 36 (a)). This might be suggested that adsorbed TA on surface of A-HMS-SP preferred CIP much more than NAL and SMX. According to the preferable interaction

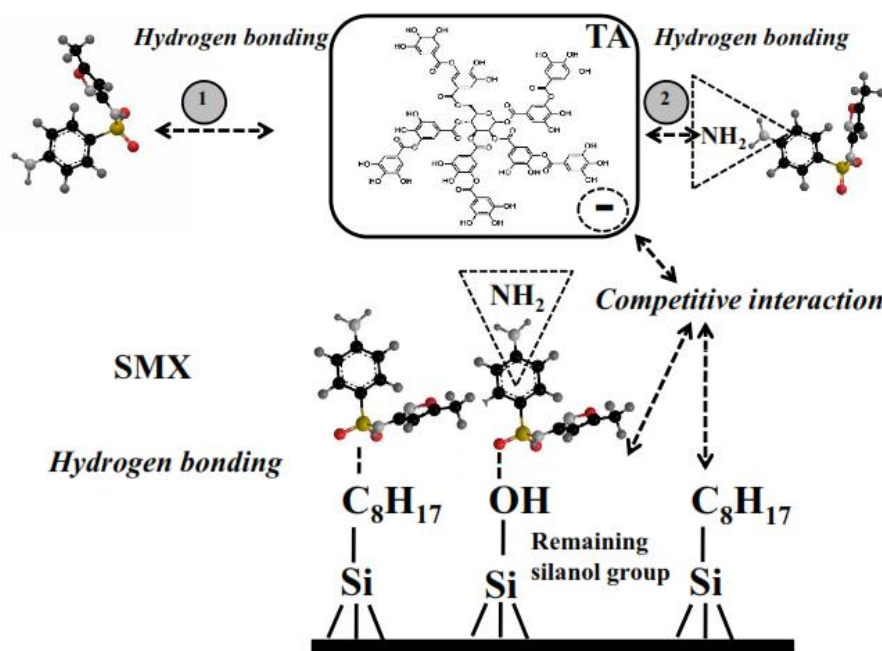


Figure 35 The proposed SMX adsorption mechanism in co-existing TA onto OD-HMS-SP.

of CIP and TA on A-HMS-SP than the other antibiotics, electrostatic interaction on second layer adsorption was suggested to be the key role in this adsorption phenomenon.

On the other hand, there was difference in the preferable adsorption order on OD-HMS-SP, being as CIP~NAL>>SMX, as showed in figure 36 (e). Considering on the adsorption capacities, the antibiotic adsorption capacities in the presence of TA were increased in the mixed solute comparing with the solute without TA excepted for SMX (as seen in figure 36 (b, e)). These might be caused by the stronger hydrophobic interaction between both CIP and NAL than SMX onto the alkyl functional surface. Furthermore, TA was preferable interacted with the quinolone antibiotic (CIP and NAL) via π - π electron donor acceptor interaction charge (CIP^{\pm}) than SMX molecule. That the higher planar aromatic ring in the molecule might be more electron donor acceptor interaction (Carabineiro et al., 2011). Therefore, the interactions between both antibiotics (CIP and NAL) with the already adsorbed TA were much more than the interacted SMX.

According to the PAC adsorption, the order of preferable antibiotic adsorption in mixed solutes in the presence of TA was slightly different from the mixed solutes solution being as NAL>>CIP~SMX as seen in figure 36 (c, f). Unexpected result, the adsorption capacity of NAL

was extremely increased when the other antibiotics were slightly increased comparing in the mixed solutes without the presence of TA. These obtained results can be suggested that the interaction between NAL and TA could be occurred in the mixed antibiotic adsorption in the presence of TA onto PAC via the same π - π electron donor acceptor as previous mention also. However, this mechanism need to be further investigated.

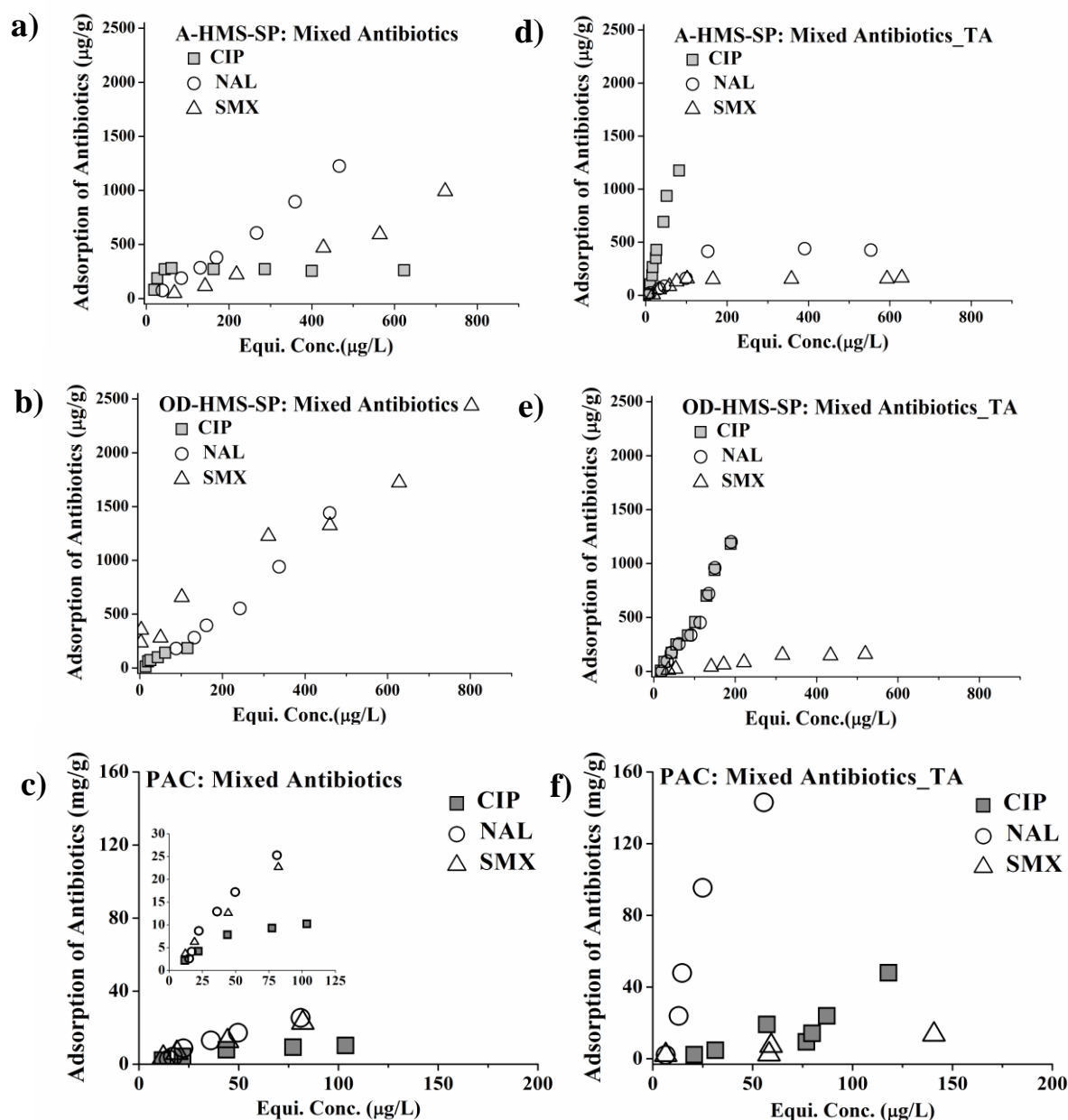


Figure 36 Adsorption isotherm of three antibiotics on A-HMS-SP, OD-HMS-SP and PAC in a mixed solute (a, b, c) without the presence of TA, and mixed solute (d, e, f) with co-existing tannic acid in 0.01 M phosphate buffer pH 7.0 (25°C).

Separation efficiencies of HMS-SPs by High Gradient Magnetic Separation filter (HGMS)

The experiments were conducted using column which has an internal diameter of 0.8 cm and height of 15 cm. The magnetic stainless filter was induced by approximately 0.2 T of magnets. P-HMS-SP was selected to study separation efficiency of HGMS filter due to the highest antibiotic adsorption capacity. The surface area per gram and volume per gram were calculated and summarized in table 4.

Table 4 Parameters characteristic of stainless filter

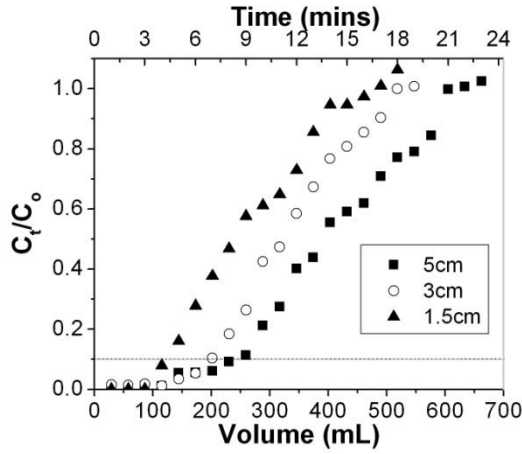
Parameters	Values
Width	0.46mm
Height	0.04mm
Surface area	98.3935cm ² /g
Density	5.5443 g/cm ³

This experiment was designed breakthrough concentration of particle at 10% removal. figure 37 (a) show breakthrough curve at different depth length of stainless filter at constant flow rate (0.95 cm/min), concentration particle (0.5 g/L) and surface area of stainless filter (37.23 cm²). It can be seen that the breakthrough time at breakthrough concentration was increased when extending bed depth due to higher surface area and contact time. For effect of flow rate, it was indicated that slower flow rate performed longer breakthrough time at 10% breakthrough by increasing contact time as shown in figure 37 (b) under fixed bed depth (5 cm), concentration particle (0.5 g/L) and porosity (97.2849%). Surface area of stainless filter at 37.23 cm² and 49.66 cm² were not significantly influence on breakthrough time and filtrate volume. Decrease of surface area to 19.32 cm² caused the reduce of service volume due to lower contact surface area, as shown in figure 37 (c).

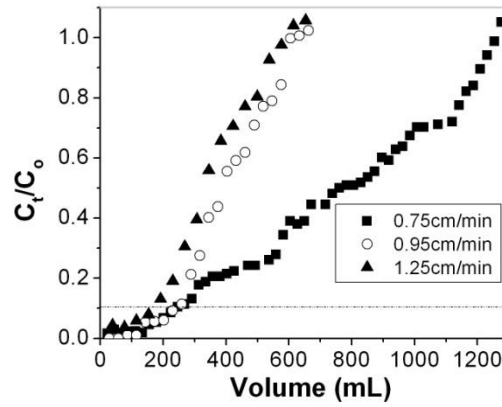
According to table 5, efficiency of stainless filter in different condition was analyzed by following equation. This Table demonstrated that the best condition is 1.5 cm of bed depth, 0.95 cm/min of flow rate and 37.23 cm² of surface area due to slightly different in flow rate between 0.95 and 0.75 cm/min.

$$Q = \frac{t \times F}{S}$$

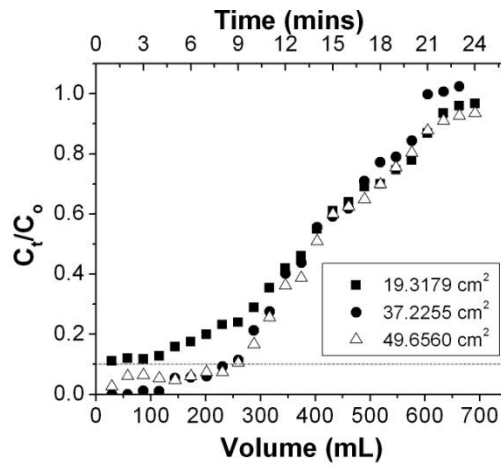
Where Q is breakthrough capacity (cm^3/cm^2), t is time at breakthrough at 10% (min), F is flow rate (cm^3/min) and S is surface area (cm^2).



(a)



(b)



(c)

Figure 37 Effect of (a) bed depth stainless filter, (b) flow rate and (c) surface area of stainless filter on breakthrough curve.

Table 5 Experiment data and breakthrough capacity of various depth, flow rate and surface area

Parameter	Breakthrough Time (min)	Filtrated Volume at Breakthrough (cm ³)	Breakthrough Capacity (cm ³ /cm ²)
Varying Depth			
1.5 cm	4.58	132.0	11.8198
3 cm	6.92	199.2	8.9186
5 cm	8.36	240.9	6.4714
Varying Flow			
0.75 cm/min	10.78	241.5	6.4883
0.95 cm/min	8.36	240.9	6.4714
1.25 cm/min	4.02	160.7	4.3170
Varying Surface area			
49.66 cm ²	8.50	244.9	4.9323
37.23 cm ²	8.36	240.9	6.4714
19.32 cm ²	-	-	-

Separation efficiencies of HMS-SPs by magnetic system applied to enhance ultrafiltration

Magnetic System Reducing Specific Cake Resistance

The core-shell magnetic silica structure of synthesized materials provided advantages on adsorbent separation after NAL removal process. Magnetic system which consists of SP adsorbent with external magnetic field were applied in ultrafiltration (UF) in this study to separate adsorbents after adsorption process. This magnetic system is suggested to enhance UF by slow-down cake formation and reduce membrane fouling. The specific cake resistance (R_c) of UF with magnetic system were determined. This value was expected to be less than of which conventional UF process to prove efficiency in reducing membrane fouling on UF.

P-HMS-SP under pH5 was selected for this experiment due to its highest adsorption capacity. The results exhibited on figure 38 were plotted follow the typical linear equation of cake building filtration (Ruth's law) can be derived in following equation.

$$t = \frac{\mu k R_c V_f}{2 \Delta p A^2} + \frac{\mu R_m}{\Delta p A} = a V_f + b$$

Where V_f is the filtrate volume (m^3), t is the time (s), A is the filter area (m^2), μ is the dynamic viscosity of the liquid phase ($Pa \cdot s$), Δp is the transmembrane pressure drop (Pa), R_m is the membrane resistance ($1/m$), R_c is the cake resistance ($1/m^2$) and k is the concentration coefficient (dimensionless). By experimentally determining slope a and intercept b the filter media resistance and the specific cake resistance can be calculated as shown in table 6 and 7.

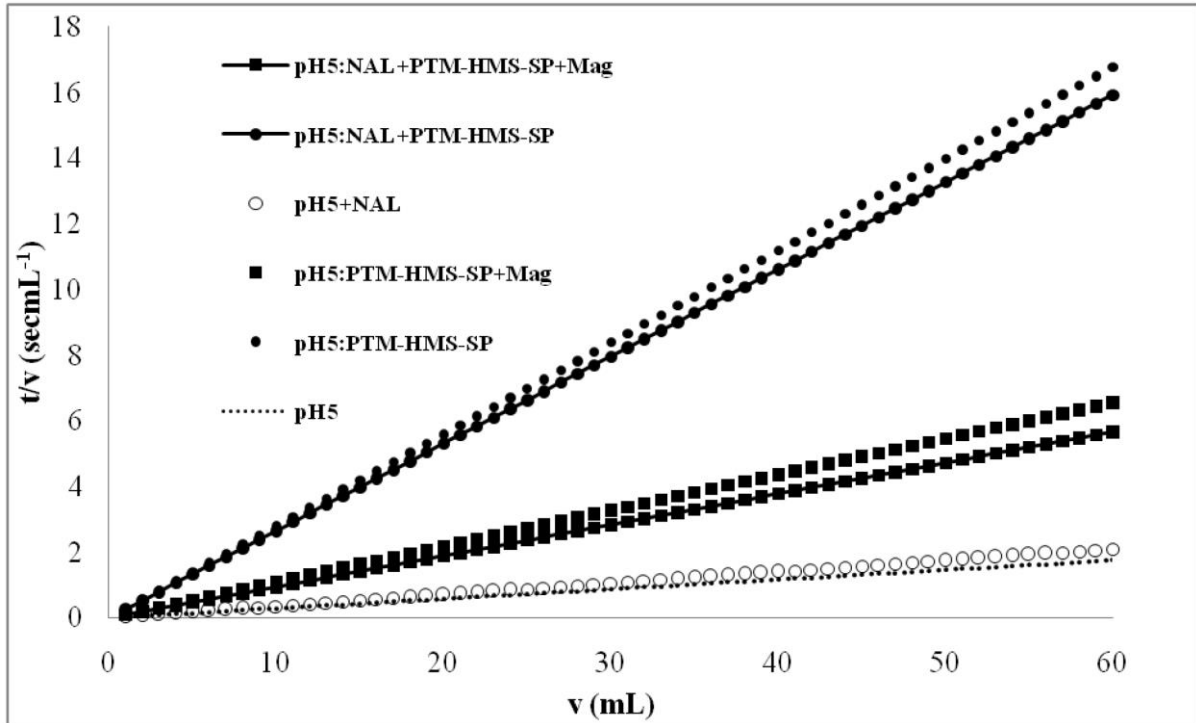


Figure 38 Relations between filtrate volume and time per filtrate volume,
at 25°C, IS = 0.01 M, pH = 5±0.2.

Table 6 Parameters for the cake building equation calculation.

Parameter		Value
A	the filter area (m ²)	0.0128
μ	the dynamic viscosity of the water at 25°C (Pa s)	8.9×10^{-4}
Δp	the transmembrane pressure drop (Pa)	10^5
k	the concentration coefficient (dimensionless)	0.001

Table 7 The Filter Media Resistance and the Specific Cake Resistance at pH = 5±0.2

Experiment	R_c (1/m ²)	R_m (1/m)
pH5	1.075	13.057
pH5:NAL	1.285	18.133
pH5:PTM-HMS-SP	10.294	5.079
pH5:PTM-HMS-SP+mag	4.021	15.238
pH5:NAL+PTM-HMS-SP	9.771	2.532
pH5:NAL+PTM-HMS-SP+Mag	3.479	10.790

R_m values were not similar to each other which might result from recycling usage of UF membrane. The lines of pH5 and NAL under pH5 (without P-HMS-SP) almost performed no slope and very low R_c which confirmed no cake formation in the system. After applied P-HMS-SP to the system under pH5 (without NAL), magnetic field greatly reduced R_c from 10.29 to 4.02 m⁻² which imply the slow-down of the cake formation.

Effects of NAL on magnetic system applied on ultrafiltration

NAL were added to the system to determine effect of NAL adsorbed by P-HMS-SP on cake formation. The filtrate flux was detected, and remained NAL concentration and adsorption

capacities are shown in table 8. The results confirmed that UF membrane could not reduce NAL concentration. And reducing of NAL concentration should be caused by adsorption on P-HMS-SP surface. The 2.85 mg/g adsorption capacity of NAL was determined. From the data obtain from table 8, the presence of NAL in the system did affect to R_c significantly.

Table 8 NAL Concentration of Initial and Filtrate Flux at pH = 5±0.2

Experiment	NAL Concentration (mg/L)		NAL Adsorption Capacity (mg/g)
	Initial	Filtrate Volume	
pH5:NAL	20.52	20.48	-
pH5:NAL+PTM-HMS-SP	20.8	19.75	2.85

From figure 38 and table 8, adsorbed NAL on P-HMS-SP surface resulted slightly decreasing of R_c (10.29 to 9.77 m²) which may caused by reducing interruption from attractive electrostatic interaction between materials and membrane surface. at pH5, surface charges of P-HMS-SP become slightly positive whereas regenerated cellulose membrane surface is negative. Attractive electrostatic interaction between virgin P-HMS-SP and membrane surface can activate fouling. Once NAL which become neutral at pH5 were adsorbed on adsorbent surface, slightly positive charges of P-HMS-SP surface were decreased or covered. The reduction of attractive electrostatic interaction between materials and membrane surface due to adsorbed NAL may lead to decreasing of R_c value. Effect of membrane surface charge, adsorbent and existing of NAL were investigated further in 4.4.3. However, according to figure 38 and table 8, application of magnetic field can significantly reduce R_c value of P-HMS-SP which adsorbed NAL on the surface as well (9.77 to 3.48 m²). The results indicated that combination of magnetic system and existing of NAL on P-HMS-SP surface under pH5 can enhance UF by slow down cake formation.

Effects of Electrostatic Interaction (by changing pH)

Electrostatic interaction was suggested to involve in cake formation on UF membrane surface. This experiment was established to study effect of membrane surface charge. Electrostatic interaction of applied membrane, adsorbents and NAL at pH 5 and 7 were summarized in table 9. Table 10 confirmed that NAL cannot interact with UF membrane surface at both of pH 5 and 7. Thus only P-HMS-SP can interact with NAL in the system.

Table 9 Electrostatic interaction of each material at pH = 5 \pm 0.2 and 7 \pm 0.2

	Electrostatic Charge		
pH	NAL	Regenerated Cellulose Membrane	P-HMS-SP
5	Neutral	Negative	Slightly Positive
7	Negative	Negative	Negative

Table 10 NAL Concentration of initial and filtrate volume at pH = 5 \pm 0.2 and 7 \pm 0.2

Experiment	NAL Concentration (mg/l)		NAL Adsorption Capacity (mg/g)
	Initial	Filtrate Volume	
pH5:NAL	20.52	20.48	-
pH5:NAL+PTM-HMS-SP	20.8	19.75	2.85
pH7:NAL	20.45	20.44	-
pH7:NAL+PTM-HMS-SP	20.1	19.08	1.02

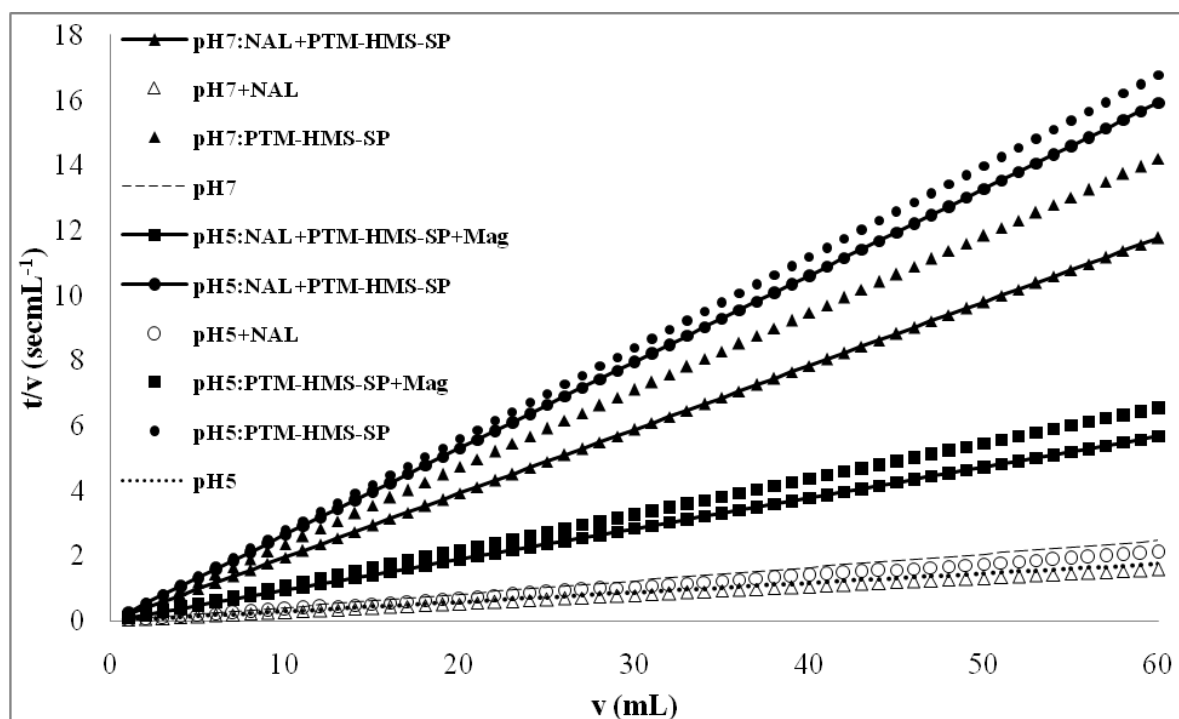


Figure 39 Relations between filtrate volume and time per filtrate volume, at at 25°C, IS = 0.01 M, pH = 5 \pm 0.2, 7 \pm 0.2.

From Figure 39 and table 11, obtained slopes and very low R_c in case of no P-HMS-SP was not significantly different between pH 5 and 7, which indicated no cake formation in the system. Presence of P-HMS-SP at pH 7 provided less R_c than at pH 5 as shown in table 11, which might be caused by the role of electrostatic interaction. Negative surface charge of P-HMS-SP under pH 7 performed repulsive electrostatic interaction with negative charge of UF membrane that might reduce the cake formation.

Table 11 The filter media resistance and the specific cake resistance at pH = 5 \pm 0.2, 7 \pm 0.2

Experiment	R_c (1/m ²)	R_m (1/m)
pH5	1.075	13.057
pH5:NAL	1.285	18.133
pH5:PTM-HMS-SP	10.294	5.079
pH5:PTM-HMS-SP+mag	4.021	15.238
pH5:NAL+PTM-HMS-SP	9.771	2.532
pH5:NAL+PTM-HMS-SP+Mag	3.479	10.789
pH7	1.513	14.335
pH7:NAL	0.965	17.431
pH7:PTM-HMS-SP	8.718	4.325
pH7:NAL+PTM-HMS-SP	7.216	7.662

The filtrate volume was also illustrated in Figure 4.18 to ensure the slow-down of membrane fouling caused by repulsive electrostatic interaction. Highest repulsive electrostatic interaction of PTM-HMS-SP with NAL adsorbed under pH 7 performed the highest filtrate flux following by PTM-HMS-SP without NAL under pH 7, PTM-HMS-SP with NAL under pH 5 and without NAL under pH 5 respectively.

Conclusions

The overall goal of this study was to systematically examine and clarify the adsorption mechanisms that controlled pharmaceutical residues (including by-products) adsorption (NAL, CIP, SMX, ACT, NAP, DCF, CBZ, HANs, etc.) on the various types of hybrid organic-inorganic adsorbents such as HMS-SPs, PMOs, porous silicas, GO modified HMSs, and GO modified SBA-15s, particularly to understand the roles and effects of hydrophobic interaction, hydrogen bonding

and electrostatic interaction of each organic functional groups on target pharmaceutical residues adsorption. Finally, the selective adsorption of pharmaceutical residues was also evaluated and quantitatively analyzed the comparison of single and mixed solutes adsorption, including the effect of tannic acid (TA) on pharmaceuticals adsorption.

From adsorption kinetics studies, all experimental data was well fitted with the pseudo-second-order kinetic model. Adsorption equilibrium stage of all antibiotics could be reached within 30 min. According to the intraparticle diffusion model, the CIP adsorption on HMS-SPs was governed by the intraparticle diffusion while the adsorption of NAL and SMX was controlled by the film diffusion. Among PMO materials, virgin PMO had the lowest initial adsorption rate. The initial adsorption rate of PMOs seemed to increase as the amount of added n-silane was increased. The adsorption kinetic of CIP, CBZ, CFA and NAP on GO modified HMS and SBA-15 including PAC were reported the best fit with the pseudo-second order model. Intraparticle diffusion mechanism of CIP, CBZ, CFA and NAP exhibited that amine functional group could reduce the rate of adsorption by steric effect as well as the contrast of hydrophilic-hydrophobic like.

For adsorption mechanism, the adsorption isotherms were investigated under the different pH function and evaluated by FT-IR spectra. Hydrophobic interaction via van der Waals force, π - π electron-donor-acceptors interaction and electrostatic interaction was suggested to be the main adsorption interaction. The adsorption capacity of organic functional groups modified HMS-SPs, HMSs and SBA-15s for pharmaceuticals increased after modification strongly related to hydrophobicity of each functional group. The adsorption capacity of PMOs for CFA increased after surface modification with mono-, di- and tri-organosilane. The adsorption capacity of PMO derivatives varied with the type and density of amine functional groups on their surface.

According to adsorption selectivity study, the active surface areas of all synthesized adsorbents were enough for three antibiotics adsorption in mixed solutes condition at concentration range lower than $1 \mu\text{g L}^{-1}$. The adsorption of adsorbents for DCF, CBZ and NAP in which hydrogen bonding and hydrophobic interactions were the main mechanism of adsorption. The adsorption capacity in this case might be related to the molecular size of the adsorbates. But in case of selective adsorption of amino functionalized adsorbents for acidic pharmaceuticals such as DCF, NAP and CFA which have negatively charged molecules, the adsorption capacity varied with the pK_a values of the adsorbates.

In addition, there was no interrupted by the co-existing TA as NOM under the antibiotics adsorption. Interestingly, there were two phenomenons in the adsorption of antibiotic in the presence of TA. Firstly, multilayer could be formed between amine functional group surface and TA, and then the antibiotic (CIP) was interacted with already adsorbed TA as the new layer. Secondly, there were the competitive between the individual antibiotic especially for both antibiotics (NAL and SMX) and TA molecule. Moreover, the presence of TA in mixed antibiotics solute can enhance the CIP adsorption capacities on A-HMS-SP and OD-HMS-SP.

To investigate separation magnetic particle by HGMS filter, the breakthrough time was increasing by extending bed depth of stainless filter and decreasing flow rate. However, higher and lower surface area of stainless filter did not affect to breakthrough curve but it can be failed when surface area was not enough. Low density of particles were captured easier than high density because low density had more remained space to catch the particle than high density. Moreover, application of BDST model can be matched with HGMS filter, due to high correlation coefficient. Nevertheless, BDST model cannot apply with changing flow rate and particle concentration.

After applying magnetic system on UF separation system, greatly reduction of cake resistance (R_c) can be observed which indicated reducing of membrane fouling from P-HMS-SP. A special configuration of the magnet system caused a slow down of the cake built-up due to by an external magnetic force and interparticulate magnetic force. Moreover, electrostatic interaction between adsorbent and membrane surface was found to affect on R_c value.

References

- Brigante, M., et al. (2010) Effect of humic acids on the adsorption of paraquat by goethite. *Journal of Hazardous Materials* 184: 241-247.
- Bui, T.X., and Choi, H. (2010) Influence of ionic strength, anions, cations, and natural organic matter on the adsorption of pharmaceuticals to silica. *Chemosphere*, 80: 681-686.
- Busca, G., et al. (2008). Removal and recovery of nitriles from gaseous streams: An IR study of acetonitrile adsorption on and desorption from inorganic solids. *Colloids and Surfaces A: Physicochemical and Engineering Aspects* 320: 205-212.
- Carabineiro, S.A.C., et al., (2011) Adsorption of ciprofloxacin on surface-modified carbon materials. *Water Research* 45: 4583-4591.

- Carabineiro, S.A.C., et al. (2012) Comparison between activated carbon, carbon xerogel and carbon nanotubes for the adsorption of the antibiotic ciprofloxacin. *Catalysis Today* 186: 29-39.
- Dai, X., et al., (2009) Adsorption characteristics of N-nitrosodimethylamine from aqueous solution on surface-modified activated carbons. *Journal of Hazardous Materials* 168:51-56.
- de Villiers, M. M., et al. (2008). *Nanotechnology in Drug Delivery*, Springer New York.
- Dimos, K., et al., (2009) Synthesis and characterization of hybrid MCM-41 materials for heavy metal adsorption. *Microporous and Mesoporous Materials*. 126: 65–71.
- Huang, Y.-L., et al. (2011). "Effect of extended polymer chains on properties of transparent graphene nanosheets conductive film." *Journal of Materials Chemistry* 21(45): 18236-18241.
- Janssen, A. H., et al. (2002). A 3D-TEM study of the shape of mesopores in SBA-15 and modified SBA-15 materials. *Chemical Communications*, 15: 1632-1633.
- Lai, L., et al. (2011). "One-step synthesis of NH₂-graphene from in situ graphene-oxide reduction and its improved electrochemical properties." *Carbon* 49(10): 3250-3257.
- Lin, A.Y.-C., et al., (2008) Pharmaceutical contamination in residential, industrial, and agricultural waste streams: Risk to aqueous environments in Taiwan. *Chemosphere* 74: 131-141.
- Nie, Y., et al. (2014). Removal of clofibric acid from aqueous solution by polyethylenimine-modified chitosan beads. *Frontiers of Environmental Science & Engineering* 8(5): 675-682.
- Prarat, P., et al., (2011) Adsorption characteristics of haloacetonitriles on functionalized silica-based porous materials in aqueous solution, *Journal of Hazardous Materials*. 192: 1210-1218.
- Pulido, A., et al. (2012). "Reconstruction of the carbon sp² network in graphene oxide by low-temperature reaction with CO." *Journal of Materials Chemistry* 22(1): 51-56.
- Saad, R., et al., (2008) Adsorption of phosphate and nitrate anions on ammonium-functionnalized mesoporous silicas, *Journal of Porous Materials*. 15: 315–323.

- Wang, C., et al., (2010) A simple method for preparation of superparamagnetic porous silica. Journal of Alloys and Compounds 493(1-2): 410-414.
- Wang, J., et al., (2011) Behaviors and mechanisms of tannic acid adsorption on an amino-functionalized magnetic nanoadsorbent. Desalination 273: 285-291.
- Wei, F., et al., (2009) Modifying MCM-41 as an efficient nitrosamine trap in aqueous solution. Solid State Sciences 11:402-410.
- Yang, A., et al. (2015). One-step amine modification of graphene oxide to get a green trifunctional metal-free catalyst. Applied Surface Science 346: 443-450.
- Yang, A., et al. (2015). One-step amine modification of graphene oxide to get a green trifunctional metal-free catalyst. Applied Surface Science 346: 443-450.
- Yi, Z., et al. (2011) Green, effective chemical route for the synthesis of silver nanoplates in tannic acid aqueous solution. Colloids and Surfaces A: Physicochemical and Engineering Aspects, 392: 131-136.
- Zhou, C. F. and Zhu, J. H. (2005) Adsorption of nitrosamines in acidic solution by zeolites. Chemosphere 58:109-114.

Output จากโครงการวิจัยที่ได้รับทุนจาก สกว.

1. ผลงานตีพิมพ์ในวารสารวิชาการนานาชาติ
 - 1) Adsorption of single and mixed haloacetonitriles on silica-based porous materials: Mechanisms and effects of porous structures
Journal of Environmental Science (impact factor 3.120)
สถานะ : Accept
(ภาคผนวก ก)
 - 2) Selective adsorption mechanism of antibiotic in the presence of co-existing tannic acid (TA) by superparamagnetic porous silicate (เอกสารแนบที่ 2)
อยู่ระหว่างเตรียมการส่งพิจารณาเพื่อตีพิมพ์ในวารสาร Separation Science and Technology ในช่วงเดือน กันยายน พ.ศ. 2561
(ภาคผนวก ข)

2. การนำผลงานวิจัยไปใช้ประโยชน์

- เชิงวิชาการ

ผลิตบัณฑิตในระดับมหาบัณฑิตภายใต้โครงการวิจัย จำนวน 5 คน ได้แก่

1) น.ส. มัณชิมา ทองจีน

วิศวกรรมศาสตรมหาบัณฑิต จุฬาลงกรณ์มหาวิทยาลัย ปีการศึกษา 2558

2) นาย พณภัทร เกิดสมุทร

วิศวกรรมศาสตรมหาบัณฑิต จุฬาลงกรณ์มหาวิทยาลัย ปีการศึกษา 2559

3) น.ส. จิตสุภา สุดโกทา

วิทยาศาสตรมหาบัณฑิต จุฬาลงกรณ์มหาวิทยาลัย ปีการศึกษา 2558

4) น.ส. วรรณชลัช เสถียรธรรมณี

วิทยาศาสตรมหาบัณฑิต จุฬาลงกรณ์มหาวิทยาลัย ปีการศึกษา 2558

5) นายต่อศักดิ์ นวนิล

วิศวกรรมศาสตรมหาบัณฑิต จุฬาลงกรณ์มหาวิทยาลัย ปีการศึกษา 2560

3. อื่นๆ (เช่น ผลงานตีพิมพ์ในวารสารวิชาการในประเทศ การเสนอผลงานในที่ประชุมวิชาการ หนังสือ การจดสิทธิบัตร)

- การนำเสนอผลงานในที่ประชุมวิชาการจำนวน 5 เรื่อง ได้แก่

1) การดูดซับคาร์บอนาซีป็นและซัลฟาเมโทซาโซลโดยถ่านกัมมันต์ชนิดผงและเกร็ด
มัณชิมา ทองจีน และ ปฏิภาณปัญญาพลกุล

การประชุมวิชาการสิ่งแวดล้อมแห่งชาติครั้งที่ 15

วันที่ 11-13 พฤษภาคม 2559 โรงแรมเดอะ ทวิน ทาเวอร์ กรุงเทพมหานคร

2) Adsorption of 17- α Methyltestosterone on Modified Graphene Oxide with
Superparamagnetic Particle

Panapatt Kerdsamut and Patiparn Punyapalakul

5th International conference on environmental engineering, science and
management, May 11-13, 2016 at The Twin Towers Hotel Bangkok,
Thailand.

3) Adsorption of clofibric acid and naproxen on graphene modified SBA-15

Wanchalach Sathienthammanee and Patiparn Punyapalakul

5th International conference on environmental engineering, science and
management, May 11-13, 2016 at The Twin Towers Hotel Bangkok,
Thailand.

4) Removal of Ciprofloxacin and Carbamazepine by Graphene Oxide Modified
Bi-functional Group Mesoporous Silica

Jitsupa Suthkota and Patiparn Punyapalakul

5th International conference on environmental engineering, science and management, May 11-13, 2016 at The Twin Towers Hotel Bangkok, Thailand.

- 5) Effect of Porous Structures on Adsorption of Pharmaceutical Residues by Metal Organic Frameworks

Patiparn Punyapalakul, Dujduan Sompornpailin and Chalita Ratanatawanate

24th Thai-Korea Conference on Environmental Engineering in Jeonju, Korea between 17-20 April 2018

- 6) Adsorption Mechanisms of Pharmaceutical Residues on Periodic Mesoporous Organosilicas in the presence of Dissolved Organic Matter

Surawut Siratham, Khemarath Osathaphan and Patiparn Punyapalakul

24th Thai-Korea Conference on Environmental Engineering in Jeonju, Korea between 17-20 April 2018

ภาคผนวก ก

Your manuscript JES_2018_528_R3 has been accepted

Journal of Environmental Sciences (Journal of Environmental Sciences) <EvisSupport@elsevier.com>

Wed 9/12/2018 3:04 PM

To: Patiparn Punyapalakul <Patiparn.P@chula.ac.th>;

Ref: JES_2018_528_R3

Title: Adsorption of single and mixed haloacetonitriles on silica-based porous materials: Mechanisms and effects of porous structures

Journal: Journal of Environmental Sciences

Dear Dr. Punyapalakul,

I am pleased to inform you that your paper has been accepted for publication. My own comments as well as any reviewer comments are appended to the end of this letter. Now that your manuscript has been accepted for publication it will proceed to copy-editing and production.

Thank you for submitting your work to Journal of Environmental Sciences. We hope you consider us again for future submissions.

Kind regards,

Journal of Environmental Sciences

Editorial office

Journal of Environmental Sciences

Comments from the editors and reviewers:

Have questions or need assistance?

For further assistance, please visit our [Customer Support](#) site. Here you can search for solutions on a range of topics, find answers to frequently asked questions, and learn more about EVISE® via interactive tutorials. You can also talk 24/5 to our customer support team by phone and 24/7 by live chat and email.

Copyright © 2018 Elsevier B.V. | [Privacy Policy](#).

Elsevier B.V., Radarweg 29, 1043 NX Amsterdam, The Netherlands, Reg. No. 33156677.

Manuscript Details

Manuscript number	JES_2018_528_R3
Title	Adsorption of single and mixed haloacetonitriles on silica-based porous materials: Mechanisms and effects of porous structures
Article type	Research Paper

Abstract

Adsorption mechanisms and the role of different porous and crystalline structures on the removal of five haloacetonitriles (HANs) over Hexagonal mesoporous silica (HMS), titanium substituted mesoporous silica (Ti-HMS), rod-shaped SBA-15 and microporous zeolite NaY were investigated. In addition, the effect of pH on adsorption mechanism and selective adsorption of five HANs individually and in an equimolar mixed solution were evaluated. The results indicated that the intraparticle diffusion rate constants of the mesoporous adsorbents were higher than that of the microporous NaY. In single solute, the order of adsorption preference (highest to lowest) was mono-HANs > di-HANs > tri-HAN. However, in mixed solute, the large molecular weight of the tri-HAN and di-HANs are more easily adsorbed than the smaller molecular weight mono-HANs. Except for SBA-15, the order of adsorption capacities in mixed HANs solute was not different compared to that observed for the single HAN solute, which might be caused by the higher accessibility to the active sites due to larger pore size. The ion-dipole electrostatic interaction was likely to be the main adsorption mechanism, and was favored at high pH values due to the high negative surface charge density of the adsorbent. The molecular structure of the HANs and hydrophilic/hydrophobic nature affected the adsorption capacities and their selective adsorption from mixed solutes.

Keywords	haloacetonitrile; adsorption mechanism; porous structure; ion-dipole electrostatic interaction; hydrophilicity
Taxonomy	Water, Emerging Contaminant
Manuscript region of origin	Asia Pacific
Corresponding Author	Patiparn Punyapalakul
Corresponding Author's Institution	Chulalongkorn University
Order of Authors	Panida Prarat, Chawalit Ngamcharussrivichai, Sutha Khaodhiar, Patiparn Punyapalakul
Suggested reviewers	Heechul Choi, Jian Xu, David Sabatini

Submission Files Included in this PDF

File Name [File Type]

Cover Letter.docx [Cover Letter]

JES_reviewer response_3rd revision.docx [Response to Reviewers]

Highlights.docx [Highlights]

Graphical Abstract.docx [Graphical Abstract]

Title page_3rd.docx [Title Page (with Author Details)]

JES_manuscript_3rd minor revised_completed.docx [Manuscript File]

Author agreement.pdf [Author Agreement]

To view all the submission files, including those not included in the PDF, click on the manuscript title on your EVISE Homepage, then click 'Download zip file'.

Research Data Related to this Submission

There are no linked research data sets for this submission. The following reason is given:
Data will be made available on request

Cover Letter

Adsorption of single and mixed haloacetonitriles on silica-based porous materials: Mechanisms and effects of porous structures

Panida Prarat, Chawalit Ngamcharussrivichai, Sutha Khaodhiar and
Patiparn Punyapalakul

Corresponding author :

Patiparn Punyapalakul, Ph.D.

Department of Environmental Engineering,
Faculty of Engineering, Chulalongkorn University,
Bangkok , Thailand, 10330

Tel: +662-218-6686; Fax: +662-218-6666;

E-mail: patiparn.p@chula.ac.th

Response to Reviewer's comments

Journal: Journal of Environmental Sciences

Ref: JES_2018_528_R2

**Title: Adsorption of single and mixed haloacetonitriles on silica-based porous materials:
Mechanisms and effects of porous structures**

Comments from the editors and reviewers:

The manuscript is still needed to a further format before final decision can be given.

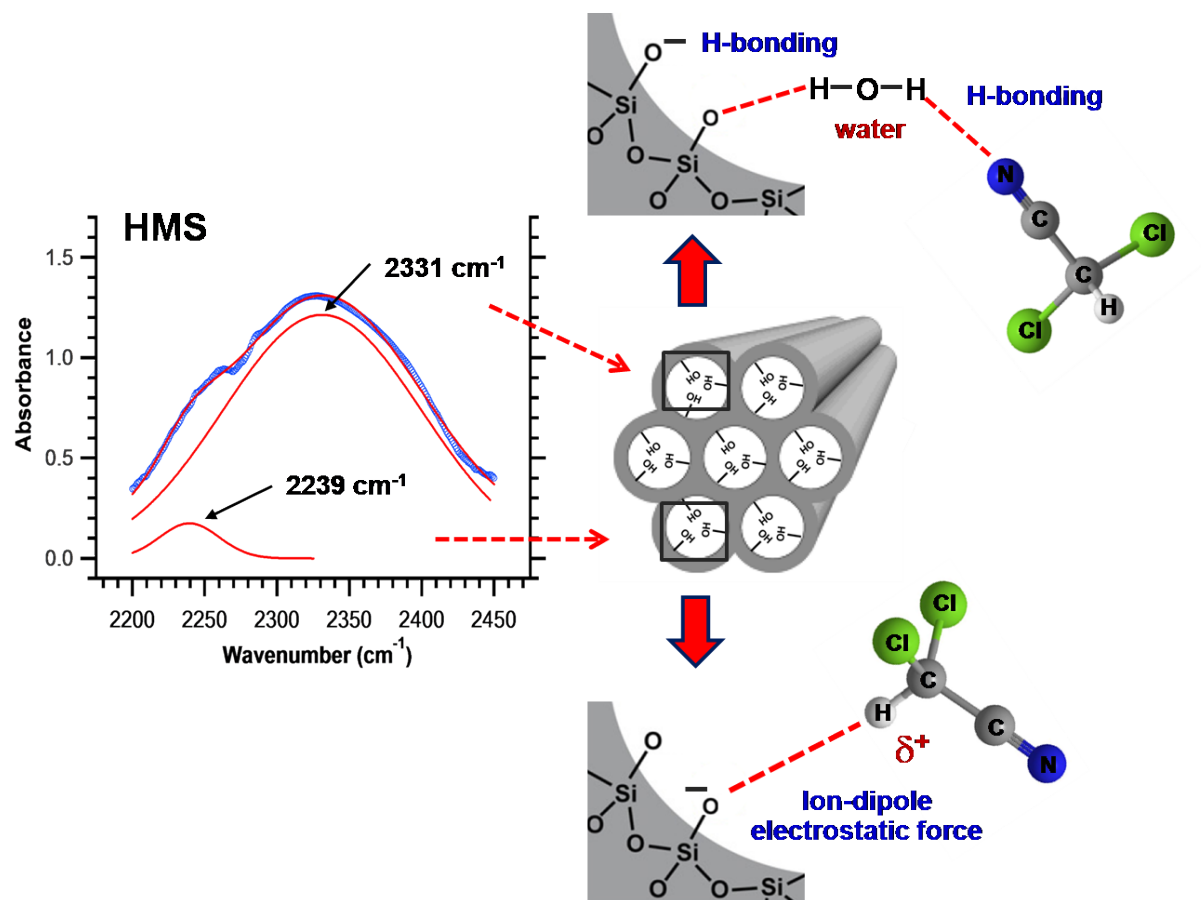
Please pay more attention on reference style, and format all figures, unit, and so on. The attached is a JES format sample.

Response: The manuscript has been rechecked following the attached file “JES sample 2018”. Reference style and format of all figures have been edited as the editor comments.

Highlights

- > First report of mixed HANs adsorption mechanisms on silica-based materials.
- > Adsorption of HANs occurs via an ion-dipole electrostatic interaction.
- > Lewis acid sites play an important role for adsorption.
- > Selective adsorption is in the order of mono-HANs > di-HANS > tri-HAN.

Graphical Abstract



Title Page

Adsorption of single and mixed haloacetonitriles on silica-based porous materials: Mechanisms and effects of porous structures

Panida Prarat ^{1,2}, Chawalit Ngamcharussrivichai ^{3,4}, Sutha Khaodhiar ⁵,

Patiparn Punyapalakul ^{2,5,6,7 *}

¹ International Postgraduate Programs in Hazardous Substance and Environmental Management, Graduate School, Chulalongkorn University, Bangkok 10330, Thailand

² Center of Excellence on Hazardous Substance Management (HSM), Chulalongkorn University, Bangkok 10330, Thailand

³ Department of Chemical Technology, Faculty of Science, Chulalongkorn University, Bangkok 10330, Thailand

⁴ Center for Petroleum, Petrochemicals and Advanced Materials, Chulalongkorn University, Bangkok 10330, Thailand

⁵ Department of Environmental Engineering, Faculty of Engineering, Chulalongkorn University, Bangkok 10330, Thailand

⁶ Research unit Control of Emerging Micropollutants in Environment, Chulalongkorn University, Bangkok, 10330, Thailand

⁷ Research Network of Chula and NANOTEC (RNN)

*Corresponding author :

Patiparn Punyapalakul, Ph.D.

Department of Environmental Engineering,

Faculty of Engineering, Chulalongkorn University,

Bangkok , Thailand, 10330

Tel: +662-218-6686; Fax: +662-218-6666;

E-mail: patiparn.p@chula.ac.th

ORCID: 0000-0001-7280-0339

**Adsorption of single and mixed haloacetonitriles on silica-based porous materials:
Mechanisms and effects of porous structures**

Panida Prarat ^{1,2}, Chawalit Ngamcharussrivichai ^{3,4}, Sutha Khaodhiar ⁵,

Patiparn Punyapalakul ^{2, 5, 6,7 *}

1. International Postgraduate Programs in Hazardous Substance and Environmental Management, Graduate School, Chulalongkorn University, Bangkok 10330, Thailand.
2. Center of Excellence on Hazardous Substance Management (HSM), Chulalongkorn University, Bangkok 10330, Thailand.
3. Department of Chemical Technology, Faculty of Science, Chulalongkorn University, Bangkok 10330, Thailand.
4. Center for Petroleum, Petrochemicals and Advanced Materials, Chulalongkorn University, Bangkok 10330, Thailand.
5. Department of Environmental Engineering, Faculty of Engineering, Chulalongkorn University, Bangkok 10330, Thailand
6. Research unit Control of Emerging Micropollutants in Environment, Chulalongkorn University, Bangkok, 10330, Thailand.
7. Research Network of Chula and NANOTEC (RNN)

Received 03 March 2018

Revised 22 August 2018

Accepted

Abstract: Adsorption mechanisms and the role of different porous and crystalline structures on the removal of five haloacetonitriles (HANs) over Hexagonal mesoporous silica (HMS), titanium substituted mesoporous silica (Ti-HMS), rod-shaped SBA-15 and microporous zeolite NaY were investigated. In addition, the effect of pH on adsorption mechanism and selective adsorption of five HANs individually and in an equimolar mixed solution were evaluated. The results indicated that the intraparticle diffusion rate constants of the mesoporous adsorbents were higher than that of the microporous NaY. In single solute, the order of adsorption preference (highest to lowest) was mono-HANs > di-HANs > tri-HAN. However, in mixed

solute, the large molecular weight of the tri-HAN and di-HANs are more easily adsorbed than the smaller molecular weight mono-HANs. Except for SBA-15, the order of adsorption capacities in mixed HANs solute was not different compared to that observed for the single HAN solute, which might be caused by the higher accessibility to the active sites due to larger pore size. The ion-dipole electrostatic interaction was likely to be the main adsorption mechanism, and was favored at high pH values due to the high negative surface charge density of the adsorbent. The molecular structure of the HANs and hydrophilic/hydrophobic nature affected the adsorption capacities and their selective adsorption from mixed solutes.

Keywords:

Haloacetonitrile

Adsorption mechanism

Porous structure

Ion-dipole electrostatic interaction

Hydrophilicity

* Corresponding author . E-mail: patiparn.p@chula.ac.th (Patiparn Punyapalakul)

Introduction

Haloacetonitriles (HANs) are nitrogenous disinfection by-products (DBPs) that have recently been reported to have a much higher toxicity than the two other major groups of DBPs, the trihalomethanes (THMs) and haloacetic acids (HAAs) (Plewa et al., 2008). A relative high HANs of 88.4 µg/L was detected in tap water in turkey (Baytak et al., 2008). Based on our preliminary survey, the most prevalent species among HANs in tap water of Bangkok, Thailand, was dichloroacetonitrile (DCAN) at range from 2.5 to 27 µg/L. Due to their health effects, the World Health Organization has suggested guideline maximal permitted values of DCAN and dibromoacetonitrile (DBAN) present in drinking water supplies at 20 and 70 µg/L, respectively (WHO, 2011). Several diverse techniques have been employed as point-of-use (POU) to remove DBPs from the (aqueous) environment, such as by adsorption (Babi et al., 2007; Kim and Kang, 2008), ozonation (Ratasuk et al., 2008), boiling (Shi et al., 2017), vacuum UV irradiation (Kiattisaksiri et al., 2016) and membrane filtration (Uyak et al., 2008). However, degradation intermediates of HANs from treatment processes such as 2-

chloropropionitrile, 2,2-dimethylpropanenitrile and fumaronitrile were detected after reactions (Kiattisaksiri et al., 2016). Among POU treatments, the adsorption process has been favored for water treatment due to its advantages of a relatively low cost, low intermediates and simplicity. Consequently, a lot of effort has been focused upon the development of various materials for the removal of DBPs from an aqueous phase (Prarat et al., 2013).

Apart from activated carbon, micropore adsorbents, such as zeolites, are widely used for water treatment and in the catalyst fields. Zeolites have a crystalline aluminosilicate structure where the Al^{3+} replacement of Si^{4+} forms a bridging hydroxyl group, the so-called Brønsted acid site. The proton of the Brønsted acid site inside the channel can introduce an electrostatic interaction towards negatively charged adsorbates. Nevertheless, its strong hydrophilicity hinders the adsorption of organic target molecules (typically of low hydrophilicity) in aqueous solution.

As an alternative to the microporous zeolites, mesoporous silicates seem to be promising adsorbents. Mesoporous silicates have a high surface area, a large pore volume and more suitable pore diameters. Pure hexagonal mesoporous silicate (HMS) and derivatives like SBA-15 are members of family of the mesoporous silicates. Due to differences in the pore system and pore size, such as a wormhole and pore size of 2 to 3 nm for HMS compared to a hexagonal with interconnected channels and a 6 to 8 nm pore size for SBA-15, the adsorption mechanism and phenomena of both materials would be expected to be different. Moreover, their surface modification with various organosilanes could improve the adsorptive capacity and selectivity (Prarat et al., 2011). Indeed, of these modifications the substitution of Si^{4+} with transition metal ions within the porous structures has received a great deal of attention due to the availability of transition metal species (such as Ti, Zr, Mn or Sn), and the presence of stable active sites. With respect to the adsorption, the incorporation of the transition metal into the mesopore framework can increase the number of surface adsorption sites. This has previously been shown to successfully allow the removal of various organic contaminants from the aqueous phase, such as surfactants (Punyapalakul and Takizawa, 2006a) and reactive dyes (Messina and Schulz, 2006) amongst others.

Moreover, only a limited amount of information on the adsorption of DBPs over micro- and meso- porous materials has been reported previously. Punyapalakul et al. (2009) found that the crystalline structure and surface area of adsorbents affected the adsorption of DCAA at low concentrations. Furthermore, the micropore size, relative pore volume and surface characteristics have all been reported to be important factors in determining the adsorption of *N*-nitrosodimethylamine (Dai et al., 2009). The adsorption phenomena of different porous

materials may be significantly different as a consequence of their porous structure (Zhang et al., 2006). However, the effect of the porous structure on the obtained adsorption is poorly understood or defined and needs further investigation.

To the best of our knowledge, the effect of the porous or crystalline structure nature of the adsorbent on the adsorption of HANs from an aqueous solution has not been studied. Towards a better understanding of the adsorption mechanism and the role of porous or crystalline structures on the adsorption, this study focused on investigating the relationship between the porous structures of the silica based adsorbent and the adsorption efficiency for HANs at a dilute concentration. For the mesoporous structures, pure silica HMS and rod-shaped SBA-15, and a metal substitute that incorporated titanium into the silica structure (Ti-HMS) were compared with the micropore zeolite NaY to investigate the effect of different porous and crystalline structures by comparison of their adsorption capacity. The experimentally derived equilibrium data were fitted with adsorption isotherm models, and the kinetic parameters were calculated to determine the likely adsorption mechanism(s). In addition, the effect of varying the solution pH (and so the surface charge density) of the adsorbents on the selective adsorption of the five different HANs (monochloroacetonitrile (MCAN), dichloroacetonitrile(DCAN), trichloroacetonitrile (TCAN), monobromoacetonitrile (MBAN) and dibromoacetonitrile (DBAN)), both as single and as an equimolar mixed solution were also investigated.

1 Materials and methods

1.1 Adsorbent synthesis

1.1.1 Siliceous HMS and titanium-substituted HMS synthesis

Synthesis of HMS was performed following the procedure described by Lee et al. (2001), and titanium-substituted HMS (Ti-HMS) was synthesized according to previously reported procedures (Punyapalakul and Takizawa, 2006b; Tanev et al., 1994).

1.1.2 SBA-15 synthesis

SBA-15 was prepared using Pluronic P123 as the template as previously reported (Imperor-Clerc et al., 2000).

1.1.3 NaY zeolite preparation

Commercial Na-form Y zeolite, denoted as NaY, was purchased from Tosoh Corporation, Japan. NaY was thermally pretreated under static conditions at 400 °C for 3 hr with a heating rate of 1 °C/min (Punyapalakul et al., 2009).

1.2 Characterization of adsorbents

Details on the methods of characterization along with the resulting physicochemical properties of HMS, Ti-HMS and NaY were as previously reported (Punyapalakul et al., 2009; Punyapalakul and Takizawa, 2006), and are summarized in **Table 1**. For SBA-15, its structural analysis was performed by X-ray diffractometry (XRD) on a powder X-ray diffractometer equipped with Cu K α radiation (DMAX 2200, Rigaku, Japan). The XRD patterns were collected in the range of $2\theta = 0.5$ -6°. Textural properties of SBA-15 were analyzed with an Autosorb-1 Quantachrome automatic volumetric sorption analyzer at 77 K. The specific surface area and pore diameter were calculated according to the Brunner-Elmer-Teller (BET) and Barrett-Joyner-Halenda (BJH) equations, respectively. X-ray photoelectron spectroscopy (XPS) spectrum was taken by using DLD system operated at 150 W (Axis ultra, Kratos, Japan). Morphology of the adsorbent samples were taken using a scanning electron microscope (SEM) (JSM-5410LV, JEOL, Japan). Hydrophilic characteristics of the adsorbent surface were evaluated by measuring the water contact angle (θ) using a tensiometer in a powder contact angle mode (DCAT-11, Dataphysics, Germany). Fourier transform infrared spectrophotometry (FT-IR) based analysis of the adsorbent surface was performed to investigate the adsorptive interaction. The adsorbent powder mixed with KBr was compressed to form a self-support wafer, and the FT-IR spectra were recorded in the transmittance mode between 4,000 and 400 cm⁻¹.

1.3 Adsorption study

The evaluation of the aqueous-phase adsorption of HANs was conducted as a batch experiment. Stock solutions of HANs were prepared in 10 mM phosphate buffer at the indicated pH. In a typical procedure, 0.025 g of adsorbent and 35 mL of HAN solution were mixed in a 100 mL Erlenmeyer flask and covered with a glass stopper. The slurry was then stirred in a rotary shaker at 200 r/min (25 °C) until equilibrium, whereupon the solid matter was removed by a glass microfiber filter (GF/C) and the eluting supernatant was analyzed with a gas chromatograph equipped with an electron capture detector (GC/ECD), according to the EPA method 551.1. Each experiment was performed in duplicate under identical conditions.

The adsorption kinetics were evaluated at pH 7 by varying the equilibrating time over 10 intervals from 0 to 48 hr with an initial DCAN concentration of 100 µg/L. The adsorption isotherms of the five different HANs evaluated (MCAN, DCAN, TCAN, MBAN and DBAN) in individual (single) solute solution were each constructed with different concentrations in the range of 25-300 µg/L. The effects of pH on the adsorption capacity were evaluated using 10 mM phosphate buffer at pH of 5, 7 and 9. In addition, the effect of the molecular structure (halogen type and degree of substitution) on the selective adsorption at pH 7 was evaluated using an equimolar mixture of the five different HANs.

2 Results and Discussion

2.1 Physicochemical characteristics of adsorbents

The XRD patterns of the as used HMS, Ti-HMS, SBA-15 and NaY samples are shown in **Fig. 1**. HMS exhibited the highest corresponding hexagonal porous structure with a clear (100) plane at $2\theta = 2.2^\circ$. A shift in the (100) plane to a higher 2θ angle was observed for the Ti-HMS, which can be attributed to a partial collapse of the HMS framework during the adsorbent synthesis. For SBA-15, three diffraction peaks were clearly revealed at $2\theta = 0.92^\circ$, 1.58° and 1.84° , which correspond to the (100), (110) and (200) planes, respectively, reflecting the well-defined hexagonal array of the mesopore. The standard peaks of the NaY were 6° , 10° , 12° , 15° , 18° , 20° , 24° , 27° and 31° (**Fig. 1b**). The patterns attained from the synthesized SBA-15 and the commercial NaY seen here are similar to those previously reported (Aguado et al., 2009; Sue-aok et al., 2010; Tao et al., 2010; Wei et al., 2005). The determined BET surface area, pore diameter and pore volume data, based on the N₂ adsorption-desorption isotherms (**Fig. 2**), are summarized in **Table 1** including the previously reported data from these same sample preparations. Additionally, the XPS technique has been used to investigate the surface chemical environment of HMS (**Fig. 3**). The survey spectrum of HMS reveals that the main elements of sample were Si and O (Si 2p at 104.6 eV and O 1s at 533.3 eV, respectively). SEM micrographs of HMS and SBA-15 are shown in **Fig. 4**. HMS exhibited an aggregated spherical particles, which is consistent with the report of Punyapalakul et al. (2009). Moreover, SBA-15 presented continuous rod-shaped structure.

The surface charge density, as Coulombs/m, of HMS, Ti-HMS, SBA-15 and NaY versus the pH are plotted in **Fig. 5**, where the three mesoporous silicates (HMS, Ti-HMS and SBA-15) showed a broadly similar pattern being positively charged at acidic ($\sim\text{pH} < 4.5$) and negatively charged at alkaline ($\sim\text{pH} > 6.0$) conditions with a broad near neutral charge range

from pH 4.5 to 6.0. In contrast, the NaY zeolite showed a markedly different profile, with a sharper transition (low near neutral pH range), being positively charged at a much higher pH range (< 7.5) and negatively charged at $\text{pH} > 7.8$ (**Table 1**), whilst the water contact angles (θ) varied over two-fold between the four adsorbents and were ranked $\text{HMS} \sim \text{SBA-15} > \text{Ti-HMS} > \text{NaY}$ (**Table 1**).

2.2. Adsorption kinetics

The kinetic curves of the DCAN adsorption on the porous materials, as plot of the relative adsorption capacity (q_t) versus time, are shown in **Fig. 6a**. The DCAN uptake by all four adsorbents (HMS, Ti-HMS, SBA-15 and NaY) was rapid at the beginning (within the first 4 h) and reached the equilibrium stage after ca. 18 hr. However, the amount of adsorbed DCAN (q_t) varied between the adsorbents being highest for HMS followed by $\text{NaY} > \text{Ti-HMS} > \text{SBA-15}$. To describe the adsorption phenomena, the adsorption kinetics were modeled using several mathematical expressions. The experimental data were fitted with the pseudo-first order and pseudo-second order equations, using Eqs. (1) and (2), respectively, as shown below:

$$q_t = q_e(1 - \exp(-k_1 t)) \quad (1)$$

$$q_t = \frac{q_e^2 k_2 t}{1 + q_e k_2 t} \quad (2)$$

where q_t and q_e are the amount of DCAN adsorbed at any given time (t) and at equilibrium ($\mu\text{g/g}$), respectively, k_1 and k_2 are the first-order rate constant ($1/\text{h}$) and the second-order rate constant ($\text{g}/\mu\text{g/h}$), respectively.

Note that in order to measure the adsorption rate, the initial adsorption rate, h ($\mu\text{g/g/h}$) at $t = 0$, and the half-life time, $t_{1/2}$ (hr), can be determined according to Eqs. (3) and (4), respectively:

$$h = k_2 q_e^2 \quad (3)$$

$$t_{1/2} = \frac{1}{k_2 q_e} \quad (4)$$

A normalized standard deviation Δq (%) was employed in this study to find out the most suitable kinetic model to fit the data. This error function has been used previously by a number of researchers in adsorption studies (Günay et al., 2007; Qin et al., 2009; Shaarani and Hameed, 2011), and is shown in Eq. (5):

$$\Delta q(\%) = 100 \times \sqrt{\frac{\sum \left[\frac{q_{\text{exp}} - q_{\text{cal}}}{q_{\text{exp}}} \right]^2}{N - 1}} \quad (5)$$

where N is the number of data points, and q_{exp} and q_{cal} ($\mu\text{g/g}$) are the experimental and the calculated adsorption capacities, respectively. The best-fit models should have the least Δq (%) values.

Both kinetic models were applied to the experimental data and the correlation coefficients (R^2) and Δq (%) were calculated by nonlinear regression using the ORIGIN version 8.0 software, with the results shown in **Table 2**. For all four adsorbents the pseudo-second order model gave a better fit to the data, as defined by the higher R^2 and significantly smaller Δq (%), than the pseudo-first order model. The adsorption mechanism on an adsorbent surface should be proportional to the driving force and area. In this study, the driving force is the adsorbate concentration in the solution, and the area is the amount of active sites on the adsorbent surface. Due to the low concentration of DCAN in this study ($100 \mu\text{g/L}$), the effect of water can essentially be neglected. Therefore, the pseudo-second order model is more suitable to describe the adsorption kinetics of DCAN on these porous adsorbents at a low solute concentration. Consistent with this notion is that Wu et al. (2009) reported that the pseudo-second order model was suitable to explain the adsorption of low molecular weight compounds on small adsorbent particles.

The pseudo-second order rate constant (k_2) value obtained was highest for HMS, followed by that for NaY, and so a higher amount of HMS sample is needed to adsorb a given amount of DCAN. In other words, overall NaY has a better adsorption performance (i.e. adsorption capacity and adsorption rate) for DCAN. Nevertheless, the initial DCAN adsorption rate (h) and the half-life time ($t_{1/2}$) of HMS was 2.13-fold higher and 1.56-fold lower, respectively, than that for NaY. Thus, NaY requires almost twice the time to achieve two-thirds the maximal level of DCAN uptake at the equilibrium stage, compared with that seen with HMS. Traditionally, the adsorption rate of a porous material is related to the porous structure of the adsorbents (Ruiz et al., 2010), and so the different adsorption behavior of HMS and NaY might be caused directly by the intrinsic characteristics of their porous structures. HMS has a much larger (3.51-fold) pore size and higher (2.37-fold) total pore volume (see **Table 1**) than NaY, which certainly favors a quicker initial adsorption rate. The molecular dimensions of DCAN, as calculated by the ACD/ChemSketch software (**Table 5**), is 0.29 nm wide and 0.36 nm long, and so the pore size clearly did not affect the accessibility of DCAN to the inner pores of the micropore NaY adsorbent.

Ti-HMS had a ~ 3.8 -fold lower initial adsorption rate than that for HMS even though Ti-HMS has a 1.22-fold larger pore size and 1.65-fold larger total pore volume than HMS. This difference in adsorption rate then might be because the surface of Ti-HMS is more hydrophilic than that of HMS, at least based on the 1.5-fold larger water contact angle (θ) of HMS compared to Ti-HMS (**Table 1**), and so the water molecules can surround the adsorbent

particle, causing a lower adsorption rate onto the Ti-HMS. Surprisingly, the initial adsorption rate (h) of the mesopore SBA-15, with a pore size of 6.0 nm, showed the lowest h value, for which a faster adsorption rate would have been expected. This is probably related to its pore feature which contains a combined micro- and meso-pore structure within the ordered mesopore structure.

2.3 Intraparticle diffusion mechanism

Theoretically, there are three mass transfer steps for a solid-liquid adsorption process; (i) film or external diffusion, (ii) pore diffusion and (iii) adsorption onto active sites at the interior of the adsorbent particle (Liu et al., 2010). However, the final step is assumed to be rapid and so is usually omitted in the kinetic analysis.

The intraparticle diffusion model developed by Weber and Morris (1963) was applied to investigate whether the adsorption process was limited by mass transfer within the film layer or by diffusion inside the adsorbent particles. The model can be defined as shown in Eq. (6):

$$q_t = k_{ip}t^{0.5} + C \quad (6)$$

where k_{ip} is the intraparticle diffusion rate constant ($\mu\text{g g}^{-1} \text{hr}^{0.5}$) and C ($\mu\text{g g}^{-1}$) is a constant that gives an idea of the thickness of the boundary layer.

The q_t versus $t^{0.5}$ relations display a differentiated linearity for all four adsorbents (**Fig. 6b**), indicating that multiple adsorption steps are associated in the adsorption process. The first linear region represents the diffusion of DCAN in the boundary layer (film or external diffusion) and is followed by the diffusion of DCAN molecules through the porosity of the adsorbent (intraparticle diffusion). Finally, the third step is the equilibrium plateau (the horizontal line at last region).

The external diffusion step, occurring in the initial period of adsorption process (at up to 0.5-2.0 $\text{hr}^{0.5}$, depending upon the adsorbent) was measured by determining the rate constant (k_f) obtained from the slope of the first linear region, where a larger k_f value means a faster external diffusion rate. The rate constant (k_f) of HMS, Ti-HMS, SBA-15 and NaY are listed in **Table 2**, and suggest that an external mass transfer is predominant at the initial contact time. Comparison of the k_f values between HMS and SBA-15 revealed, surprisingly, that the external diffusion rate of SBA-15 was 2.56-fold lower than that for HMS even though its pore size is 2.3-fold larger. However, the external diffusion rate may be related to the particle size of the adsorbent. Because the external/internal surface area ratio of SBA-15, with its smaller particles,

is larger than that for HMS with its larger particle size, this might make it difficult for the DCAN molecules to diffuse through the boundary layer.

The second region in **Fig. 6b**, from 1.5-2.0 to 4-4.5 hr^{0.5}, represents the step at which the intraparticle diffusion starts to control the rate of adsorption. Here, the pore size of the adsorbent material might influence the adsorption rate. Thus, for instance, the intraparticle diffusion rate constants (k_{ip1}) of the silica-based mesoporous adsorbents (HMS, Ti-HMS and SBA-15) were higher than that of the microporous NaY (**Table 2**). Consequently, DCAN can diffuse more easily in the larger pore size of the mesoporous silicate based adsorbents than in the smaller pore size of NaY. Moreover, it can be seen that SBA-15 had four apparent mass transfer steps in the adsorption process, where the second region of the plot seems to refer to the diffusion into the wider mesopores and, for the third region with the lowest slope, the adsorption into narrow micropores.

The intercept of the second region corresponds to the boundary layer thickness, where the larger the observed interception is then the greater is the boundary layer effect. The existence of a boundary layer effect was apparent in all four adsorbents, suggesting that intraparticle diffusion was not the only rate-controlling step for DCAN adsorption.

2.4 Adsorption isotherms

2.4.1. Adsorption mechanism evaluation from FT-IR analysis

Considering the molecular structure of each of the five different HANs and their charge distribution (**Table 3**), calculated by minimum energy optimization using MOPAC, two important mechanisms are revealed to be involved in the adsorption process; namely, hydrogen bonding and electrostatic interactions (ion-dipole interaction). Hydrogen bonding occurs via an interaction between the surface functional groups of the silanol group –OH moiety, and the nitrogen atom (N3) of the respective HAN molecule. The surface functional groups are ionized under different pH conditions, so the electrostatic force (ion-dipole interaction) derived from the interaction between $\equiv\text{Si-O}^-$, Lewis acid sites of Ti-HMS, Na^+ , etc., and the opposite charge positions of the HAN molecules are pH dependent.

To identify the adsorptive interaction during the surface adsorption, HMS was saturated with a 500 $\mu\text{g/mL}$ DCAN solution in 10 mM phosphate buffer (pH 7) and FT-IR analysis was conducted on the surface of HMS and the FT-IR spectrum was analyzed by the IGOR Pro version 6.0 software. The $\text{C}\equiv\text{N}$ stretching of the nitrile group has been reported to be located at around 2,250 cm^{-1} (Busca et al., 2008; Kozyra et al., 2006). Here, the spectrum of HMS

showed two peaks (**Fig. 7a**). The downward shift of the minor peak at 2,239.39 cm^{-1} can be assigned to the interaction of the silanol group ($\equiv\text{Si-O}^-$) and the positive dipole of the H-atom (H6) in DCAN. The DCAN nitrile group may be weak after interacting with the silanol group ($\equiv\text{Si-O}^-$) via ion-dipole electrostatic interaction, causing a downward shift of the $\text{C}\equiv\text{N}$ stretching. Due to the low concentration of the DCAN solute in our case study, the single intensive upward shift at 2,331.17 cm^{-1} might be evidence of hydrogen bonding between the physisorbed water molecule on the HMS surface and the DCAN nitrile group.

In the region of the O-H bending of the adsorbed water (**Fig. 7b**), the band at 1,630.39 cm^{-1} represents the physisorbed water molecules. Interestingly, there was a new peak formed at 1,701.00 cm^{-1} (**Fig. 7b**) that corresponds to the $\text{C}=\text{N}$ stretching, which might be caused by a weaker nitrile group due to ion-dipole electrostatic interactions. This result is consistent with the appearance of a downward shift in the $\text{C}\equiv\text{N}$ stretching at 2,239.39 cm^{-1} (**Fig. 7a**). From the FT-IR results, ion-dipole electrostatic interactions between the nitrile and silanol groups (deprotonated form) were identified as a mechanism that likely plays an important role in HAN adsorption.

2.4.2. Effect of porous and crystalline structures on HANs adsorption

The effect of the porous and crystalline structures of the four adsorbents on the adsorption capacities of the five different HANs (MCAN, DCAN, TCAN, MBAN and DBAN) at pH 7 are shown in **Fig. 8**. To exclude the effect of the differences in surface area between the four adsorbents, the adsorption capacities were standardized for the surface area and are presented accordingly as $\mu\text{g}/\text{m}^2$. Ti-HMS had the highest adsorption capacities of both mono-HANs (MCAN and MBAN). Of the three mesoporous adsorbents, although HMS had a somewhat similar mean pore size to Ti-HMS (81.8% of the Ti-HMS level), the observed adsorption capacities of MCAN and MBAN were slightly and significantly lower, respectively, for HMS than that for Ti-HMS. This is probably due to the significantly (1.65-fold) higher pore volume of Ti-HMS (**Table 1**), as determined by N_2 adsorption. Thus, the accessibility of the mono-HANs molecules to the internal pores of Ti-HMS is better than that for HMS leading to a higher adsorption capacity. In addition, the Lewis acid site on the Ti-HMS surface, is a stronger acid than the weak acidic silanol group in the pure silica-based HMS and SBA-15, and so could enhance the adsorption capacity by the synergic adsorption of the ion-dipole interactions from both functional groups. Previous reports have found that the active Lewis and Brønsted acid sites can promote adsorption by interacting with the nitrile ($\text{N}\equiv\text{C}$) and nitroso ($\text{N}=\text{NO}$) groups

in the adsorbate molecules (Busca et al., 2008; Dai et al., 2009). Thus, the surface functional group of the adsorbent also plays an important role in adsorption.

However, the mesopore SBA-15 showed the lowest adsorption capacity of all four adsorbents for the two mono-HANs, MCAN and MBAN, compared with the other adsorbents. The negative surface charge derived from dissociation of silanol groups could contribute to the electrostatic interaction with the ion-dipole of the HANs and thus HAN adsorption. The significantly larger mean pore size (6.0 nm) of SBA-15 might reduce its ability to confine smaller sized adsorbates, such as these two mono-HANs. A similar result has been reported previously, where the adsorption capacity of nitrosamine on SBA-15 was lower than on the smaller (2.22-fold) pore diameter of MCM-41 (2.7 nm) (Wei et al., 2009). Thus, the pore size is clearly likely to be a key factor controlling mono-HAN adsorption.

In the case of NaY, the positively charged surface is due to the combination of the protonated silanol group and the Na^+ at pH 7. Since the N-atom (N3) of each HAN possesses a negative dipole, they can be electrostatically adsorbed onto the positively charged surface. As seen, the adsorption of the mono-HANs exhibited a comparable adsorption capacity to that for HMS and Ti-HMS (excepting for the adsorption of MBAN that was less than Ti-HMS), although NaY has a relatively low surface area and pore volume (see **Table 1**). One possible explanation is that the small pore size (0.74 nm) and porous structure of NaY could be effective in retaining the mono-HANs. In this scenario, the crystalline structure and narrow diameter pore size (micropores) of zeolite NaY provides a delicate geometric confinement of small adsorbate molecules (Zhou and Zhu, 2005), and so suggests that the crystalline structure of the adsorbent can affect the adsorption capacity of mono-HANs.

The adsorption capacities of the di-HANs (DCAN and DBAN) on HMS, Ti-HMS and NaY (**Fig. 8c & 8d**) were less than that of the mono-HANs, whereas, in contrast, SBA-15 showed a slightly higher capacity. However, the adsorption capacities are likely to be related to the molecular structure of the HANs in terms of the amount of halogen atoms in the molecule and their molecular weight, as will be discussed in Section 3.4.5. Moreover, that the adsorption capacity of DBAN is higher than DCAN might be because of the stronger positive dipole of the H-atom in DBAN.

The TCAN adsorption isotherm (**Fig. 8e**) showed the adsorption capacity followed the sequence $\text{Ti-HMS} > \text{NaY} > \text{SBA-15} > \text{HMS}$, and suggests that the Lewis acid sites of Ti-HMS and the Na^+ of NaY significantly influenced the adsorption capacities. This supports the notion that the surface functional group plays a crucial role in adsorption.

2.4.3 Isotherm models

In order to model the adsorption isotherm, four isotherm models (Linear, Langmuir, Freundlich and Dubinin and Radushkevich (D-R)) were employed to describe the different adsorption behaviors on the adsorbents seen in this study. Due to the linear-shaped adsorption response observed at these low initial concentrations of HANs, the adsorption isotherm of HMS, Ti-HMS, SBA-15 and NaY were fitted with a Linear isotherm, as shown in Eq. (7):

$$q_e = K_p C_e \quad (7)$$

where K_p is linear partition coefficient that is obtained from the slope of a plot of q_e versus C_e .

The Langmuir isotherm model (Eq. (8)) is based on the assumption that a monolayer coverage of adsorbate occurs over homogeneous sites, whilst the Freundlich isotherm model (Eq. (9)) is an empirical equation employed to describe a heterogeneous system.

$$q_e = \frac{q_m K_L C_e}{1 + K_L C_e} \quad (8)$$

$$q_e = K_F C_e^{1/n} \quad (9)$$

where q_m is the maximum adsorption capacity ($\mu\text{g/g}$), K_L is Langmuir constant, and K_F ($\mu\text{g/g}$) and n are Freundlich constants.

The derived Linear, Langmuir and Freundlich isotherm parameters are listed in **Table 4**. Since the equilibrium concentration was low, the Linear isotherm fits well to the experimental results with a high R^2 (> 0.91), except for the case of MCAN adsorption on NaY ($R^2 = 0.855$). A high K_p value indicates a high affinity of adsorbent for HAN adsorption. For the adsorption of HANs onto the Ti-HMS and NaY adsorbents, the data best fits the Freundlich model, as evidenced from the R^2 values, which supports the heterogeneous distribution of the silanol groups and the Lewis acid sites in the titanium substitution of Ti-HMS, and the Na^+ and silanol groups on the NaY surface. On the other hand, the adsorption equilibrium of HANs on SBA-15 was likely to be described by both models, implying a multilayer coverage may occur on homogeneous surface of silanol group uniformity on SBA-15 surface. However, the HAN adsorption data distribution on HMS fitted well with the Freundlich model rather than the Langmuir one, despite the fact that the surface of HMS has a relatively uniform silanol group distribution. Note, however, that the evaluation of the adsorption at high HAN concentrations is required for confirmation.

The isotherm data were also applied to the D-R isotherm model to evaluate whether the adsorption energy best fitted a physical or chemical adsorption. The non-linearized equation of the D-R model can be written as Eq. (10):

$$q_e = q_m \exp^{-K_D \varepsilon^2} \quad (10)$$

where q_e (mol/g) is the amount of HANs adsorbed on the adsorbent; q_m (mol/g) is the maximum adsorption capacity; K_D (mol² /kJ²) is the constant related to adsorption energy; ε is the Polanyi potential, which is equal to $RT \ln(1+1/C_e)$; C_e (mol/L) is the equilibrium concentration of HANs; R (kJ/ mol / K) is the universal gas constant and T (K) is the temperature in Kelvin. The q_m and K_D values were obtained from the experimental data after plotting as q_e versus ε^2 .

The mean free energy of adsorption (E , kJ/mol), defined as the free energy change when 1 mol of adsorbate is transferred to the surface of a solid from infinity in solution (Zhan et al., 2011), can be calculated from Eq. (11):

$$E = (2K_D)^{-0.5} \quad (11)$$

The adsorption energy (E) is then used to estimate the type of adsorption. If the E value is below 4 (kJ/mol), then the adsorption mechanism can be explained by physical adsorption (i.e. Van der Waals force), whilst E values between 4 and 38 (kJ/mol) are explained by physical adsorption (ion-dipole, dipole-dipole forces including hydrogen bonding) (Solomons, 1996). The E values for the adsorption of the five different HANs on the four adsorbents (HMS, Ti-HMS, SBA-15 and NaY) ranged from between 6.39 to 10.86 kJ/mol, suggesting that electrostatic interactions (i.e. ion-dipole force) are likely to be the main adsorption mechanism. However, in general a low adsorption energy was measured for the two mono-HANs (MCAN and MBAN), which could be explained as that they are more easily adsorbed onto the adsorbents.

2.4.4 Effect of pH on DCAN adsorption

The adsorption capacities of DCAN on the adsorbents at pH 5, 7 and 9 are presented in **Fig. 9**. Increasing the pH of the solution from 5 to 7 and especially from 7 to 9 resulted in a higher DCAN adsorption on all four adsorbents. The surface of these four adsorbents is more negatively charged at pH 9 due to the increasing dissociation of the silanol group, the major functional group on the surface of these adsorbents. The charge of the H-atom in DCAN is supposed to be more positive, as calculated by the ChemOffice Ultra 2005 (**Table 3**). Therefore, the negative surface silanol charges could attract the positive dipole of the DCAN H-atom (H6) via an ion-dipole electrostatic interaction. In addition, the density of the negative surface charge (per square meter) of adsorbents at pH 9 was higher than that at pH 5 and 7 (see **Fig. 5**), leading to a higher adsorption capacity. The low adsorption capacities at pH 5 might be due to the hydrogen ion strongly competing with the positive H6 dipole of DCAN for the

same negatively charged adsorptive sites on the surface of the four adsorbents. This supports an ionic interaction adsorption mechanism, in agreement with the D-R isotherm model and suggesting that the adsorption mechanism is believed to occur via an ion-dipole electrostatic interaction.

2.4.5. Selective adsorption of five-HANs in single-solute and mixed-solute solutions

Adsorption isotherms for the five-HANs alone (single solutes) on HMS, Ti-HMS, SBA-15 and NaY are shown in **Fig. 10a, 10c, 10e and 10g**, respectively. The order of adsorption preference (highest to lowest) was MCAN > MBAN > DCAN > DBAN > TCAN on HMS, Ti-HMS and NaY, which implies that the adsorption capacities may relate to the strength of the positive/negative dipoles in the respective HANs. The strongest positive dipole of the two H-atom of the mono-HANs provides an enhancement of the ion-dipole electrostatic force and the strongest negative dipole of N-atom in mono-HANs molecule (**Table 4**) could interact with Lewis acid site of Ti-HMS and Na⁺ of NaY, leading to a higher adsorption capacity. Moreover, these selective adsorption behaviors might be linked to the surface characteristics of each adsorbent. The hydrophilic surface characteristics of all four adsorbents would be expected to selectively adsorb a hydrophilic adsorbate in the order of mono-HANs > di-HANs > tri-HAN. However, except for SBA-15, the adsorption of the five HANs displayed a reverse order of adsorption preference (**Fig. 10e**). For SBA-15, the larger molecular weight of tri-HAN was adsorbed more than the di-HANs and mono-HANs. This difference may be related to the porous structure of SBA-15, which seems to be a more important factor in controlling adsorption. A larger pore size might enhance the internal surface accessibility and let the larger molecular structure HANs (**Table 3**) be adsorbed better than on adsorbents with smaller sized pores. Regardless, these results indicate that the adsorption capacity of the five different HANs on the four adsorbents is related to the molecular structure of the HANs. Moreover, the hydrophilic / hydrophobic nature of both the adsorbent and the adsorbate can influence the selective adsorption.

The adsorption isotherms for the five HANs when presented as an equimolar mixed solute on the four adsorbates (**Fig. 10**) are consistent with the notion that the active surfaces of each adsorbent had been divided between all five-HAN species causing a decrease in the observed adsorption capacity of each HAN. The order of adsorption capacities in this equimolar mixed HAN solute on HMS, Ti-HMS and NaY were significantly different from the single solute results (TCAN > DBAN \cong DCAN > MBAN \cong MCAN). The large molecular weight

of the tri-HAN and the two di-HANs are more easily adsorbed than the smaller molecular weight mono-HANs at low concentrations. Unlike SBA-15, the order of adsorption capacities of all five HANs was not different compared to that observed for the single HAN solute (**Fig. 10f**), which might be caused by the higher accessibility to the active sites due to larger pore size.

3 Conclusions

The adsorption of DCAN on all four adsorbents followed a pseudo-second order model, and the adsorption rate seemed to be controlled by external diffusion followed by the intraparticle diffusion in the pores. The adsorption of HANs was significantly influenced by the porous and crystalline structures, in terms of the pore size and volume, as well as by the surface functional group of the adsorbent. The experimentally derived isotherm data fitted well with the Linear, Langmuir, Freundlich and Dubinin-Redushkevich models. The adsorptive interactions between the five different HANs and the four types of adsorbents involve ion-dipole electrostatic interactions that are related to the pH_{PZC} of adsorbents. The molecular structure of the five HANs and their hydrophilic / hydrophobic nature affect their adsorptive capacity and selectivity.

Acknowledgements

The authors would like to acknowledge the financial support from The Thailand Research Fund, Thailand under grant no. RSA5880018 and the 90th Anniversary of Chulalongkorn University Fund (Ratchadaphiseksomphot Endowment Fund). This work was carried out as a part of research of research program in “Hazardous Substance Management in Agricultural Industry” granted by the Center of Excellence on Hazardous Substance Management (HSM). This work has been partially supported by the National Nanotechnology Center (NANOTEC), NSTDA, Ministry of Science and Technology, Thailand, through its program of Research Network NANOTEC (RNN).

References

- Aguado, J., Arsuaga, J. M., Arencibia, A., Lindo, M., Gascón, V., 2009. Aqueous heavy metals removal by adsorption on amine-functionalized mesoporous silica. *J. Hazard. Mater.* 163, 213-221.

- Babi, K.G., Koumenides, K.M., Nikolaou, A.D., Makri, C.A., Tzoumerkas, F.K., Lekkas, T.D., 2007. Pilot study of the removal of THMs, HAAs and DOC from drinking water by GAC adsorption. *Desalination* 210, 215-224.
- Baytak, D., Sofuoglu, A., Inal, F., Sofuoglu, S.C., 2008. Seasonal variation in drinking water concentrations of disinfection by-products in IZMIR and associated human health risks. *Sci. Total. Environ.* 407, 286-296.
- Busca, G., Montanari, T., Bevilacqua, M., Finocchio, E., 2008. Removal and recovery of nitriles from gaseous streams: An IR study of acetonitrile adsorption on and desorption from inorganic solids. *Colloids Surf. A. Physicochem. Eng. Asp.* 320, 205-212.
- Dai, X., Zou, L., Yan, Z., Millikan, M., 2009. Adsorption characteristics of N-nitrosodimethylamine from aqueous solution on surface-modified activated carbons. *J. Hazard. Mater.* 168, 51-56.
- Günay, A., Arslankaya, E., Tosun, I., 2007. Lead removal from aqueous solution by natural and pretreated clinoptilolite: Adsorption equilibrium and kinetics. *J. Hazard. Mater.* 146, 362-371.
- Imperor-Clerc, M., Davidson, P., Davidson, A., 2000. Existence of a Microporous Corona around the Mesopores of Silica-Based SBA-15 Materials Templated by Triblock Copolymers. *J. Am. Chem. Soc.* 122, 11925-11933.
- Kiattisaksiri, P., Khan, E., Punyapalakul, P., Ratpukdi, T., 2016. Photodegradation of haloacetonitriles in water by vacuum ultraviolet irradiation: Mechanisms and intermediate formation. *Water Res.* 98, 160-167.
- Kim, J., Kang, B., 2008. DBPs removal in GAC filter-adsorber. *Water Res.* 42, 145-152.
- Kozyra, P., Salla, I., Montanari, T., Datka, J., Salagre, P., Busca, G., 2006. FT-IR study of the adsorption of carbon monoxide and of some nitriles on Na-faujasites: Additional insight on the formation of complex interactions. *Catal. Today*, 114, 188-196.
- Lee, B., Kim, Y., Lee, H., Yi, J., 2001. Synthesis of functionalized porous silicas via templating method as heavy metal ion adsorbents: the introduction of surface hydrophilicity onto the surface of adsorbents. *Microporous Mesoporous Mater.* 50, 77-90.
- Liu, Q.S., Zheng, T., Wang, P., Jiang, J.P., Li, N., 2010. Adsorption isotherm, kinetic and mechanism studies of some substituted phenols on activated carbon fibers. *Chem. Eng. J.* 157, 348-356.
- Messina, P.V., Schulz, P.C., 2006. Adsorption of reactive dyes on titania-silica mesoporous materials. *J. Colloid Interface Sci.* 299, 305-320.

- Plewa, M.J., Wargner, E.D., Muellner, M.G., Hsu, K. M., Richardson, S. D., 2008. Comparative mammalian cell toxicity of N-DBPs and C-DBPs. Symposium Series 995, Washington, District of Columbia, US.
- Prarat, P., Ngamcharussrivichai, C., Khaodhiar, S., Punyapalakul, P., 2011. Adsorption characteristics of haloacetonitriles on functionalized silica-based porous materials in aqueous solution. *J. Hazard. Mater.* 192, 1210-1218.
- Prarat, P., Ngamcharussrivichai, C., Khaodhiar, S., Punyapalakul, P., 2013. Removal of haloacetonitriles in aqueous solution through adsolubilization process by polymerizable surfactant-modified mesoporous silica. *J. Hazard. Mater.* 244-245, 151-159.
- Punyapalakul, P., Soonglerdsongpha, S., Kanlayaprasit, C., Ngamcharussrivichai, C., Khaodhiar, S., 2009. Effects of crystalline structures and surface functional groups on the adsorption of haloacetic acids by inorganic materials. *J. Hazard. Mater.* 171, 491-499.
- Punyapalakul, P., Takizawa, S., 2006a. Selective adsorption of nonionic surfactant on hexagonal mesoporous silicates (HMSs) in the presence of ionic dyes. *Water Res.* 40, 3177-3184.
- Punyapalakul, P., Takizawa, S., 2006b. Effect of surface functional group on adsorption of organic pollutants on hexagonal mesoporous silicate. *Water Sci. Tech. Water Supply.* 6, 17-25.
- Qin, Q., Ma, J., Liu, K., 2009. Adsorption of anionic dyes on ammonium-functionalized MCM-41. *J. Hazard. Mater.* 162, 133-139.
- Ratasuk, C., Kositanont, C., Ratanatamskul, C., 2008. Removal of haloacetic acids by ozone and biologically active carbon. *Sci. Asia*, 34, 293-298.
- Ruiz, B., Cabrita, I., Mestre, A. S., Parra, J. B., Pires, J., Carvalho, A. P., et al., 2010. Surface heterogeneity effects of activated carbons on the kinetics of paracetamol removal from aqueous solution. *Appl. Surf. Sci.* 256, 5171-5175.
- Shaarani, F.W., Hameed, B.H., 2011. Ammonia-modified activated carbon for the adsorption of 2,4-dichlorophenol. *Chem. Eng. J.* 169, 180-185.
- Shi, W., Wang, L., Chen, B., 2017. Kinetics, mechanisms, and influencing factors on the treatment of haloacetonitriles (HANs) in water by two household heating devices. *Chemosphere*, 172, 278-285.
- Solomons, T.W.G., 1996. *Fundamentals of Organic Chemistry* (5th ed.). Wiley, New York.
- Sue-aok, N., Srithanratana, T., Rangsriwatananon, K., Hengrasmee, S., 2010. Study of ethylene adsorption on zeolite NaY modified with group I metal ions. *Appl. Surf. Sci.* 256, 3997-4002.

- Tanev, P.T., Chibwe, M., Pinnavaia, T.J., 1994. Titanium-containing mesoporous molecular sieves for catalytic oxidation of aromatic compounds. *Nature*, 368, 321-323.
- Tao, Q., Xu, Z., Wang, J., Liu, F., Wan, H., Zheng, S., 2010. Adsorption of humic acid to aminopropyl functionalized SBA-15. *Microporous Mesoporous Mater.* 131, 177-185.
- Uyak, V., Koyuncu, I., Oktem, I., Cakmakci, M., Toroz, I., 2008. Removal of trihalomethanes from drinking water by nanofiltration membranes. *J. Hazard. Mater.* 152, 789-794.
- Weber, W.J., Morris, J.C., 1963. Kinetics of adsorption on carbon from solution. *J. Sanit. Eng. Div. ASCE*. 89, 561-578.
- Wei, F., Gu, F.N., Zhou, Y., Gao, L., Yang, J., Zhu, J.H., 2009. Modifying MCM-41 as an efficient nitrosamine trap in aqueous solution. *Solid State Sci.* 11, 402-410.
- Wei, Q., Nie, Z., Hao, Y., Chen, Z., Zou, J., Wang, W., 2005. Direct synthesis of thiol-ligands-functionalized SBA-15: Effect of 3-mercaptopropyltrimethoxysilane concentration on pore structure. *Mater. Lett.* 59, 3611-3615.
- WHO, 2011. Guidelines for drinking-water quality. WHO, Geneva, Switzerland.
- Wu, F.C., Tseng, R.L., Huang, S.C., Juang, R.S., 2009. Characteristics of pseudo-second-order kinetic model for liquid-phase adsorption: A mini-review. *Chem. Eng. J.* 151, 1-9.
- Zhan, Y., Lin, J., Zhu, Z., 2011. Removal of nitrate from aqueous solution using cetylpyridinium bromide (CPB) modified zeolite as adsorbent. *J. Hazard. Mater.* 186, 1972-1978.
- Zhang, X., Li, A., Jiang, Z., Zhang, Q., 2006. Adsorption of dyes and phenol from water on resin adsorbents: Effect of adsorbate size and pore size distribution. *J. Hazard. Mater.* 137, 1115-1122.
- Zhou, C.F., Zhu, J.H., 2005. Adsorption of nitrosamines in acidic solution by zeolites. *Chemosphere*, 58, 109-114.

List of tables

Table 1 Physicochemical characteristics of the synthesized adsorbents

Materials	Surface functional group	Mean pore diameter (nm)	V_P (mm ³ /g)	S_{BET} (m ² /g)	pH _{PZC}	Contact angle (θ)
HMS	Silanol	3.48	917	524	4.5	45.1
Ti-HMS	Lewis acid site and silanol	2.74	1214	938	4.7	30.9
SBA-15	Silanol	6.00	981	654	4.8	44.2
NaY	Lewis acid site and silanol	0.74 ^a	326 ^a	653 ^a	7.8 ^a	20.4

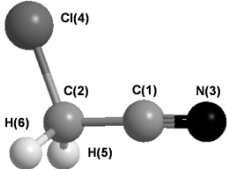
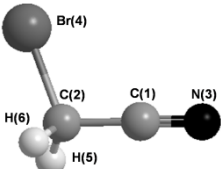
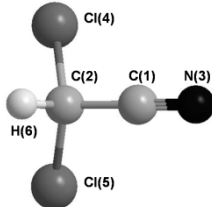
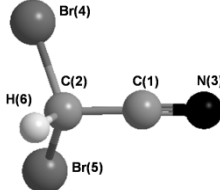
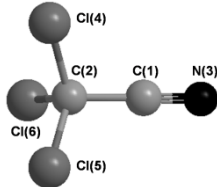
^a Punyapalakul (2009)

Table 2 Kinetic parameters of DCAN adsorption onto the adsorbents using the pseudo-first-order, pseudo-second-order and intraparticle diffusion models.

Materials	$q_{e,exp}$ ($\mu\text{g/g}$)	Pseudo-first-order				Pseudo-second-order						Weber and Moris (Intraparticle diffusion)						
		$q_{e,cal}$ ($\mu\text{g/g}$)	k_1 (1/h)	R^2	Δq (%)	$q_{e,cal}$ ($\mu\text{g/g}$)	k_2 (g/ $\mu\text{g/h}$)	R^2	Δq (%)	h ($\mu\text{g/g/h}$)	$t_{1/2}$ (h)	k_f ($\mu\text{g/g/h}^{0.5}$)	K_{ip1} ($\mu\text{g/g/h}^{0.5}$)	Intercept (C)	R^2	K_{ip2} ($\mu\text{g/g/h}^{0.5}$)	Intercept (C ₂)	R^2
HMS	29.10	26.87	0.452	0.942	4.398	29.29	0.021	0.962	2.008	18.063	1.611	11.506	5.219	7.985	0.999	-	-	-
Ti-HMS	18.41	17.86	0.225	0.968	0.852	20.33	0.015	0.979	0.063	4.745	3.880	9.183	2.326	7.646	0.918	-	-	-
SBA-15	15.35	15.06	0.113	0.978	2.361	18.29	0.007	0.984	1.304	1.532	10.023	4.490	2.653	3.083	0.944	0.867	9.552	0.961
NaY	21.39	20.29	0.289	0.958	1.595	22.36	0.018	0.982	0.068	8.496	2.518	7.433	2.295	9.493	0.997	-	-	-

Abbreviations used; q_e =Adsorption capacity (amount of DCAN adsorbed at equilibrium), experimental ($_{exp}$) or theoretical ($_{cal}$); k_1 and k_2 = the first and second order rate constant; h = initial adsorption rate; $t_{1/2}$ = half life for maximal adsorption; Δq = normalized standard deviation; k_f = external diffusion rate constant; k_{ip} = interparticle diffusion rate constant; and C = boundary layer constant.

Table 3 Molecular structure, molecular dimension, water solubility and charge distribution of MCAN, MBAN, DCAN, DBAN and TCAN molecules.

Parameters	HANs									
	MCAN		MBAN		DCAN		DBAN		TCAN	
Molecular structure										
MW (g/mol)	75.50		119.95		109.94		198.85		144.39	
Width (Å)	2.43		2.52		2.89		2.52		2.90	
Length (Å)	3.10		3.15		3.61		3.75		3.60	
Solubility (mg/mL)	100		50-100		10-50		10-50		< 1	
Charge distribution ^a	C(1)	-0.1304	C(1)	-0.1205	C(1)	-0.1254	C(1)	-0.1089	C(1)	+0.1136
	C(2)	-0.1324	C(2)	-0.2513	C(2)	-0.0239	C(2)	-0.2460	C(2)	-0.1298
	N(3)	-0.0537	N(3)	-0.0542	N(3)	-0.0177	N(3)	-0.0219	N(3)	+0.0027
	Cl(4)	-0.0838	Br(4)	+0.0094	Cl(4)	-0.0362	Br(4)	+0.0633	Cl(4)	+0.0044
	H(5)	+0.2002	H (5)	+0.2083	Cl(5)	-0.0364	Br(5)	+0.0632	Cl(5)	+0.0044
	H(6)	+0.2002	H(6)	+0.2083	H(6)	+0.2399	H(6)	+0.2504	Cl(6)	+0.0048

^a Calculated by ChemOffice Ultra 2005

Table 4 Isotherm parameters derived from the Linear, Langmuir, and Freundlich models for the adsorption of HANs from a single solute onto HMS, Ti-HMS, SBA-15 and NaY adsorbents.

Materials	HANs	Linear		Langmuir			Freundlich			D-R			
		K_p	R^2	q_m (μg/g)	K_L (L/μg)	R^2	K_F (μg/g)	$1/n$	R^2	q_m (mol/g)	K_d (mol ² /kJ ²)	E (kJ/mol)	R^2
HMS	MCAN	1.122	0.990	107.18	0.013	0.725	0.0002	3.007	0.876	0.9530	0.0120	6.46	0.9843
	DCAN	0.237	0.958	140.85	0.015	0.993	1.563	1.261	0.996	5.53E-05	0.0043	10.85	0.9824
	TCAN	0.189	0.926	12.41	0.004	0.983	0.028	1.245	0.987	0.0340	0.0101	7.05	0.9785
	MBAN	0.731	0.924	96.15	0.024	0.902	0.286	3.502	0.935	0.8006	0.0122	6.39	0.9172
	DBAN	0.263	0.984	102.56	0.005	0.920	0.004	1.749	0.981	0.0179	0.0099	7.12	0.9804
Ti-HMS	MCAN	1.028	0.954	166.76	0.009	0.902	0.172	1.399	0.925	5.08E-04	0.0054	9.62	0.9152
	DCAN	0.170	0.957	250.00	0.044	0.965	1.430	0.713	0.948	4.06E-04	0.0067	8.65	0.9622
	TCAN	0.464	0.911	172.41	0.002	0.774	0.155	1.232	0.966	3.97E-04	0.0058	9.28	0.8895
	MBAN	1.369	0.978	454.54	0.002	0.854	0.001	3.013	0.916	0.0485	0.0092	7.36	0.9421
	DBAN	0.441	0.989	188.68	0.001	0.954	0.002	1.980	0.971	0.0254	0.0096	7.22	0.9747
SBA-15	MCAN	0.224	0.966	41.67	0.002	0.887	0.0003	2.266	0.995	0.0015	0.0080	7.93	0.8487
	DCAN	0.215	0.962	118.48	0.003	0.991	2.679	1.152	0.991	7.05E-05	0.0049	10.12	0.9889
	TCAN	0.229	0.994	60.98	0.007	0.999	0.823	0.756	0.988	3.49E-05	0.0042	10.86	0.9994
	MBAN	0.197	0.960	61.39	0.006	0.852	0.001	2.041	0.975	0.0213	0.0103	6.98	0.9637
	DBAN	0.280	0.979	133.33	0.002	0.966	0.075	1.248	0.960	9.13E-04	0.0069	8.49	0.9782
NaY	MCAN	1.629	0.855	117.65	0.002	0.928	0.0001	3.071	0.940	1.3554	0.0121	6.42	0.9638
	DCAN	0.150	0.985	95.24	0.002	0.922	0.007	1.966	0.873	3.42E-05	0.0044	10.71	0.9862
	TCAN	0.581	0.948	90.09	0.010	0.800	0.128	1.315	0.987	0.0013	0.0066	8.70	0.9394
	MBAN	0.504	0.933	222.22	0.003	0.964	0.006	1.915	0.916	9.90E-04	0.0066	8.70	0.8990
	DBAN	0.168	0.955	72.99	0.003	0.980	0.0002	2.287	0.821	0.0022	0.0081	7.84	0.9566

Abbreviations used; K_p = linear partition coefficient; q_m = maximum adsorption capacity; K_L = Langmuir constant; K_F = Freundlich constant; n = Freundlich constant related to adsorption intensity; K_d = the constant related to adsorption energy; and E = mean free energy of adsorption.

List of figures

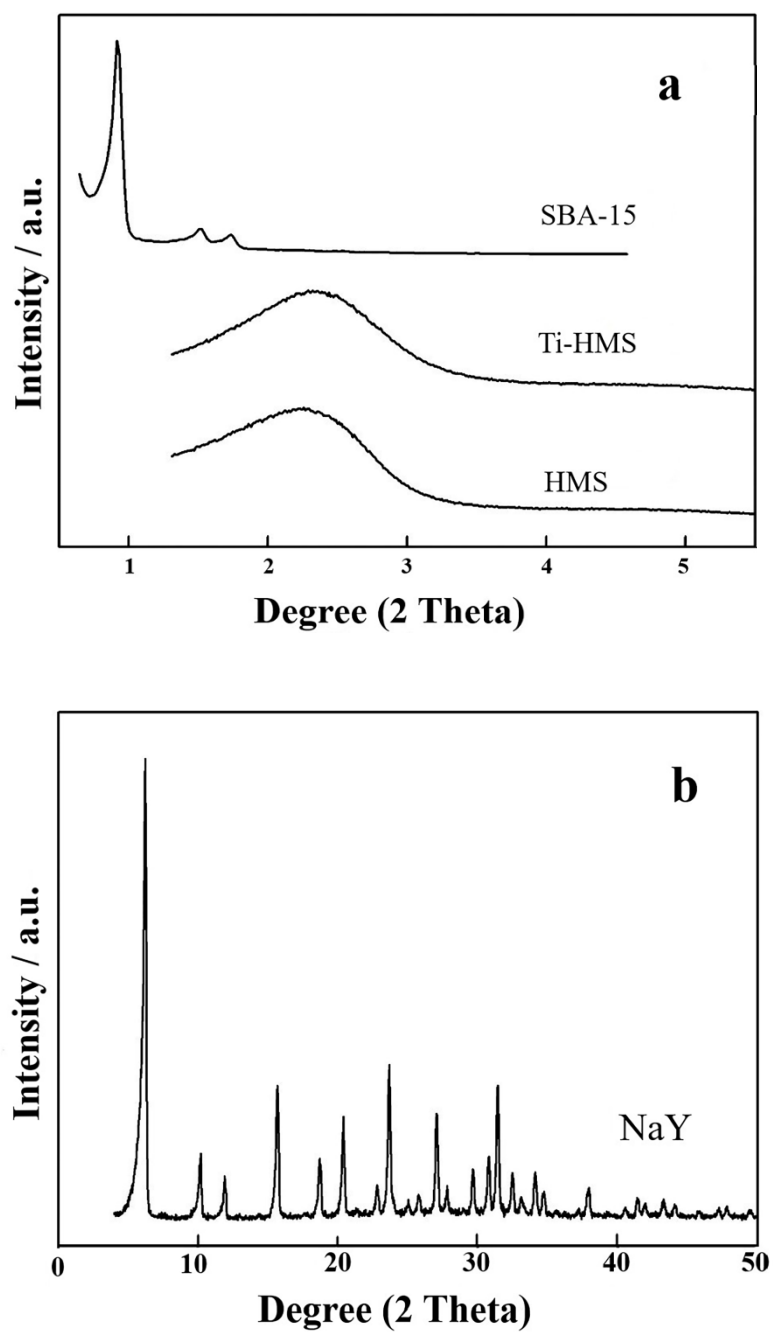


Fig. 1 Representative XRD patterns of (a) HMS, Ti-HMS and SBA-15 and (b) NaY.

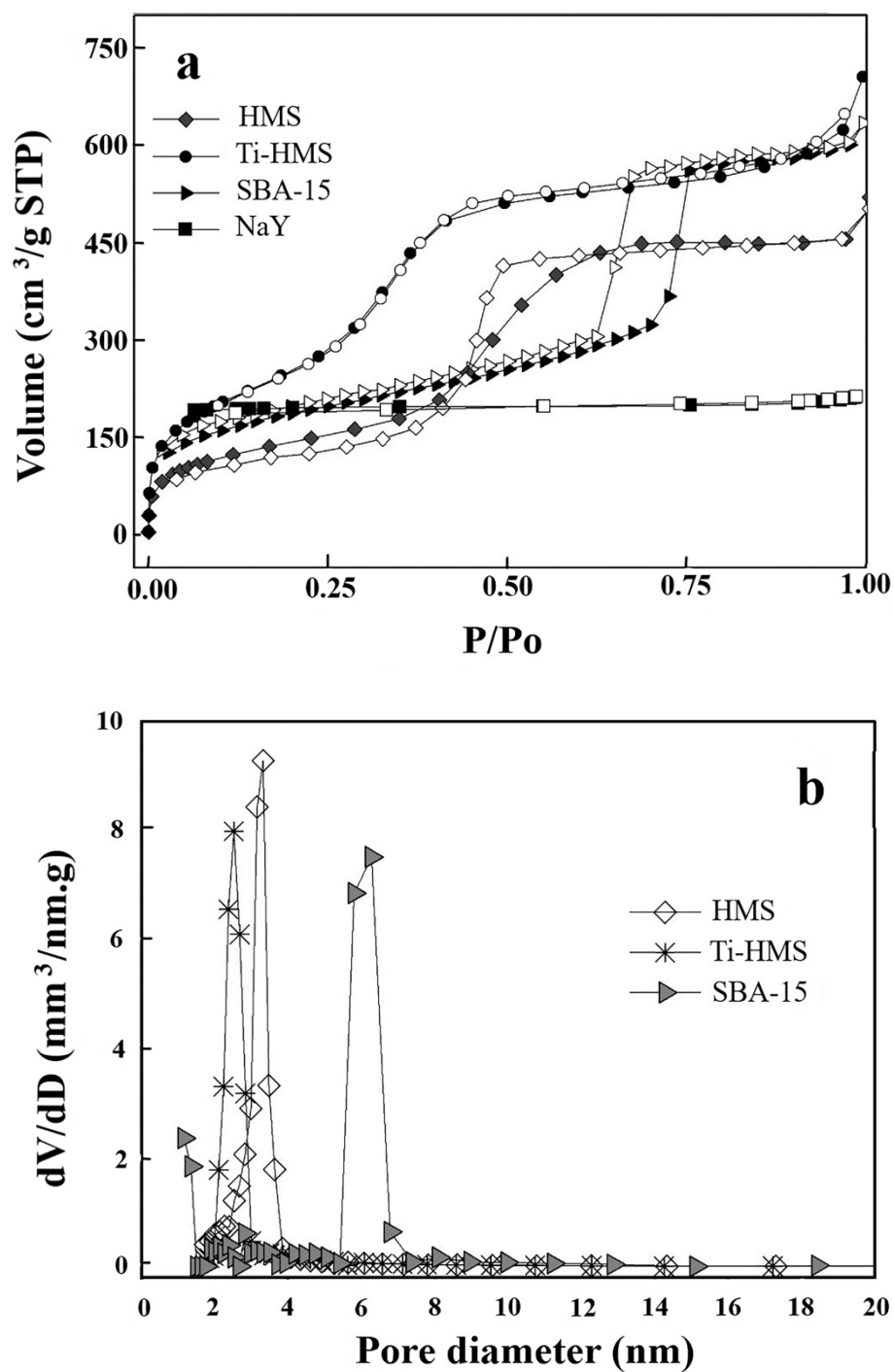


Fig. 2 (a) N_2 adsorption-desorption isotherms of HMS, Ti-HMS, SBA-15 and NaY. Closed symbol: N_2 adsorption; and open symbol: N_2 desorption; (b) Pore size distribution (BJH method) of HMS, Ti-HMS and SBA-15.

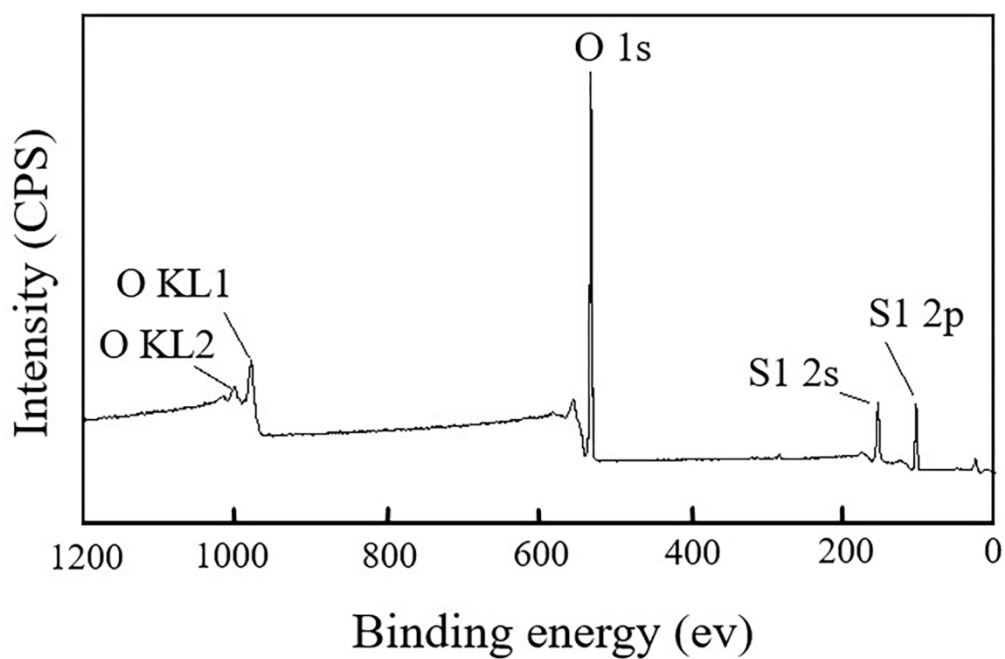


Fig. 3 XPS wide scan spectrum of HMS adsorbent.

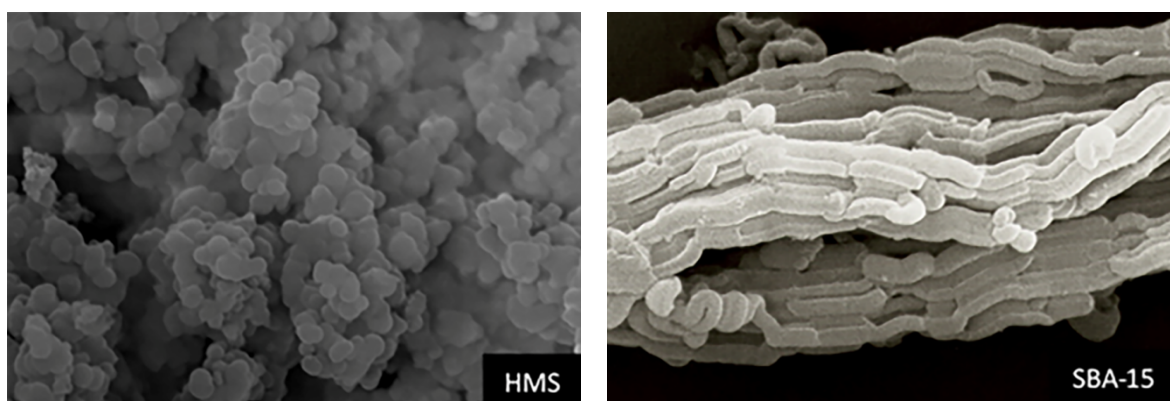


Fig. 4 Representative SEM pictures of HMS and SBA-15 at 10,000 X magnifications.

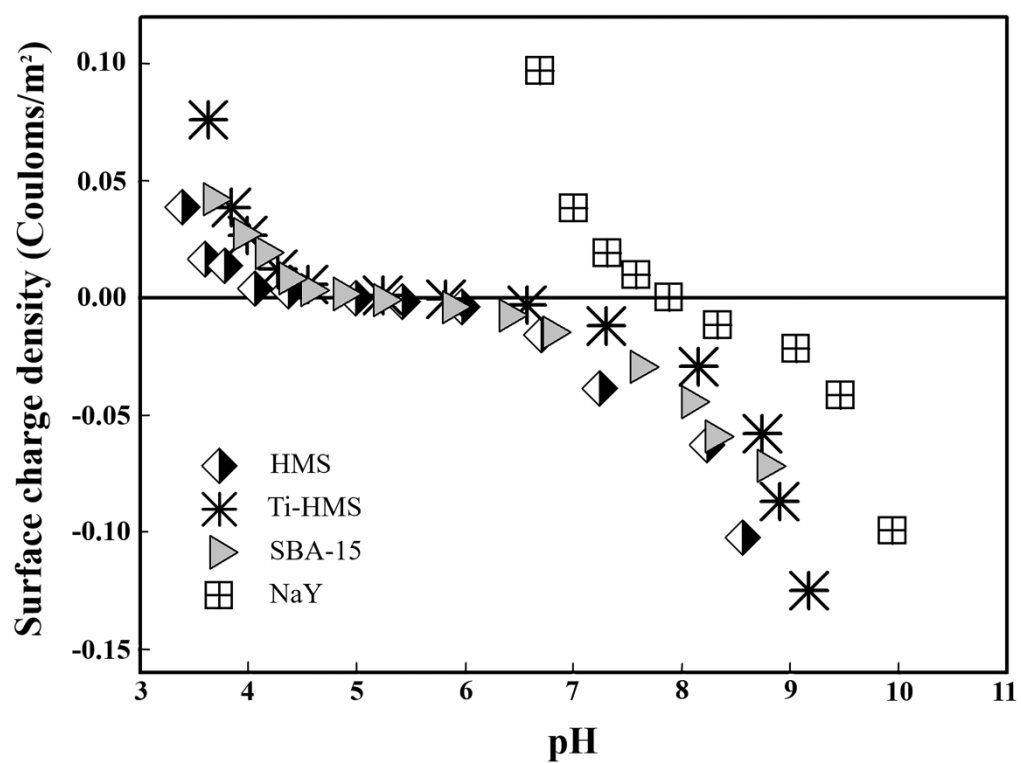


Fig. 5 Surface charge density of HMS, Ti-HMS, SBA-15 and NaY as a function of the solution pH at ionic strength of 10 mM.

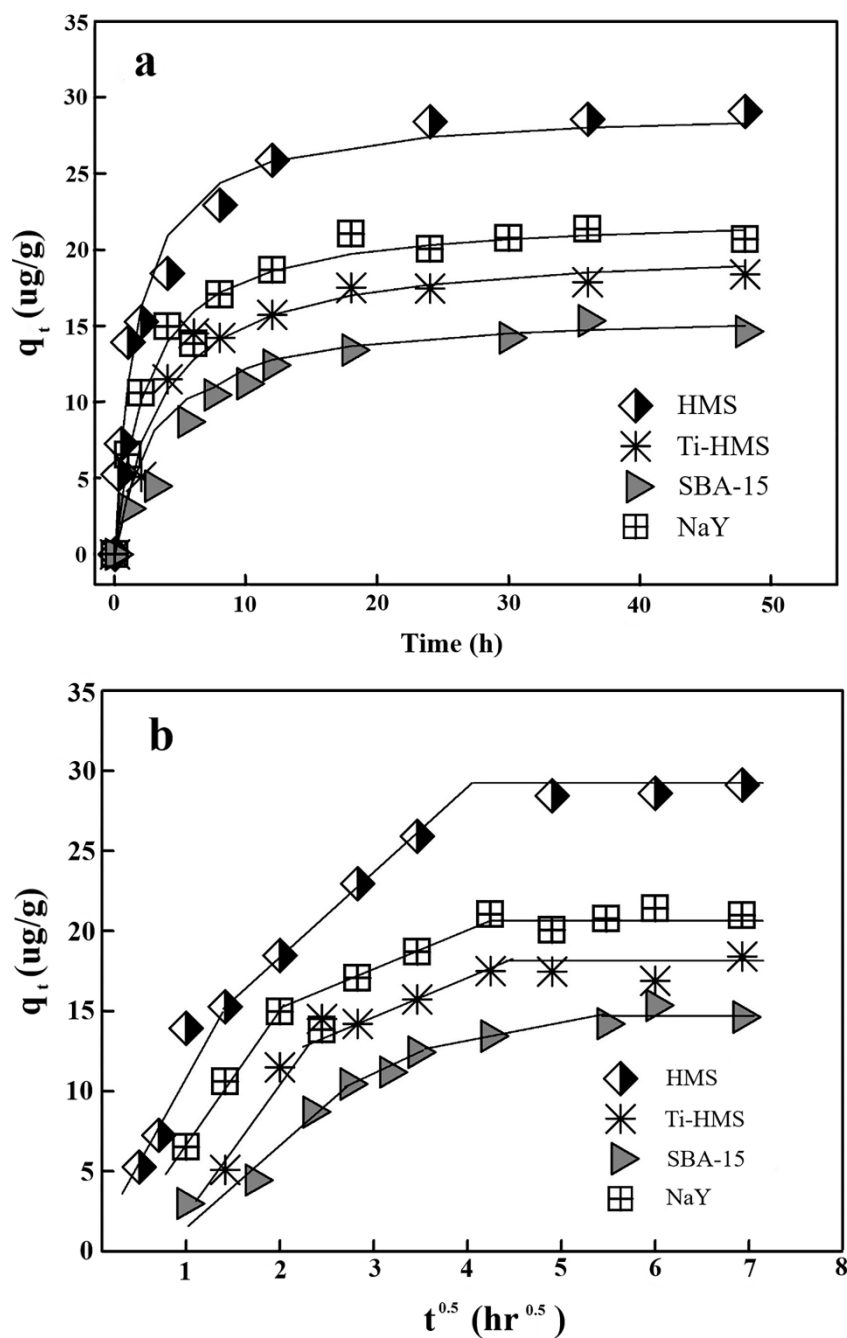


Fig. 6 (a) DCAN adsorption kinetics of HMS, Ti-HMS, SBA-15 and NaY at 100 $\mu\text{g/L}$ at pH solution of 7 (ionic strength of 10 mM). Solid lines present the data derived from the pseudo-second-order kinetic model. (b) Plot of intraparticle diffusion model (Weber and Morris) for the adsorption of DCAN on HMS, Ti-HMS, SBA-15 and NaY.

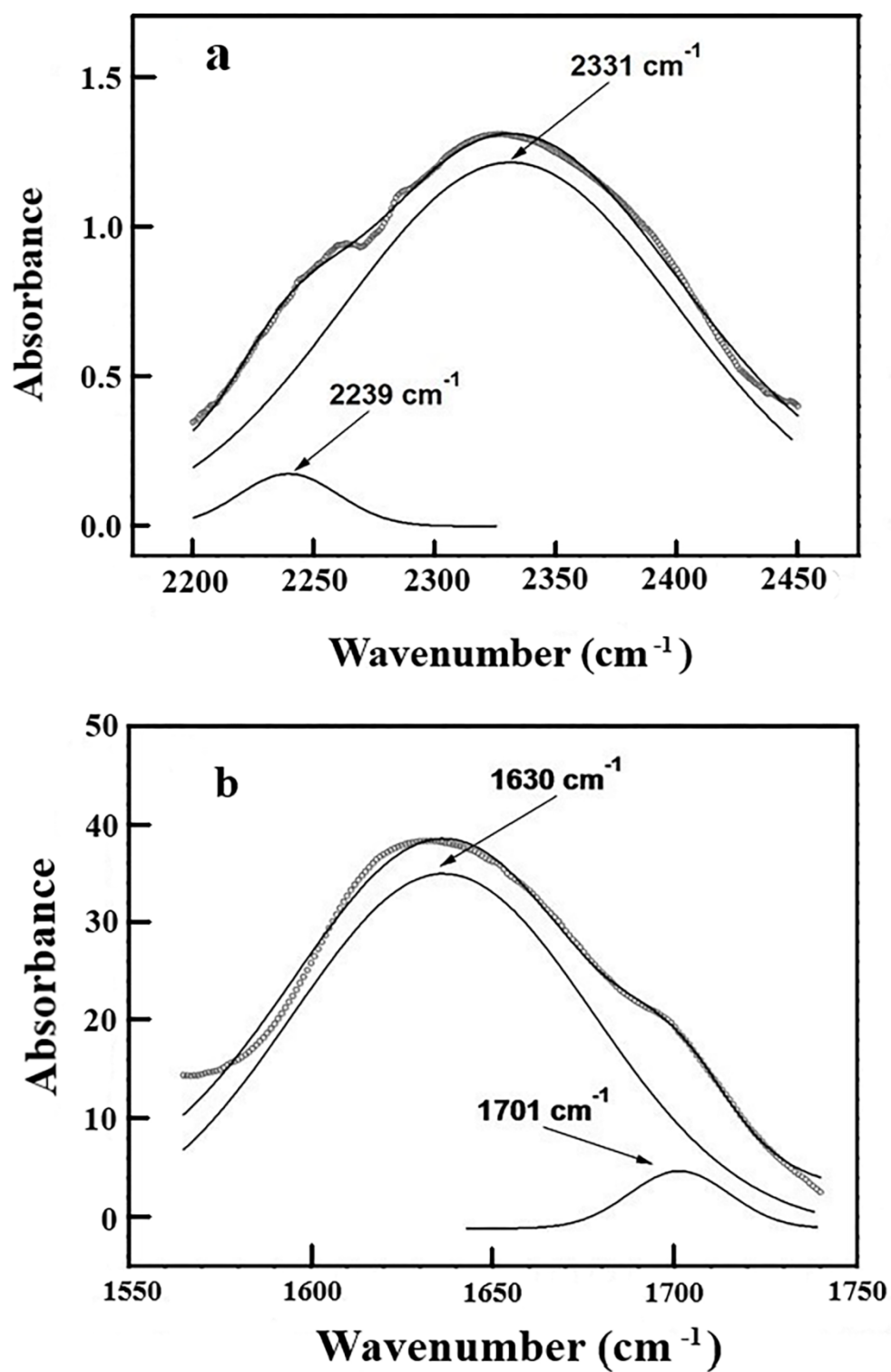


Fig. 7 FT-IR spectra of HMS after DCAN adsorption. Spectra show the DCAN adsorption on HMS in the region of (a) C-N stretching and (b) O-H bending of physisorbed water molecule.

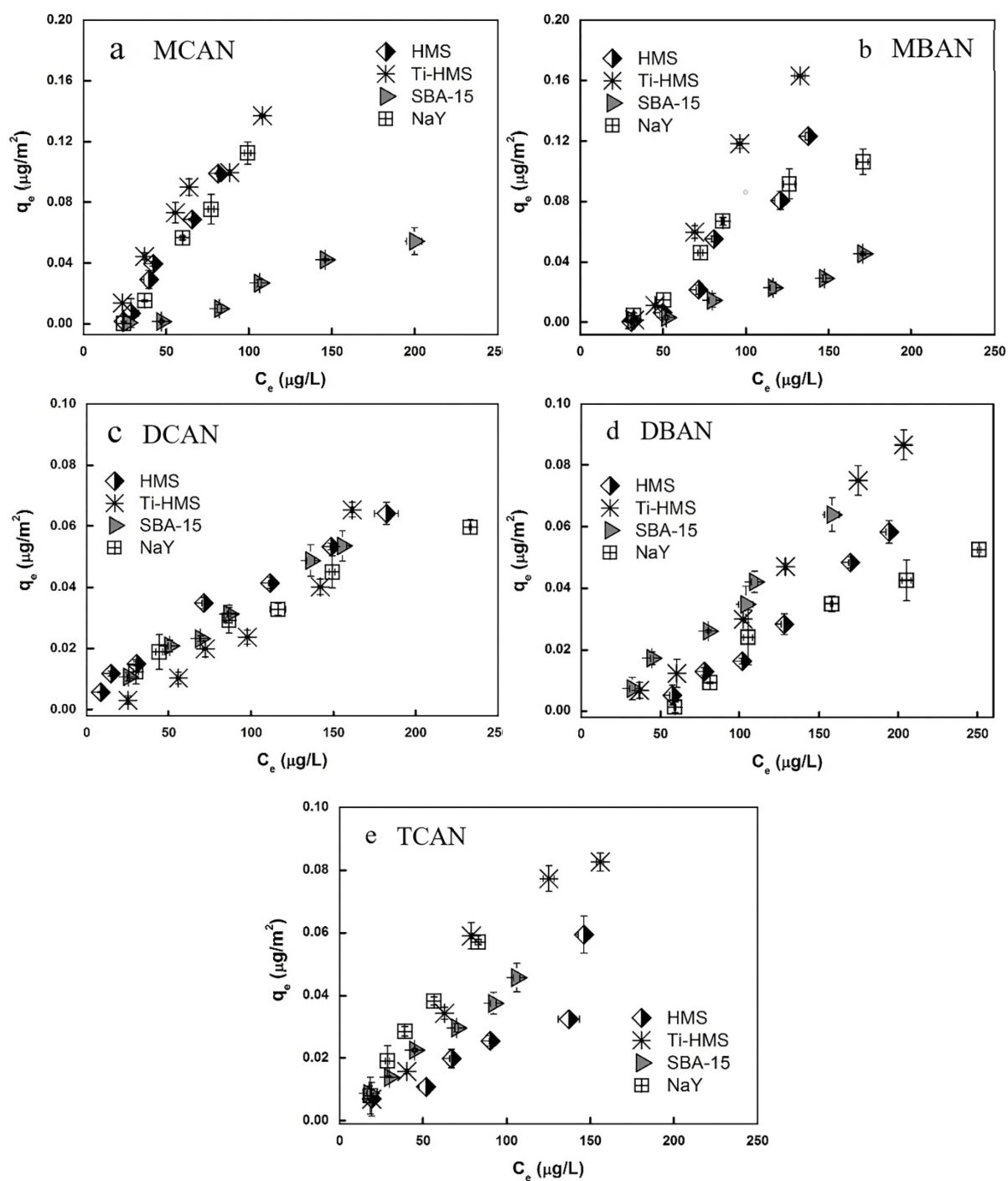


Fig. 8 Adsorption isotherms of the five different HANs on the four adsorbents (HMS, Ti-HMS, SBA-15 and NaY) at pH solution of 7 (ionic strength of 10 mM). Isotherms are shown for (a) MCAN, (b) MBAN, (c) DCAN, (d) DBAN and (e) TCAN.

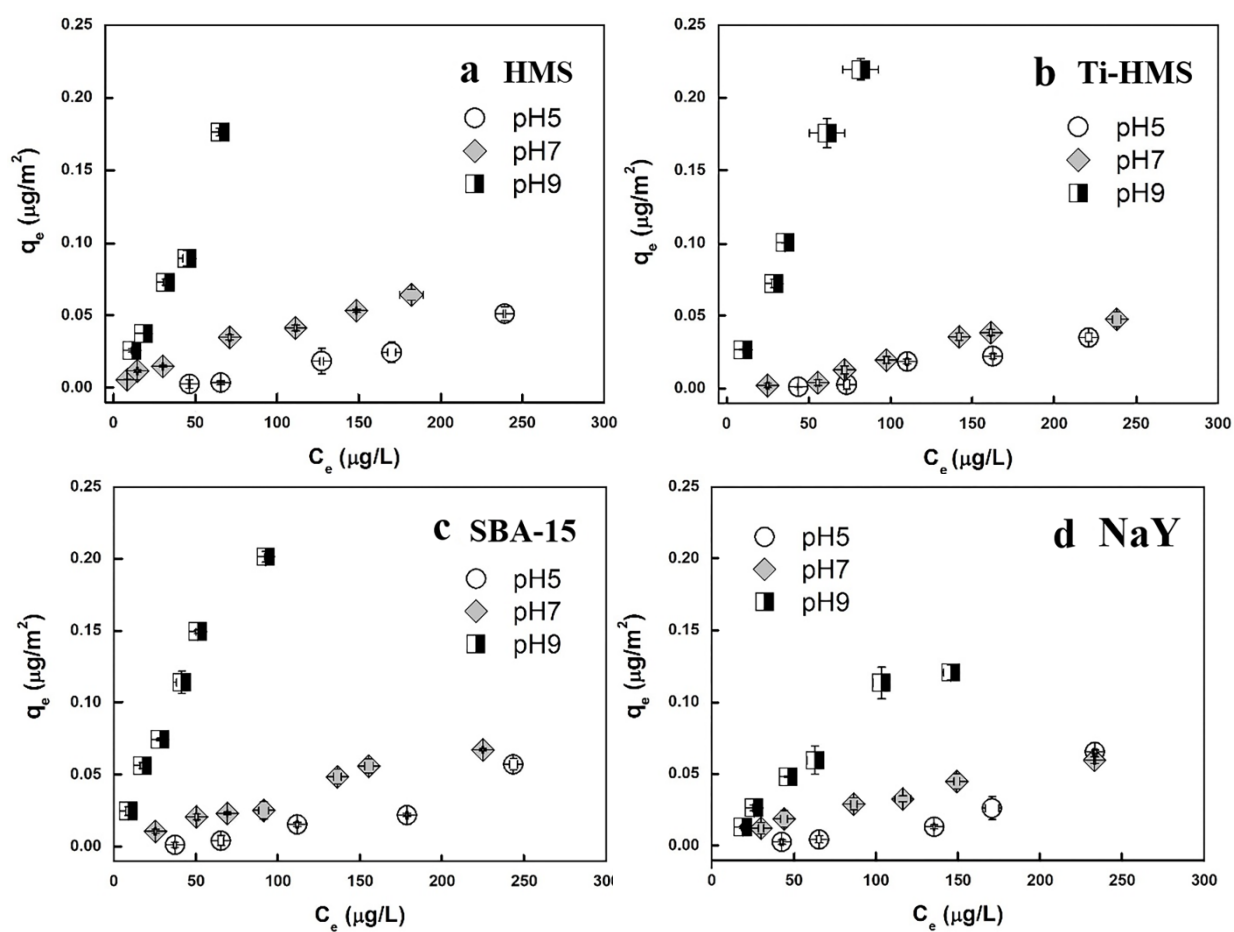


Fig. 9 Effect of pH on the adsorption of DCAN on the four adsorbents at pH solutions of 5, 7 and 9 (ionic strength of 10 mM).

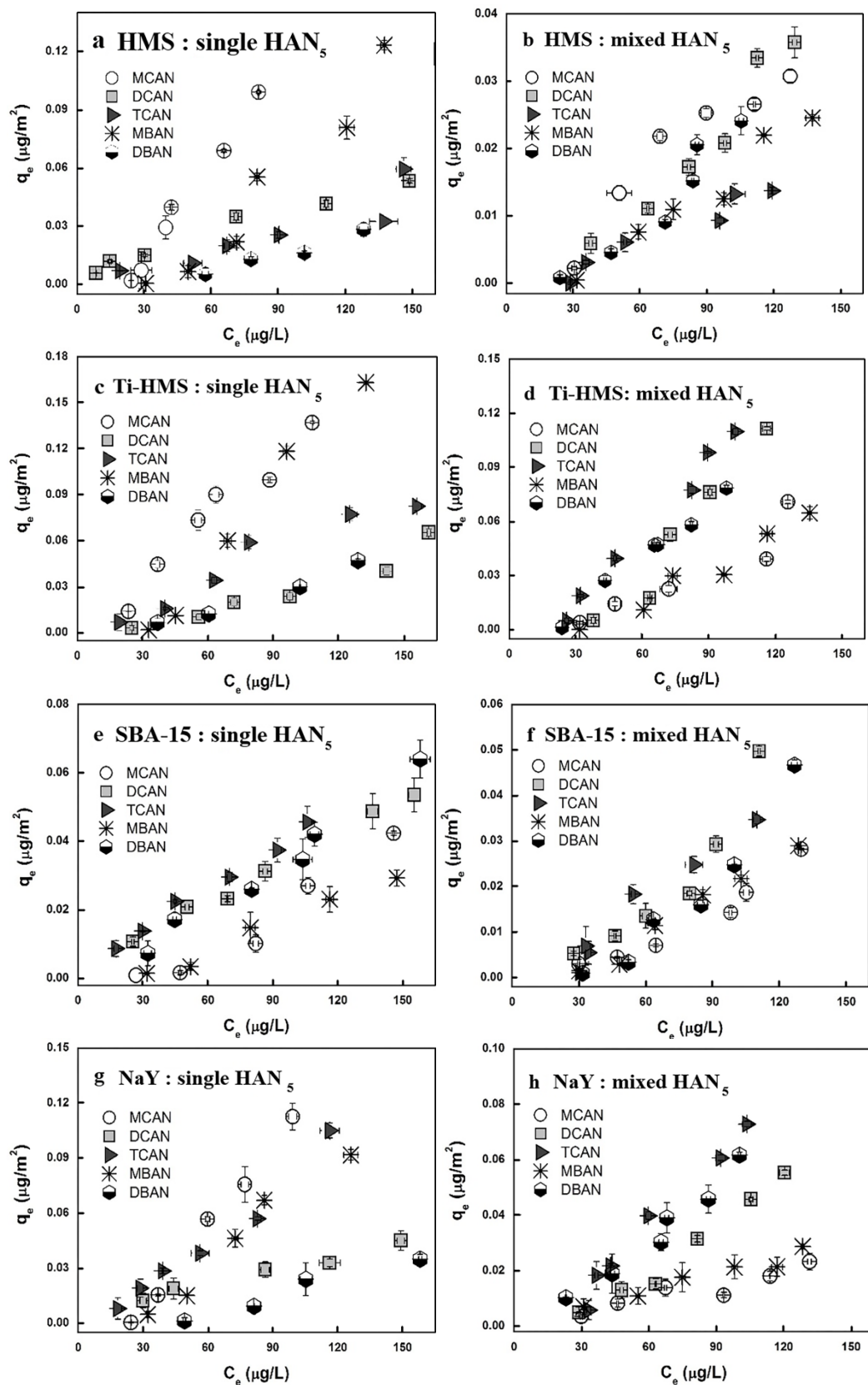


Fig. 10 Adsorption isotherms of the five different HANs alone (single solute) or as an equimolar mixture on the four adsorbents (HMS, Ti-HMS, SBA-15 and NaY) at pH solution of 7 (ionic strength of 10 mM).

Editorial Department
P. O. Box 2871
Beijing 100085
China
Tel: 86-10-62920553
E-mail: jesc@rcees.ac.cn

Journal Publishing Agreement

Author(s): Panida Prarat, Chawalit Ngamcharussrivichai, Sutha Khaodhiar, Patiparn Punyapalakul

Title: Adsorption of single and mixed haloacetonitriles on silica-based porous materials: Mechanisms and effects of porous structures

The undersigned authors, with the consent of all authors, hereby assign to *Journal of Environmental Sciences*, the copyright in the above identified article to be transferred, including supplemental tables, illustrations or other information submitted in all forms and media throughout the world, in all languages and format, effective when and if the article is accepted for publication.

Authors also agree to the following terms:

- A. The article submitted is not subject to any prior claim or agreement and is not under consideration for publication elsewhere.
- B. The article contains no libelous or other unlawful statements and does not contain any materials that violate proprietary right of any other person, company, organization, and nation.
- C. If the article was prepared jointly with other authors, the author(s) agree with the authorship sequence.

Please sign and date the document.

First Author: Panida Prarat

Panida P.

Date:

Feb 26, 2018

Corresponding author: Patiparn Punyapalakul

P. Prarat

Date:

Feb 26, 2018

ภาคผนวก ข

Selective adsorption mechanism of antibiotic in the presence of co-existing tannic acid (TA) by superparamagnetic porous silicate

Parnuch Hongsawat^{a,b}, Chawalit Ngamcharussrivichai^{c,d}, and Patiparn Punyapalakul^{b,f*}

^aInternational Postgraduate Programs in Environmental Management, Graduate School, Chulalongkorn University, Bangkok, 10330, Thailand

^bCenter of Excellence for Environmental and Hazardous Waste Management (EHWM), Chulalongkorn University, Bangkok, 10330, Thailand

^dDepartment of Chemical Technology, Faculty of Science, Chulalongkorn University, Bangkok 10330, Thailand

^dCenter for Petroleum, Petrochemicals and Advanced Materials, Chulalongkorn University, Bangkok 10330, Thailand

^eDepartment of Environmental Engineering, Faculty of Engineering, Chulalongkorn University, Bangkok 10330, Thailand

Abstract

Selective adsorption mechanism of two important antibiotic micropollutant (nalidixic acid (NAL) and sulfamethoxazole (SMX)) from the synthetic solution in the presence of co-existing tannic acid (TA), was investigated using superparamagnetic mesoporous silicate (HMS-SP) and two surface functional group (3-aminopropyltriethoxy- and n-octyldimethylsilane) modified HMS-SPs. A pseudo-second order rate kinetics model was the best fitted for both antibiotics. For the intraparticle diffusion and Boyd model, the film diffusion was the rate controlling step. When the adsorption isotherm models, Sips, and Redlich-Peterson isotherm model were the best fitted on the adsorption of NAL and SMX, respectively. According to the antibiotic adsorption mechanism with the co-existing TA, π - π electron donor acceptor interaction between benzene ring of the already adsorbed TA on the adsorbent surface and each antibiotic molecule (NAL and SMX) can be occurred. Nevertheless, the competitive adsorption interaction between TA and both NAL and SMX should be considered in the adsorption phenomena also.

Keywords: Superparamagnetic hexagonal mesoporous silicas; Adsorption; Antibiotic; Tannic acid

* Corresponding author. Tel.: +66 2 218 6686; Fax: +66 2 218 6666

E-mail address: patiparn.p@chula.ac.th (P. Punyapalakul)

1. INTRODUCTION

Antibiotic contaminated in the environment has been rising concerned since the extensive use of antibiotic in human, animal farming, and agriculture. Quinolones and sulfonamides, antibiotic group compound, is widely detected and attributed in the various environmental fate which depending on their adsorption behavior such as the adsorption interaction to soil and sediment, the distribution of antibiotic and aqueous phase, solid surfaces, and the natural organic compound in the aquatic phase (Fernando et al., 2008, Rossner et al., 2009, Hong et al., 2008, Halling-Sørensen et al., 2000).

Tannic acid (TA), a water soluble polyphenolic compounds, is a natural organic matter (NOM) in surface, ground water, wastewater discharged from cork process, paper and leather industries, and plant medicine. On the other hand, TA is considering as the toxic compound to the aquatic organism and may act as the precursor of carcinogenic disinfection byproducts also (Wang et al., 2011, Lin et al., 2011). As the consequence of the persistence and toxicity of both antibiotic contaminant and TA in the ecosystem, the selective adsorbents has been investigated and applied in the adsorption treatment system for each compound.

In addition, porous silicate material has been well known as the selective adsorbents with high adsorption efficiency for micropollutant and or disinfection byproduct adsorption treatment due to their advantages such as high surface area, large pore volume, narrow pore size distribution, and easily to modified adsorbent surface with various organosilanes (Prarat et al., 2011, Punyapalakul and Takizawa, 2006). Whereas superparamagnetic particle coated with porous silicate has reported and elucidated as the interesting adsorbent for the adsorption treatment process that can be enhance the separation efficiencies, and reduced the cake filtration etc... (Wang et al., 2010, Eichholz et al., 2008). Since the adsorption behavior between adsorbent surface and antibiotic or TA were reported thus the effective adsorption efficiencies including of adsorption capacity and adsorption kinetic in the adsorption process was concerning (Wang et al., 2010). However, to our best knowledge there were a few knowledge about the adsorption mechanism among them that might be occurred for example competitive adsorption between antibiotic and TA.

The results of this study aim to improve our understanding of the adsorption interaction among antibiotics, TA, and silica base adsorbent that elucidated fate and transport of the micropollutant in the environment. According to investigate the adsorption mechanism, nalidixic acid (NAL), and sulfamethoxazole has been selected as the representative quinolone and sulfonamide antibiotic contaminant, respectively. Furthermore, ciprofloxacin (CIP), the widely detected quinolone antibiotic in ecosystem, is adding for selective adsorption investigation as the natural environment.

2. MATERIALS AND METHODS

2.1 Adsorbent synthesis

2.1.1 Superparamagnetic hexagonal mesoporous silicas (HMS-SP) synthesis

Superparamagnetic iron oxide particles (SP), the core-shell adsorbent, were carried out through co-precipitation from aqueous alkaline solutions as following procedure; $\text{FeCl}_3 \cdot 6\text{H}_2\text{O}$ (0.046 mol) and $\text{FeSO}_4 \cdot 7\text{H}_2\text{O}$ (0.023 mol) were dissolved in 150 ml de-ionized water for 3 min. Then, 20 ml ammonium hydroxide (25%) was quickly added into the mixture solution. After 30 min, 3 ml of oleic acid was added into the previous iron solution. The mixture was heated to 75 °C and kept at this temperature for 1 h. The SP was collected through magnetic separation and washed with de-ionized water and ethanol three times, then subsequently dried in vacuum conditions. After that pristine superparamagnetic hexagonal mesoporous silicas (HMS-SP) were prepared following the procedure described by Tian *et al.* (Tian et al., 2009).

2.1.2 Organic functionalized HMS-SPs synthesis

Organic functionalized HMS-SPs were prepared via post-synthesis by following procedure: 0.5 g of pristine HMS-SP was dehydrated at 105 °C in an oven for 24 h, and then stirred in 30 ml of toluene containing 0.5 g of each organosilane: 3-aminopropyltriethoxy-silane, and n-octyldimethylchlorosilane, under refluxing conditions for 24 h, denoted as A-HMS-SP and OD-HMS-SP, respectively. The product was filtrated and then washed with 30 ml of toluene. Then, the A-HMS-SP was washed with 30 ml of ethanol while OD-HMS-SP was washed with toluene instead. After that, the adsorbent was dried under a vacuum at 85 °C for 2 h.

2.2 Characterization of adsorbents

Surface area, pore volume, and pore size were calculated from nitrogen adsorption isotherms measured at 77 K using an Autosorb-1 Quantachrome automatic volumetric sorption analyzer. Then, the specific surface area, the pore diameter and the pore volume were all calculated using the Brunauer-Emmett-Teller (BET) theory. Pore size distribution was also calculated using the Barrett-Joyner-Halenda (BJH) equation. The particle diameter was measured by Scanning Electron Microscopy (SEM JSM 5800 LV) from ten randomly obtained particles. The presence of organo-functional groups on the synthesized adsorbents' surface was confirmed by a Fourier Transform Infrared spectrometer (FTIR) (Perkin Elmer Spectrum One). The quantity of nitrogen content on the surface of A-HMS-SP was determined following the procedure described by Smart *et al.* (Smart *et al.*, 1983). The hydrophobic/hydrophilic characteristics of the adsorbent surface were evaluated by measuring the water contact angle (θ) using a Dataphysics DCAT-11 tensiometer in a powder contact angle mode. An electrophoresis apparatus (Zeta-Meter System 3.0, Zeta Meter Inc.) was used to measure the surface charge.

2.3 Analytical antibiotic method

The filtrated solute underwent a solid-phase extraction (SPE) with PEP cartridges (200 mg/6 ml, Cleanert PEP-H). The cartridges were equilibrated with methanol (5 ml) and water (10 ml), and then the filtrate sample was taken, eluted with methanol (10 ml), evaporated and resuspended with 0.5 ml of methanol. The quantities of antibiotic concentration in equilibrium solutions were analyzed by a reverse phase high performance liquid chromatography (HPLC) equipped with a photodiode array detector (260-280 nm). The determination of antibiotic in solution was performed at 50 °C on a HPLC column (5mm, 250 mm x 4.6 mm; LiChrosorb NH₂, GLS Sciences, USA). The elution gradient was conducted using acetonitrile (A) and water (B). The initial elution condition was a mobile phase A 100% v/v reach to 0% v/v within 15 min. The flow rate was 1 ml min⁻¹. Sulfamethoxazole was spiked in the obtained sample solution as the surrogate standard in CIP and NAL adsorption experiment. In case of SMX adsorption, CIP was used as the surrogate standard instead.

2.4 Adsorption study

2.4.1 Adsorption kinetics study

Adsorption kinetics were performed by varying the contact time and initial antibiotic concentration between 500-800 $\mu\text{g.L}^{-1}$ and 1 g.L^{-1} of adsorbent in 0.01 M phosphate buffer pH7.0. The sample was shaken at 220 rpm at 25 °C, and then the remaining antibiotic concentration was analyzed as described in analytical method. The important kinetic parameters were analyzed using the pseudo-second-order kinetic models are expressed as follows:

$$\frac{t}{q_t} = \frac{1}{k_2 q_e^2} + \frac{t}{q_e} \quad (1)$$

$$h = k_2 q_e^2 \quad (2)$$

$$t_{0.5} = \frac{1}{k_2 q_e} \quad (3)$$

Where k_2 is the rate constant for pseudo-second-order, and q_t and q_e are the amount of antibiotic adsorbed at time t (min) and at equilibrium ($\mu\text{g g}^{-1}$), respectively. According to the pseudo-second-order model, h and $t_{0.5}$ is the initial adsorption rate ($\mu\text{g g}^{-1}\text{min}^{-1}$) and the half-life time, $t_{0.5}$ (min), respectively.

Intraparticle diffusion model based on the theory proposed by Weber and Morris was applied in this study to identify the deep diffusion mechanism of the porous material. The governing equation is shown as;

$$q_t = k_{IPi} \cdot t^{0.5} + C_i \quad (4)$$

Where q_t , k_{IPi} , and C_i are the amount adsorbed at time t ($\mu\text{g/g}$), the intraparticle rate constant of stage i ($\mu\text{g/g.h}^{-0.5}$), and the intercept of stage i , respectively.

According to determine the actual rate controlling step in the antibiotics adsorption; the kinetic data are analyzed by using the procedure of Boyd *et al.*, express as;

$$F(t) = q/q_e \quad (5)$$

$$\text{For } F(t) \text{ values} > 0.85, \quad B_t = 0.4977 - \ln(1 - F(t)) \quad (6)$$

$$\text{For } F(t) \text{ values} < 0.85, \quad Bt = \left(\sqrt{\eta} - \sqrt{\eta - (\eta^2 F(t)/3)} \right)^2 \quad (7)$$

Where $F(t)$ is the fractional attainment of equilibrium, at different times t , and Bt is a function of $F(t)$.

Since these obtained results are still not enough to clarify the rate controlling step thus the film diffusion coefficient (D_1) and pore diffusion coefficient (D_2) are determined by using the following;

$$\frac{q_1}{q_e} = 6 \left(\frac{D_1}{r^2} \right)^{0.5} t^{0.5} \quad (8)$$

$$B = \pi^2 D_2 / r^2 \quad (9)$$

Where r represents the radius of the particle, assuming spherical particles. The film diffusion coefficient (D_1) value is calculated from the slope of the plots of q/q_e versus $t^{0.5}$. When the pore diffusion coefficient (D_2) value is calculated from the slope (B) of the plot of Bt versus t .

2.4.2 Adsorption isotherm study

Adsorption isotherm was conducted with an initial antibiotics concentration range between 20-3000 $\mu\text{g.L}^{-1}$ and 1 g.L^{-1} of adsorbent. The ionic strength of the solution was fixed using 0.01 M phosphate buffer at pH 7. The sample was shaken at 220 rpm at 25 °C, and then the remaining antibiotic concentration was analyzed as described in analytical method. The experimental data were fitted to the typical isotherms:

$$\text{Freundlich:} \quad q_e = K_F C_e^{1/n} \quad (10)$$

$$\text{Sips:} \quad q_e = q_m K_S C_e^{1/n} / (1 + K_S C_e^{1/n}) \quad (11)$$

$$\text{Redlich-Peterson:} \quad q_e = K_{RP} C_e / (1 + \alpha C_e^\beta) \quad (12)$$

Where C_e and $1/n$ is the equilibrium concentration ($\mu\text{g.L}^{-1}$) and the equilibrium constant ($\text{L } \mu\text{g}^{-1}$), respectively; K_F , K_S and K_{RP} the equilibrium constant ($\text{L } \mu\text{g}^{-1}$) in Freundlich, Sips, and Redlich-Peterson isotherm model, respectively. When α is also a constant having unit of $(\text{L } \mu\text{g}^{-1})^\beta$, and β is an exponent that lies between 0 and 1.

2.5 Selective adsorption study

2.5.1 Selective adsorption of three antibiotics in mixed solute solution

Adsorption selectivity was determined via a mixture of three selected antibiotic, CIP, NAL and SMX, on the synthesized adsorbents. The experiment was conducted in the same condition of the single solute solution at pH 7.0. The remaining antibiotic concentration was analyzed as described in analytical method.

2.5.2 Effect of Tannic acid on antibiotic adsorption

Adsorption isotherm of TA was conducted an initial concentration range between 5-100 mg.L⁻¹ and 1 g.L⁻¹ of adsorbent. According to the effect of tannic acid (TA) on antibiotic adsorption, the experiment was investigated by adjusting TA solution (40 mg/L) to different antibiotic concentration at pH 7.0 and 0.01 M phosphate buffer. The residual concentration of TA in solution was analyzed by the HPLC equipped with a photodiode array detector (280 nm). The separation was performed at 50 °C on a C18 HPLC column (5mm, 250 mm x 4.6 mm; Intersil, GLS Sciences, USA) using an acetonitrile-water mixture (85:15%, v) as the mobile phase at a flow rate of 1 ml min⁻¹. The quantities of antibiotic in the presence of TA were analyzed via the same adsorption procedure. The recovery of antibiotics was interfered by the presence of TA, therefore, double PEP cartridges (200 mg/6 ml, Cleanert PEP-H) were used in the same SPE procedure to increase the recovery efficiencies.

3. RESULTS AND DISCUSSION

3.1 Physical characteristics of adsorbents

Surface area, pore size, and pore volume of HMS-SP and two functional groups modified HMS-SPs (A-HMS-SP and OD-HMS-SP) are calculated from nitrogen adsorption isotherm data and summarized in Table 1. The results revealed that pristine HMS-SP had more pore volume than the others functionalized HMS-SPs, but OD-HMS-SP had the largest BET surface area. The amine group content onto the A-HMS-SP surface was 39.28 $\mu\text{mol}_\text{N}.\text{m}^{-2}$ confirming the presence of 3-aminopropyltriethoxy functional groups on the surfaces by determining the nitrogen content. While the hydrophobic can be revealed by the contact angle value, OD-HMS-SP had the highest hydrophobic surface followed by A-HMS-SP and pristine HMS-SP, respectively as shown in Table 1.

The surface charge density of synthesized adsorbents as the function of pH were determined and shown in Figure 1. The surface charge of pristine HMS-SP and OD-HMS-SP were close to zero at pH 3.5 and 4.5, respectively. Whereas the pH at a zero point charge (pH_{zpc}) of A-HMS-SP was increasing significantly that functionalized 3-aminopropyltriethoxy functional groups affected the surface charge of pristine HMS-SP.

3.2 Adsorption kinetics and intraparticle diffusion mechanism

Adsorption kinetics of NAL and SMX onto pristine-HMS-SP and two functionalized-HMS-SPs as a function of contact time were shown in Figure 2. Their concentration decreased gradually in the first 15 min, and then the equilibrium stages were reached after approximately 30 min on all synthesized adsorbents. Both pseudo-first-order and pseudo-second-order adsorption kinetics model were determined; however, the experimental data was well-fitted with the pseudo-second-order kinetic model (Table 2). Considering the pseudo-second-order kinetic parameters by comparison on the initial adsorption rate (h), initial adsorption rate of NAL increased in order of A-HMS-SP < HMS-SP << OD-HMS-SP. Whereas A-HMS-SP had the higher adsorption efficiencies of SMX in the term of equilibrium adsorption capacities and initial adsorption rate at the same adsorption condition as showed in Table 2. The different adsorption behavior was consistent with the previous research that fluoroquinolone and sulfonamide antibiotic had the different adsorption affinities (Hao et al., 2011). However, initial adsorption rate and adsorption capacity of all synthesized HMS-SPs were still lower than conventional powdered activated carbon (PAC) due to complexation of organo-functional group on its surface.

As the pseudo-second-order kinetic model was not able to identify the deep diffusion mechanism of the porous material, an intraparticle diffusion model based on the theory proposed by Weber and Morris is applied. The multi-linearized plot of q_t versus $t^{0.5}$ based on intraparticle diffusion model of NAL and SMX were determined on all synthesized adsorbents as showed in Figure. 3. The slope- fitting plots did not pass through the origin for all adsorbents. It could be implied that not only the intraparticle diffusion in the adsorption mechanism, but also film diffusion, affects adsorption interaction (Wu et al., 2009). Generally, the first linear segment refer to the adsorption is controlled by film diffusion for the multi-

linear intraparticle diffusion stages. The obtained results showed two or three linear diffusion stages in most of the antibiotic adsorption onto the synthesized adsorbents. The different intraparticle diffusion linear stages might be caused by the narrow and wide pore onto the synthesized mesoporous adsorbents.

The intraparticle diffusion rate parameter was evaluated and expressed in Table 3. The obtained results showed the higher K_{IP1} than K_{IP2} onto the entire synthesized adsorbents. Excepted the adsorption of NAL on A-HMS-SP, it was observed that the higher K_{IP2} than K_{IP1} onto the synthesized adsorbent. It can be implied that the two antibiotic adsorption rates might be controlled by intraparticle diffusion.

However, to determine the actual rate controlling step in the antibiotics adsorption; the kinetic data were analyzed by using the procedure of Boyd *et al.* The film diffusion coefficient (D_1) and pore diffusion coefficient (D_2) was evaluated and shown in Table 3. According to the obtained results, the higher hydrophilic adsorbent surface revealed the higher diffusion rate (K_{IP1}) and higher D_1 values than hydrophobic surface. That can be suggesting that the antibiotic adsorption was governed by film diffusion (except the adsorption of SMX onto HMS-SP). Thus, hydrophilic functional group surface might reduce the film resistance of water to mass transfer of antibiotic to the external adsorbent surface.

3.3 Adsorption isotherms

3.3.1 Effect of surface functional groups on antibiotic adsorption

The adsorption capacity per specific area of NAL and SMX was shown in Figure 4. The obtained results revealed that pristine HMS-SP had the lowest adsorption capacity per specific area that the organo functional group surface can be affected the both antibiotic adsorption. In comparison among synthesized adsorbents, A-HMS-SP had the high adsorption capacity per specific area of both NAL and SMX; hence the hydrogen bonding between the amine group of adsorbent surface and the active functional group of antibiotic was supposed to be the key role in the adsorption mechanism. However, the high adsorption affinity between SMX and OD-HMS-SP could be found similarly to A-HMS-SP thus the hydrophobic interaction might be involved in the main adsorption mechanism also. According to hydrogen bonding between silanol group of HMS-SP and active functional group, the low adsorption capacity per specific area was revealed that might be caused by the competitive adsorption between

water and antibiotic molecule with silanol group surface. Due to the silanol surface might be surrounded with water molecules hence it was no free for antibiotics adsorption. Therefore, hydrogen bonding between the amine functional group was supposed to be the main interaction for antibiotic adsorption onto the synthesized adsorbents.

3.3.2 Adsorption isotherm model

To describe the antibiotic adsorption interaction onto the synthesized adsorbents, the correlation of the experimental equilibrium data using the four adsorption isotherm models; Langmuir, Freundlich, Sips, and Redlich-Peterson model, were applied to fit the experimental equilibrium isotherm data. Two traditional approaches of determining the isotherm parameters, Langmuir and Freundlich isotherm models, were applied for the fitting of the experimental data. The Langmuir isotherm model is based on the assumption of the homogeneous surface sites within the adsorbent and a monolayer adsorption. While the heterogeneous and multilayer adsorption can be assumed via Freundlich isotherm model.

The equilibrium adsorption isotherm parameters, the correlation coefficients (R^2) and chi-square (χ^2) from the nonlinear equation were estimated using the Origin Pro version 8.5 software and shown in Table 4. Most of the obtained results revealed no relationship with the Langmuir and Redlich-Peterson isotherm (data were not shown), but the data were well-fitted with the Freundlich- and Sips isotherm base on the R^2 values ($R^2 > 0.90$) for both NAL and SMX adsorption. Additionally the best fit model can be evaluated via the nonlinear chi-square (χ^2), the higher χ^2 value indicates the variation of the experimental data thus the lower one reveals the better isotherm model. The NAL adsorption data were best fitted with the Sips isotherm model for the entire synthesized adsorbents except for OD-HMS-SP that Freundlich isotherm model reveal better performance than the other via both R^2 and χ^2 values (as shown in Table 4). While the entire adsorption data of SMX were best fitted with the Freundlich isotherm model, hence these obtained results indicating that the Sips and Freundlich isotherm model was the best fit isotherm model for NAL and SMX, respective. On the other word, the heterogeneous and a multilayer formation was occurred on the synthesized adsorbent surface through all antibiotic adsorptions.

Comparison on the K_s and K_F value of each adsorbent as show in Table 4, the higher adsorption affinity of SMX was performed on the pristine HMS-SP and A-HMS-SP; the hydrophilic adsorbents, that was unlike the NAL adsorption behavior which was no relevant between the hydrophobicity and the adsorption affinity. Nevertheless, the other important adsorption interaction, electrostatic interaction might be the involved as the key role in antibiotic adsorption mechanism also.

3.3.3 Effect of pH on antibiotic adsorption

With regard to the effect of pH on the antibiotic adsorption, adsorption experiments were conducted at pH 5-9 and expressed Figure 5. Beside the adsorption of NAL, NAL molecule consist of the aromatic ring with carboxylic- and amine functional group. Base on its pK_a value, NAL is anionic and neutral speciation at $pH > 6.04$, and $pH < 6.04$, respectively. While the cationic speciation, the protonated NAL, could be existed at low pH values ($pH < 0$), that were not considered in these experiment (Robberson et al., 2006). Focusing on the effect of the adsorption capacity caused by the pH condition on A-HMS-SP and OD-HMS-SP; the two highest NAL adsorption capacities (as seen in Figure 5 (b, c)), was not revealed therefore the electrostatic interaction was involved in the NAL adsorption mechanism but not the main interaction.

As the SMX molecular structure that is consisting of two active sites; the nitrogen atom of amine group (NH_2), and nitrogen atom of ionized form. The major SMX speciation are cationic (SMX^+), neutral (SMX^0), and anionic (SMX^-), depend on its pK_a value. The adsorption capacity of SMX on the synthesized adsorbents under different pH function were shown in Figure 5 (d, e, f). The obtained results showed the decreased repulsion between SMX^- and less negatively surface adsorbent onto OD-HMS-SP. Which indicating the SMX adsorption could be affected by the electrostatic interaction on these synthesized adsorbent. In contrasting with HMS-SP, the higher negatively surface enhanced the anion species (SMX^-) adsorption in the solution. Thus, the electrostatic via ion-dipole might be involved in the SMX adsorption mechanism.

3.4 Selective antibiotic adsorption

3.4.1 The single adsorption of antibiotic in co-existing with Tannic acid on A-HMS-SP and OD-HMS-SP

As the component of naturally organic matter (NOM), tannic acid (TA), is present through the environment, which expected to interact and/or affect to the antibiotic adsorption process. Therefore, the adsorption capacities of antibiotic in co-existing with TA onto synthesized adsorbents were investigated and shown in Figure 6. In addition, the adsorption capacities of TA onto synthesized adsorbents; HMS-SP, A-HMS-SP, and OD-HMS-SP, were 24 mg C/g, 12 mg C/g, and 12 mg C/g, respectively. As A-HMS-SP had the highest adsorption capacity of TA comparing with all the synthesized adsorbents. In this respect, electrostatic interaction between the positively charge of adsorbent surface and negatively charge of TA molecule was suggesting to be the main interaction mechanism in this condition. Consistent with previous reports, the interaction between TA and the amino-functional group on A-HMS-SP had been suggested to be the main adsorption mechanism (Wang et al., 2011, Lin et al., 2011, Wang et al., 2010). In order to the adsorption of TA on OD-HMS-SP, the lowest TA adsorption capacities, the hydrophobic interaction without the specified active site was suggesting to involve in this adsorption mechanism.

While, the adsorption capacities of both antibiotics (NAL and SMX) were increased in the presence of TA as a co-existing compound. According to adsorption of NAL and SMX, the increased adsorption capacities of NAL and SMX might be caused by the driven force of the repulsive charge between negatively antibiotic and negatively TA molecule in this pH solution. That might be enhanced the driving force of NAL and SMX for adsorption on the surface of A-HMS-SP and OD-HMS-SP.

Additionally, TA preferred to be adsorbed to amine functional group as described above, hence the TA adsorption capacity should be related to the amino functional groups of A-HMS-SP. From the Figure 6 (a), the adsorption of TA on A-HMS-SP did not change significantly, which might indicate that the NAL was not be adsorbed via amino functional groups of A-HMS-SP. However, the increasing of NAL adsorption capacity might be caused by the interaction between NAL and already adsorbed TA

via π - π electron donor acceptor between benzene ring of both TA and NAL. The expected adsorption of NAL onto A-HMS-SP surface was illustrated as showed in Figure 7 (a).

In case of TA adsorption on OD-HMS-SP in the presence of NAL (Figure 6 (b)), the adsorption of TA might be occurred via the hydrophobic interaction and hydrogen bonding via free silanol groups of OD-HMS-SP which was supposed to be the same mechanism as NAL adsorption. This Figure clearly indicated that the surface of OD-HMS-SP preferred to adsorb higher hydrophobic NAL much more than TA. Moreover, the adsorption capacity of NAL on OD-HMS-SP was increased by π - π electron donor acceptor between benzene ring of both adsorbed TA and NAL. This phenomenon was illustrated as showed in Figure 7 (b).

On the other hand, the adsorption capacities of TA in the presence of SMX on both adsorbents (A-HMS-SP, and OD-HMS-SP) were decreased as showed in Figure 6 (c, d). Although TA can be absorbed by amino groups on A-HMS-SP surface very well, the hydrogen bonding between SMX molecule and amino groups (and/or remained silanol group) on the A-HMS-SP surface seem to be stronger than the TA adsorption. Therefore, there was the competitive adsorption between SMX and TA onto the active sites of the surface (amine- and remained silanol groups). Considering on the increased adsorption capacities of SMX in the presence of TA, that might be caused by the interaction between SMX and TA via hydrogen bonding of the active functional site of both molecules such as carboxylic- and amine-group, together with π - π electron donor acceptor between benzene ring. The expected adsorption mechanism of SMX in the presence of TA onto A-HMS-P was illustrated and showed in Figure 8 (a).

Similarly to the adsorption behavior onto A-HMS-SP, the competitive interaction between SMX and TA was supposed to be occurring onto the OD-HMS-SP surface. That revealed on the increased SMX adsorption capacity but the adsorption capacity of TA was decreased as showed in Figure 6 (d). The adsorption capacities of SMX could be increased by two possible phenomenons; the adsorption of SMX onto the OD-HMS-SP surface via hydrogen bonding (the carboxylic group of SMX and the active site of adsorbent surface) and the interaction of SMX and the already adsorbed TA via π - π electron donor acceptor between benzene ring between SMX and TA,. The expected adsorption mechanism of SMX in the presence of TA onto OD-HMS-P was illustrated and showed in Figure 8 (b).

3.4.2 Selectivity of antibiotics in the presence of co-existing Tannic acid on A-HMS-SP and OD-HMS-SP

The adsorption selectivity was investigated by comparing the adsorption capacities of the mixed three antibiotics which widely detection in the environment; represent the quinolone (ciprofloxacin (CIP), and nalidixic acid (NAL)) and sulfonamide (sulfamethoxazole (SMX)) antibiotics group in the actual environment, in the presence of co-existing TA. As revealed in Figure 9 (a), the order of adsorption preferable on A-HMS-SP was $CIP \gg NAL > SMX$. There were different from the mixed antibiotic solution without the TA (as showed in Figure S5). Whereas, the adsorption capacities of NAL and SMX on A-HMS-SP with the co-existing TA were not as high as in mixed antibiotic solute without TA, this might be suggested that adsorbed TA on surface of A-HMS-SP preferred CIP much more than NAL and SMX. According to the preferable interaction of CIP and TA on A-HMS-SP than the other antibiotics, electrostatic interaction on second layer adsorption was suggested to be the key role in this adsorption phenomenon.

On the other hand, there was difference in the preferable adsorption order on OD-HMS-SP, being as $CIP \sim NAL \gg SMX$, as showed in Figure 9 (b). Considering on the adsorption capacities, the antibiotic adsorption capacities in the presence of TA were increased in the mixed solute comparing with the solute without TA excepted for SMX (as seen in Figure S4). These might be caused by the stronger hydrophobic interaction between both CIP and NAL than SMX onto the alkyl functional surface. Furthermore, TA was preferable interacted with the quinolone antibiotic (CIP and NAL) via π - π electron donor acceptor interaction charge (CIP^{\pm}) than SMX molecule. That the higher planar aromatic ring in the molecule might be more electron donor acceptor interaction (Carabineiro et al., 2011). Therefore, the interactions between both antibiotics (CIP and NAL) with the already adsorbed TA were much more than the interacted SMX.

4. CONCLUSIONS

Both NAL and SMX antibiotic adsorption onto the three synthesized adsorbent, HMS-SP, A-HMS-SP, and OD-HMS-SP followed a pseudo-second order rate kinetics model. Beside the intraparticle

diffusion and Boyd model, the film diffusion was suggested to be the rate controlling step in the NAL and SMX adsorption. Sips, and Redlich-Peterson isotherm model were the best fitted on the adsorption of NAL and SMX, respectively. Since antibiotic adsorption efficiency by synthesized superparamagnetic porous silicate was no significantly reduced in the presence of TA as the co-existing organic compound while the adsorption mechanism, π - π electron donor acceptor interaction between benzene ring of the already adsorbed TA on the adsorbent surface and each antibiotic molecule (NAL and SMX) can be occurred. Furthermore, the competitive adsorption interaction between TA and both NAL and SMX should be considered in the adsorption phenomena also.

ACKNOWLEDGEMENTS

The authors are grateful for the financial support from the 90th Anniversary of Chulalongkorn University Fund (Ratchadaphiseksomphot Endowment Fund). This work was carried out as part of the research cluster “Fate and Removal of Emerging Micropollutants in Environment” granted by the Center of Excellence for Environmental and Hazardous Waste Management (EHWM) and Special Task Force for Activating Research (STAR), both of Chulalongkorn University. The authors are also grateful for support from the Thailand Research Fund, Thailand under grant no. RSA5880018. The authors wish to express their gratitude to Hitachi Scholarship Foundation for full support via the Hitachi Research Fellowship 2011. The technical support from Department of Environmental Engineering, Faculty of Engineering and the Center for Petroleum, Petrochemicals and Advanced Materials, Chulalongkorn University are also acknowledged.

REFERENCES

- CARABINEIRO, S. A. C., THAVORN-AMORNSRI, T., PEREIRA, M. F. R. & FIGUEIREDO, J. L. 2011. Adsorption of ciprofloxacin on surface-modified carbon materials. *Water Research*, 45, 4583-4591.
- EICHHOLZ, C., STOLARSKI, M., GOERTZ, V. & NIRSCHL, H. 2008. Magnetic field enhanced cake filtration of superparamagnetic PVAc-particles. *Chemical Engineering Science*, 63, 3193-3200.
- FERNANDO, B., JOSE L., M. & CANTON, R. 2008. Antibiotics and antibiotic resistance in water environments. *Current Opinion in Biotechnology*, 19, 260-265.

- HALLING-SØRENSEN, B., HOLTEN LÜTZHØFT, H.-C., ANDERSEN, H. R. & INGERSLEV, F. 2000. Environmental risk assessment of antibiotics: comparison of mecillinam, trimethoprim and ciprofloxacin. *Journal of Antimicrobial Chemotherapy*, 46, 53-58.
- HAO, C., GAO, B., LI, H. & MA, L. Q. 2011. Effects of pH and Ionic Strength on Sulfamethoxazole and Ciprofloxacin Transport in Saturated Porous Media. *Journal of Contaminant Hydrology*, 126, 29-36.
- HONG, A. D., NGOC, H. P., HOANG, T. N., THI THUONG HOANG, HUNG VIET PHAM, VAN CA PHAM, MICHAEL BERG, WALTER GIGER & ALDER, A. C. 2008. Occurrence, fate and antibiotic resistance of fluoroquinolone antibacterials in hospital wastewaters in Hanoi, Vietnam. *Chemosphere*, 72, 968-973.
- LIN, J., ZHAN, Y., ZHU, Z. & XING, Y. 2011. Adsorption of tannic acid from aqueous solution onto surfactant-modified zeolite. *Journal of Hazardous Materials*, 193, 102-111.
- PRARAT, P., NGAMCHARUSSRIVICHAI, C., KHAODHIAR, S. & PUNYAPALAKUL, P. 2011. Adsorption characteristics of haloacetonitriles on functionalized silica-based porous materials in aqueous solution. *Journal of Hazardous Materials*, 192, 1210-1218.
- PUNYAPALAKUL, P. & TAKIZAWA, S. 2006. Selective adsorption of nonionic surfactant on hexagonal mesoporous silicates (HMSs) in the presence of ionic dyes. *Water Research*, 40, 3177-3184.
- ROBBERTSON, K. A., WAGHE, A. B., SABATINI, D. A. & BUTLER, E. C. 2006. Adsorption of the quinolone antibiotic nalidixic acid onto anion-exchange and neutral polymers. *Chemosphere*, 63, 934-941.
- ROSSNER, A., SNYDER, S. A. & KNAPPE, D. R. U. 2009. Removal of emerging contaminants of concern by alternative adsorbents. *Water Research*, 43, 3787-3796.
- SMART, M. M., RADA, R. G. & DONNERMEYER, G. N. 1983. Determination of total nitrogen in sediments and plants using persulfate digestion. An evaluation and comparison with the Kjeldahl procedure. *Water Research*, 17, 1207-1211.
- TIAN, H., LI, J., SHEN, Q., WANG, H., HAO, Z., ZOU, L. & HU, Q. 2009. Using shell-tunable mesoporous Fe₃O₄@HMS and magnetic separation to remove DDT from aqueous media. *Journal of Hazardous Materials*, 171, 459-464.
- WANG, J., ZHENG, C., DING, S., MA, H. & JI, Y. 2011. Behaviors and mechanisms of tannic acid adsorption on an amino-functionalized magnetic nanoadsorbent. *Desalination*, 273, 285-291.
- WANG, J., ZHENG, S., LIU, J. & XU, Z. 2010. Tannic acid adsorption on amino-functionalized magnetic mesoporous silica. *Chemical Engineering Journal*, 165, 10-16.
- WU, F.-C., TSENG, R.-L. & JUANG, R.-S. 2009. Initial behavior of intraparticle diffusion model used in the description of adsorption kinetics. *Chemical Engineering Journal*, 153, 1-8.

Table 1 Physicochemical characteristic of the synthesized adsorbents

Adsorbents	Surface functional groups	Surface Characteristic ^a	Contact angle (°)	Pore diameter (nm)	BET surface area (m ² /g)	Pore volume (mm ³ /g)	Particle Diameter (µm)	pH _{zpc}
SP	-	-	-	-	95	-	-	-
HMS-SP	Silanol	Hydrophilic	45	3.28	380	344	0.33	4.5
A-HMS-SP	Amino	Hydrophilic	50	3.70	141	265	0.15	9.0
OD-HMS-SP	Octyl	Hydrophobic	90	3.21	403	237	0.18	3.5
PAC	Carbonyl, phenyl and others	Hydrophobic	58	1.90	980	276	-	6.9

Table 2 Kinetic parameters of antibiotics adsorption on HMS-SP, A-HMS-SP, OD-HMS-SP and PAC adsorbents at 500 µg L⁻¹ (pH 7 and IS 0.01M).

Adsorbent	$q_{e, \text{exp}}$ (μg/g)	Pseudo-second-order			R^2	h^a (μg/g.min)	$t_{0.5}$ (min)
		$q_{e, \text{cal}}$ (μg/g)	k_2 (g/μg.min)				
Nalidixic acid (NAL)							
HMS-SP	147	149	0.0014	0.9997	31	4.66	
A-HMS-SP	263	270	0.0004	0.9965	28	9.14	
OD-HMS-SP	491	526	0.0003	0.9968	68	6.78	
PAC	4520	5000	0.0007	0.9995	14286	0.29	
Sulfamethoxazole (SMX)							
HMS-SP	600	625	0.0007	0.9992	263	2.19	
A-HMS-SP	637	625	0.0022	0.9999	909	0.71	
OD-HMS-SP	440	417	0.0010	0.9966	185	2.51	
PAC	5100	5000	0.0005	0.9999	12500	0.36	

^a h = initial adsorption rate (µg/gmin) calculated from $h = k_2 q_e^2$ ^b $t_{0.5}$ = half life of antibiotic adsorption calculated from $t_{0.5} = 1/k_2 q_e$

Table 3 Intraparticle rate parameters and diffusion coefficients for adsorption of antibiotics on adsorbents in 0.01 M phosphate buffer pH 7.

Adsorbents	Intraparticle diffusion						Film	Pore
	k_{IP1}^a	C_1	R^2	k_{IP2}^b	C_2	R^2	Diffusion ^c	Diffusion ^d
	($\mu\text{g/g.min}^{1/2}$)			($\mu\text{g/g.min}^{1/2}$)			$D_{1 \times 10^{-4}}$ ($\mu\text{m}^2/\text{min}$)	$D_{2 \times 10^{-4}}$ ($\mu\text{m}^2/\text{min}$)
Nalidixic acid (NAL)								
HMS-SP	50	0	0.96	6	89	0.96	1.31	0.79
A-HMS-SP	33	0	0.98	36	-23	0.99	0.07	0.08
OD-HMS-SP	104	-85	0.99	-	-	-	0.07	0.12
Sulfamethoxazole (SMX)								
HMS-SP	321	0	0.90	62	337	0.94	3.93	5.35
A-HMS-SP	246	0	1.00	27	497	0.97	0.12	1.08
OD-HMS-SP	61	216	0.99	-	-	-	0.12	1.10

^a Calculated at the first stage of the diffusion

^c Calculated from Eq. (5.8)

^b Calculated at the second stage of the diffusion

^d Calculated from Eq. (5.9)

Table 4 Adsorption kinetic parameters of antibiotics by HMS-SP, A-HMS-SP and OD-HMS-SP in 0.01 M phosphate buffer pH 7.

Adsorbents	Freundlich				Sips					Redlich-Peterson				
	K_F^b	$1/n$	R^2	χ^2	q_m^a	K_s^b	$1/n$	R^2	χ^2	K_{RP}^b	α	β	R^2	χ^2
Nalidixic acid (NAL)														
HMS-SP	0.03	0.44	0.85	0.01	0.69	0.00	3.26	0.92	0.01					
A-HMS-SP	0.17	0.48	0.87	0.92	5.72	0.00	4.52	0.99	0.07					
OD-HMS-SP	0.002	0.05	0.99	0.017	24.1	0.0001	1.02	0.99	0.02					
Sulfamethoxazole (SMX)														
HMS-SP	0.16	0.23	0.96	0.003	1.01	0.12	0.48	0.99	0.001	0.12	0.44	0.85	0.99	0.001
A-HMS-SP	0.19	0.46	0.92	0.26										
OD-HMS-SP	0.05	0.70	0.99	0.07										

Figure 1 Surface charges density of pristine HMS-SP, A-HMS-SP and OD-HMS-SP as a function of pH at ionic strength (IS) 0.01 M.

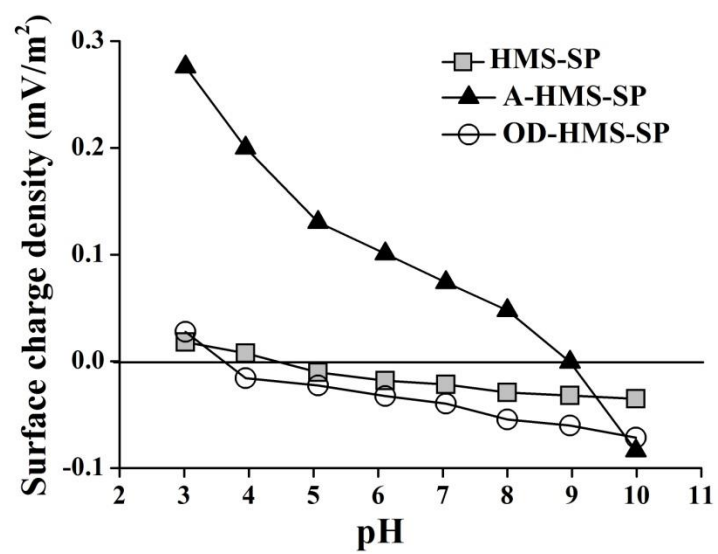


Figure 2 Adsorption kinetics of NAL (a), and SMX (b) by pristine HMS-SP, and functionalized HMS-SPs at $250 \mu\text{g L}^{-1}$ (pH 7 and IS 0.01 M).

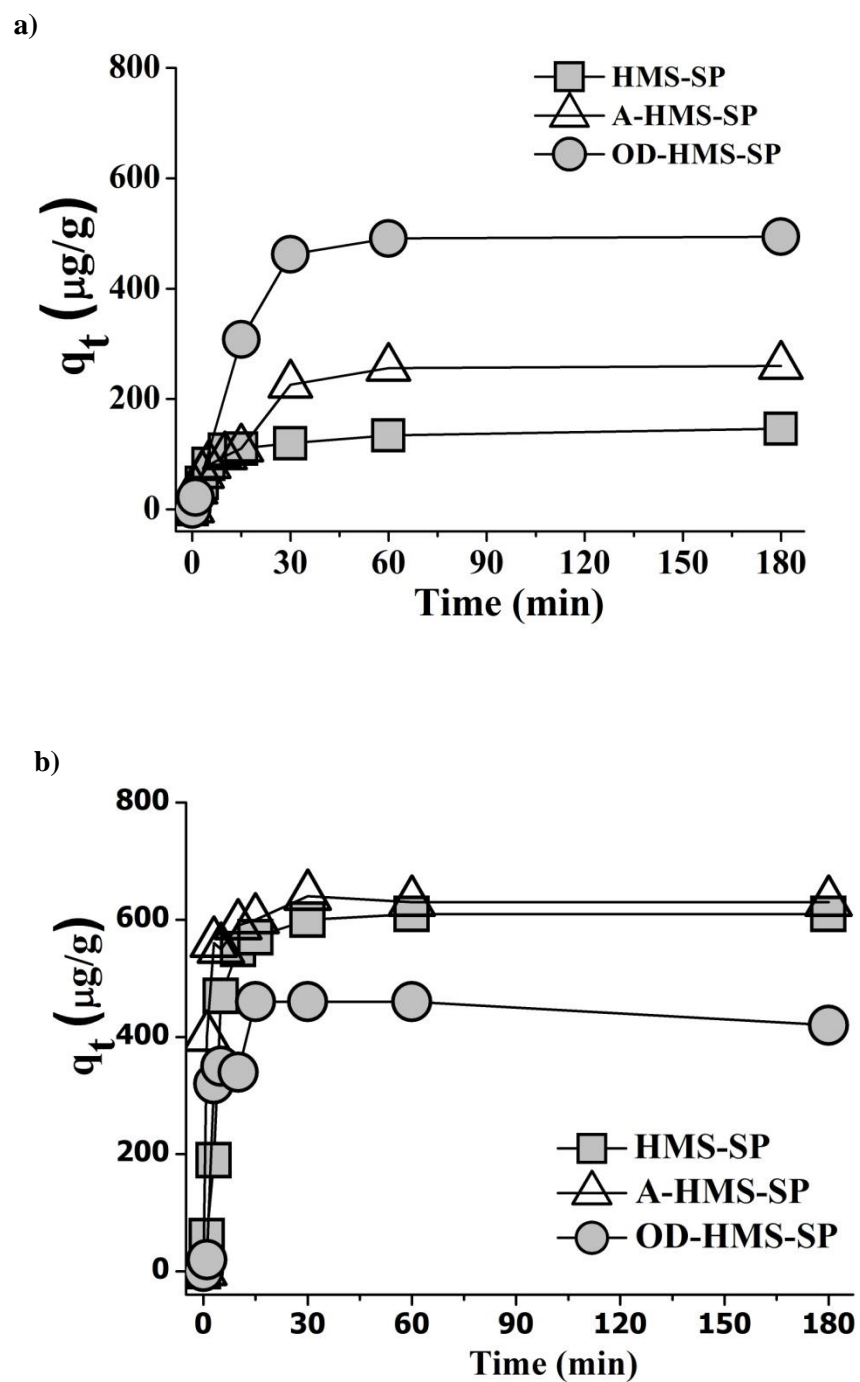
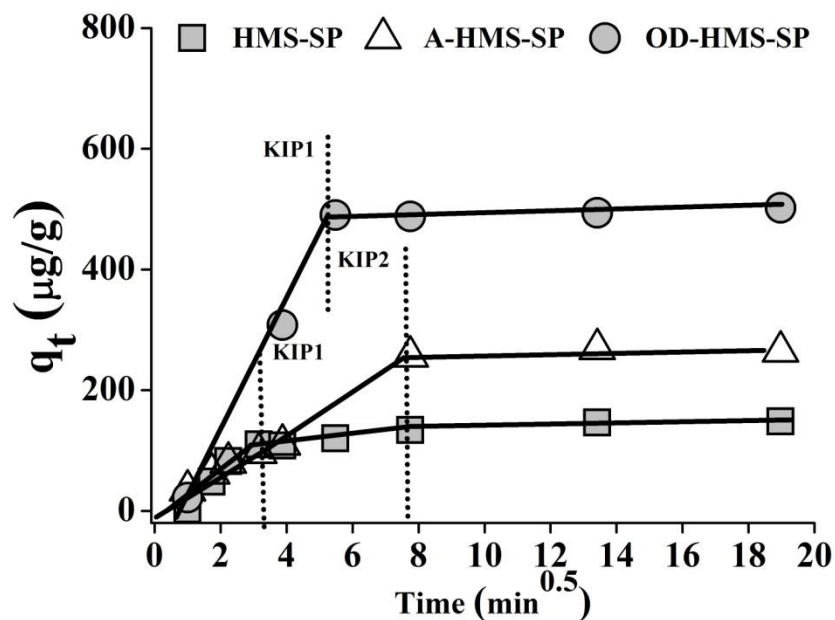


Figure 3 Intraparticle model fitting of the NAL (a), and SMX (b) adsorption kinetics on HMS-SP, A-HMS-SP and OD-HMS-SP in phosphate buffer at pH 7 and IS 0.01 M.

a)



b)

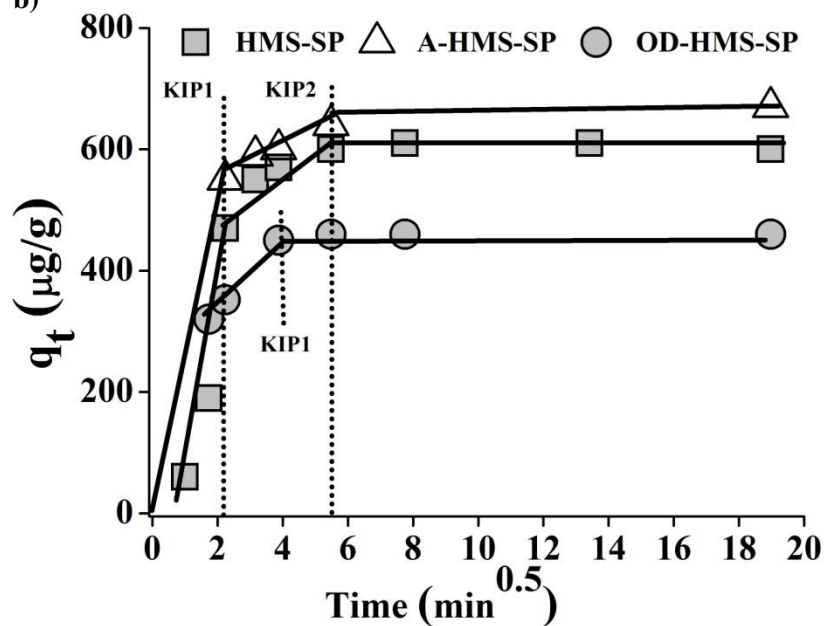


Figure 4 Effect of surface functional group on the adsorption of (a) NAL and (b) SMX by HMS-SP, A-HMS-SP and OD-HMS-SP in phosphate buffer at pH 7 and IS 0.01 M.

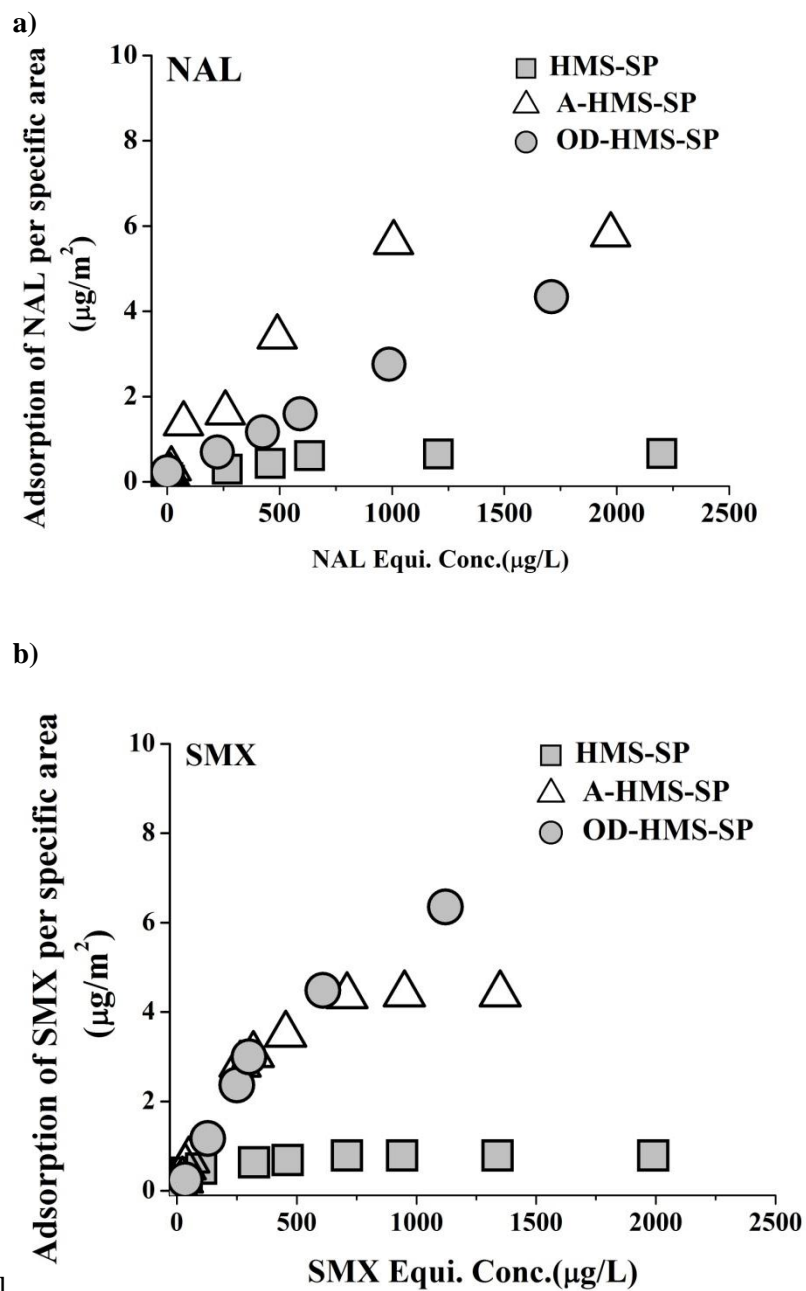


Figure 5 Effect of pH on the adsorption of NAL (a, b, c) and SMX (d, e, f) on HMS-SP, A-HMS-SP, and OD-HMS-SP at pH 5, 7 and 9 with IS 0.01 M at 25 °C.

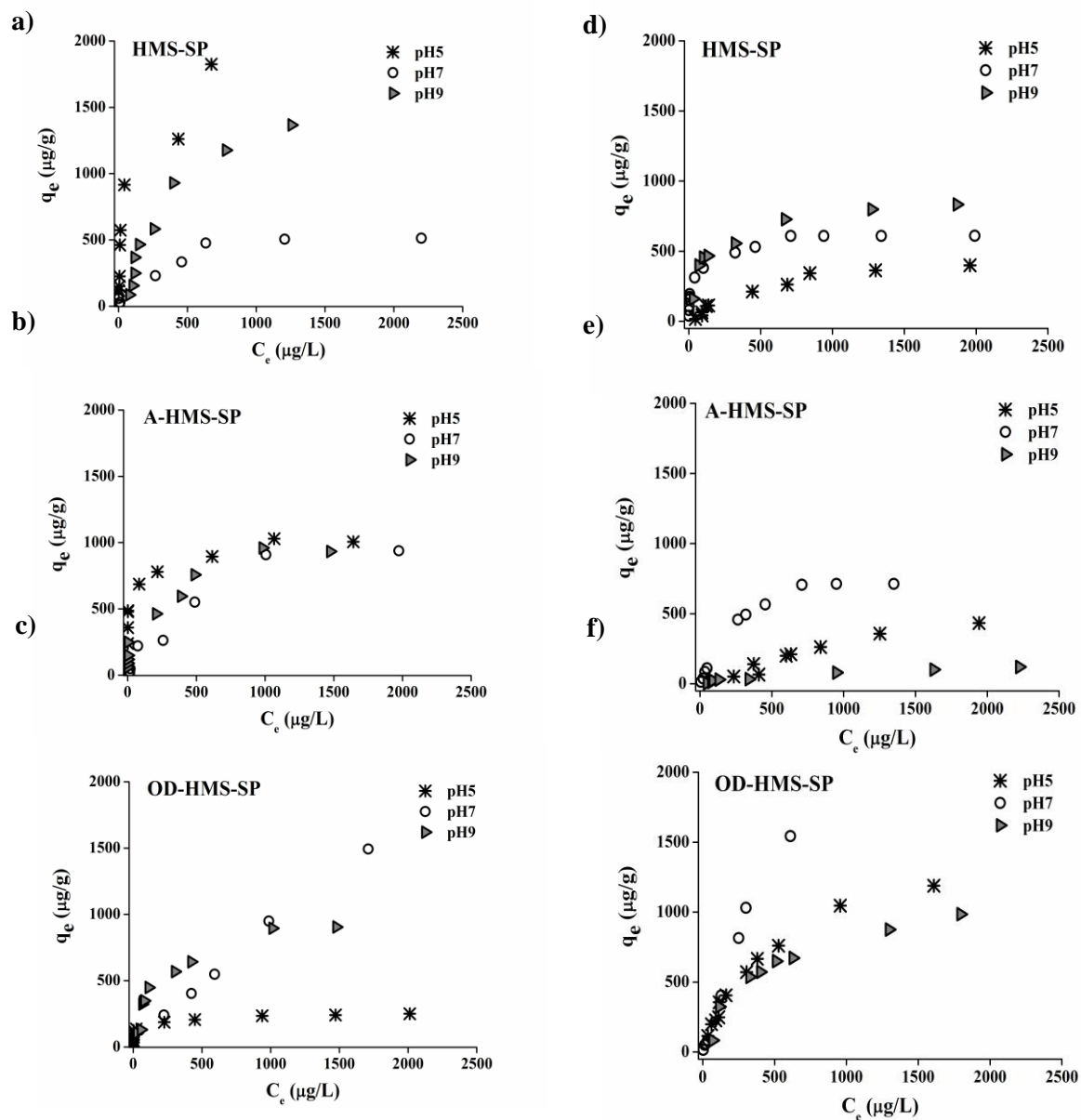


Figure 6 Effect of tannic acid on the adsorption of NAL (a, b) and SMX (c, d) onto A-HMS-SP and OD-HMS-SP at pH 7 with IS 0.01 M at 25 °C.

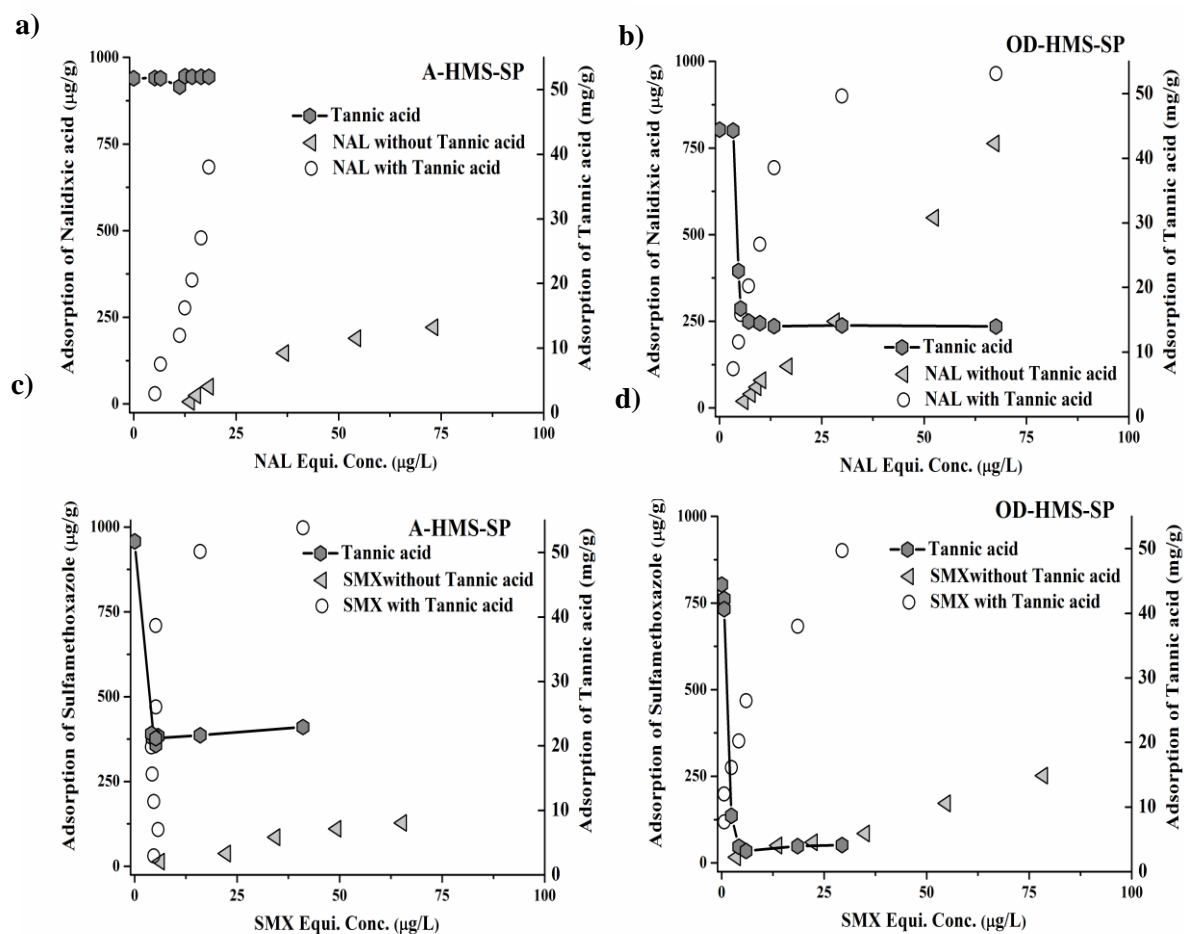


Figure 7 Proposed adsorption mechanism of nalidixic acid in co-existing Tannic acid onto (a) A-HMS-SP and (b) OD-HMS-SP

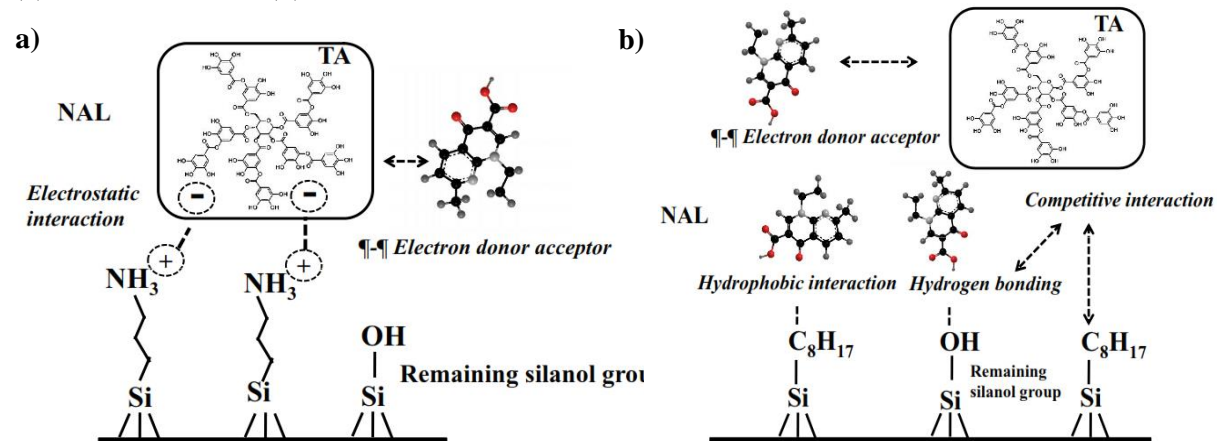


Figure 8 Proposed adsorption mechanism of sulfamethoxazole antibiotic in co-existing Tannic acid onto (a) A-HMS-SP and (b) OD-HMS-SP

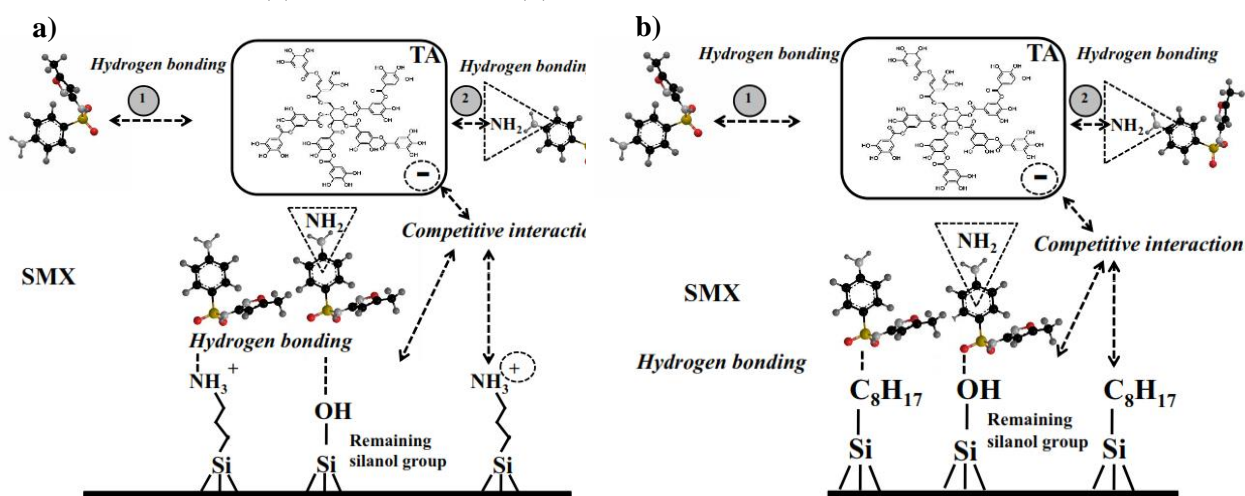
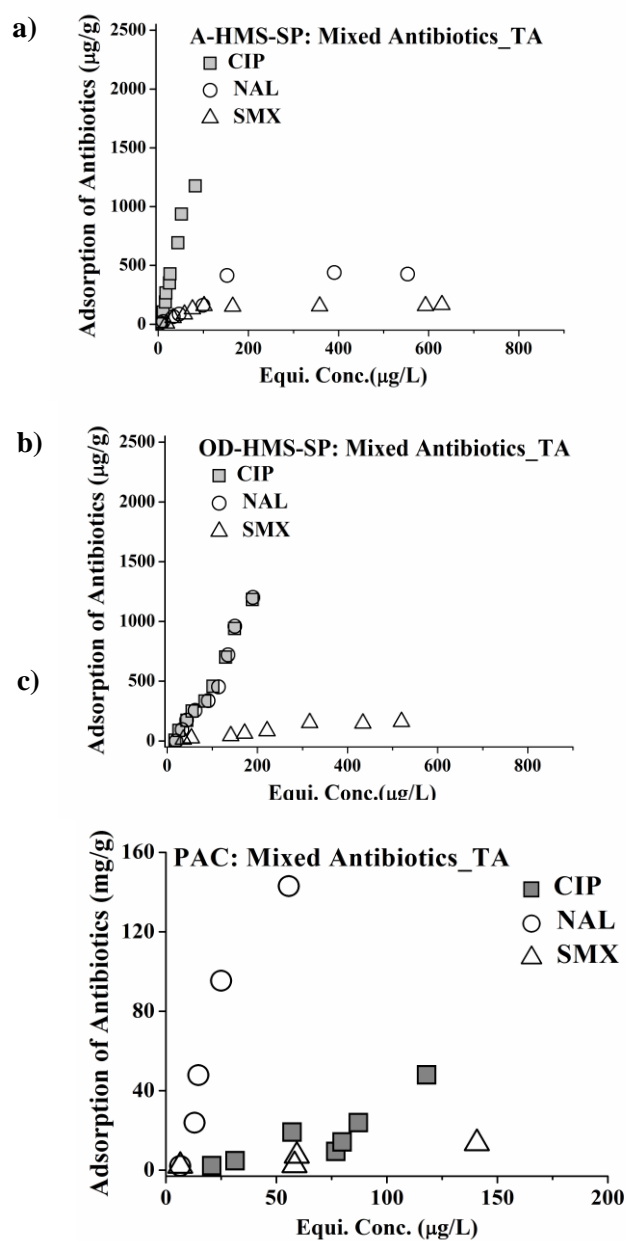


Figure 9 Adsorption isotherm of three antibiotics on A-HMS-SP, OD-HMS-SP and PAC in a mixed solute (a, b, c) with co-existing tannic acid in 0.01 M phosphate buffer pH 7.0 (25°C).



Supplement

Figure S1 Mixed solute adsorption

